EXPERIMENTAL INVESTIGATION FOR MECHANICAL PROPERTIES OF FILAMENT WOUND COMPOSITE TUBES

A THESIS SUBMITTED TO
THE GRADUATE SCHOOL OF NATURAL AND APPLIED SCIENCES
OF
MIDDLE EAST TECHNICAL UNIVERSITY

BY

EMRAH SALIM ERDILLER

IN PARTIAL FULFILLMENT OF THE REQUIREMENTS
FOR
THE DEGREE OF MASTER OF SCIENCE
IN
MECHANICAL ENGINEERING

JULY 2004

Approval of the Graduate School of Natural and Applied Sciences

Prof. Dr. Canan ÖZGEN

Director

I certify that this thesis satisfies all the requirements as a thesis for the degree of Master of Science.

Prof. Dr. S. Kemal IDER

Head of Department

This is to certify that we have read this thesis and that in our opinion it is fully adequate, in scope and quality, as a thesis for the degree of Master of Science.

Assoc. Prof. Dr. Cevdet KAYNAK	Prof. Dr. Levend PARNAS
Co-Supervisor	Supervisor

Examining Committee Members

Asst. Prof. Dr. Ergin TÖNÜK	(METU,ME)	
Prof. Dr. Levend PARNAS	(METU,ME)	
Assoc. Prof. Dr. Cevdet KAYNAK	(METU,METE)	
Prof. Dr. Mehmet A. AKGÜN	(METU,AE)	
Asst. Prof. Dr. Serkan DAG	(METU,ME)	

I hereby declare that all information in this document has been obtained and presented in accordance with academic rules and ethical conduct. I also declare that, as required by these rules and conduct, I have fully cited and referenced all material and results that are not original to this work.

Name, Last name : Emrah Salim Erdiller

Signature :

ABSTRACT

EXPERIMENTAL INVESTIGATION FOR MECHANICAL PROPERTIES OF FILAMENT-WOUND COMPOSITE TUBES

Erdiller, Emrah Salim
M.S., Department of Mechanical Engineering
Supervisor: Prof. Dr. Levend Parnas
Co-Supervisor: Assoc. Prof. Dr. Cevdet Kaynak

July 2004, 129 pages

The aim of this study is to investigate the mechanical properties of continuous fiber reinforced composite tubes, produced by filament winding technique. For this purpose, tensile and split-disk tests were performed with specimens produced with five different fiber materials and two different resin systems. Longitudinal tensile and hoop tensile properties of the selected specimens were determined and the effect of reinforcement direction on the mechanical performance of these composites was investigated. In addition, the effect of a filament-winding processing variable (fiber tension) on longitudinal and hoop tensile properties of the selected composites was obtained. A slight increase in hoop/longitudinal tensile properties of specimens was observed for specimens wounded with tension and with winding angles greater than 60^{o}. The tests were performed according to American Society for Testing and Materials (ASTM) standards.

The split-disk tests of selected composite specimens were simulated by the finite element method. For this purpose, a commercial finite element package

program was used. Experimental results were used both as input in terms of material data for the finite element study and for comparison purposes. A good agreement was obtained between the simulation results and the experimental data.

Keywords : Filament winding, composite tube, longitudinal tensile properties, hoop tensile properties, finite element method, split-disk test, tensile test.

ÖZ

FILAMAN SARIM YÖNTEMI ILE ÜRETILMIS KOMPOZIT BORULARIN MEKANIK ÖZELLIKLERININ DENEYSEL OLARAK BELIRLENMESI

Erdiller, Emrah Salim
Yüksek Lisans. Makine Mühendisligi Bölümü
Tez Yöneticisi: Prof. Dr. Levend Parnas
Ortak Tez Yöneticisi: Doç. Dr. Cevdet Kaynak

Temmuz 2004, 129 sayfa

Bu çalismanin amaci, filaman sargi yöntemi ile üretilmis, sürekli fiber destekli kompozit borularin mekanik özelliklerinin deneysel olarak belirlenmesidir. Bu amaçla, bes farkli elyaf malzemesi ve iki farkli reçine sistemi kullanilarak üretilmis numunelerle, tüp çekme ve disk-ayirma testleri gerçeklestirilmistir. Bu testler sonucunda, numunelerin, eksenel çekme ve çevresel çekme özellikleri deneysel olarak belirlenmis, elyaf yönünün, kompozit malzemenin mekanik özelliklerine olan etkisi incelenmistir. Buna ek olarak, bir filaman sargi yöntemi üretim parametresi olan, elyaf gerginlik ayarinin, söz konusu mekanik özelliklere olan etkisi belirlenilmeye çalisilmistir. Buna göre, gerginlikli olarak sarilmis ve 60^o üzerinde sarim açisina sahip numunelerin mekanik özelliklerinde kismi bir artis gözlenmistir. Testler, Amerikan Test ve Malzeme Standartlari Kurumu (ASTM) standartlarina uygun olarak gerçeklestirilmistir.

Tez kapsaminda, belirlenen kompozit numunelerin mekanik özelliklerinin disk-ayirma test yöntemi ile karakterizasyonunun, sonlu elemanlar yöntemi ile simulasyonu gerçeklestirilmistir. Bu amaçla, ticari bir sonlu elemanlar paket programi kullanilmistir. Deneyler sonucunda elde edilen veriler, hem analiz sirasinda malzeme verisi olarak, hem de karsilastima amaci ile kullanilmistir. Analiz sonuçlari ve deneysel sonuçlar arasinda iyi bir uyum gözlenmistir

Anahtar Kelimeler: Filaman sargi metodu, kompozit boru, eksenel çekme özellikleri, çevresel çekme özellikleri, sonlu elemanlar yöntemi, disk-ayirma testi, çekme testi.

To my parents

ACKNOWLEDGEMENTS

I must express my sincere thanks to Prof. Dr. Levend Parnas and Assoc. Prof. Dr. Cevdet Kaynak for their guidance, insight, and patience throughout the research. I also want to thank to Askin Üstad, Erkan Akay, Fikret Senel and Bora Balya, for their help and understanding.

Special thanks to Hülya Arslan for her sacrifices and moral support over the years. Finally, I specially wish to thank my family for their neverending patience, motivation and moral support.

TABLE OF CONTENTS

LIST OF TABLES

LIST OF FIGURES

CHAPTER 1

INTRODUCTION

Development of new composites and new applications of composites is accelerating due to the requirement of materials with unusual combination of properties that cannot be met by the conventional monolithic materials. Actually, composite materials are capable of covering this requirement in all means because of their heterogeneous nature. Properties of composites arise as a function of its constituent materials, their distribution, and the interaction among them and as a result an unusual combination of material properties can be obtained.

From the wide family of composites, fiber reinforced composites have taken much attention due to their better mechanical properties. A fibrous reinforcement is characterized by its length being much greater than its cross-sectional dimension. Composites produced by long fibers with high aspect ratio give what are called continuous fiber reinforced composites. These composites have found a wide range of application area due to their anisotropic nature, that is; the direction dependence of their properties results in much better design flexibility that cannot be obtained by monolithic materials or particle reinforced composites.

Anisotropic nature of fibrous composites, however, makes their mechanical characterization much more complicated compared to monolithic materials. There are several analytical, computational and experimental studies, concerning the analysis of mechanical performance of filament-wound composites in literature. However, this concept is still under development, and requires additional scientific effort.

This study was aimed to fulfil a part of this requirement. Carbon, and glass fiber reinforced filament-wound composite tubes were selected as the target of this study since these reinforcements are commonly used in most of the applications of filament-winding technique. Variation of longitudinal tensile and hoop tensile properties of these composites was investigated as a function of mainly the direction of fiber reinforcements inside the composite. By evaluating the experimental data, a general distribution of the prespecified properties as a function of winding angle was obtained. In addition, split disk testing of filament-wound composite structures was modelled by using the finite element method, to supply a comprehensive base to the study.

Several production methods have been developed for the synthesis of fiber reinforced composites, mainly according to the continuous/matrix phase of the composite, under consideration. Filament winding technique can be accepted as one of the most common production techniques, for the synthesis of polymer matrix composites (PMC). In the following section, filament-winding technique, its advantages, limitations, applications and potential raw materials will be explained.

1.1 Filament Winding Technique

Filament winding is a continuous fiber reinforced composite production technique, in which resin – impregnated band of continuous fibers are wound over a rotating mandrel. Wounding of continuous fibers are performed either as adjacent bands or in the form of repeating bands that are stepped the width of the band to eventually cover the mandrel surface and to produce one complete layer. The process continues with the wounding of additional layers, until the design requirements are achieved. The production is completed by curing of the filament-wound product in an oven and the removal of the mandrel. A schematic representation of the technique is given in Figure 1.1.

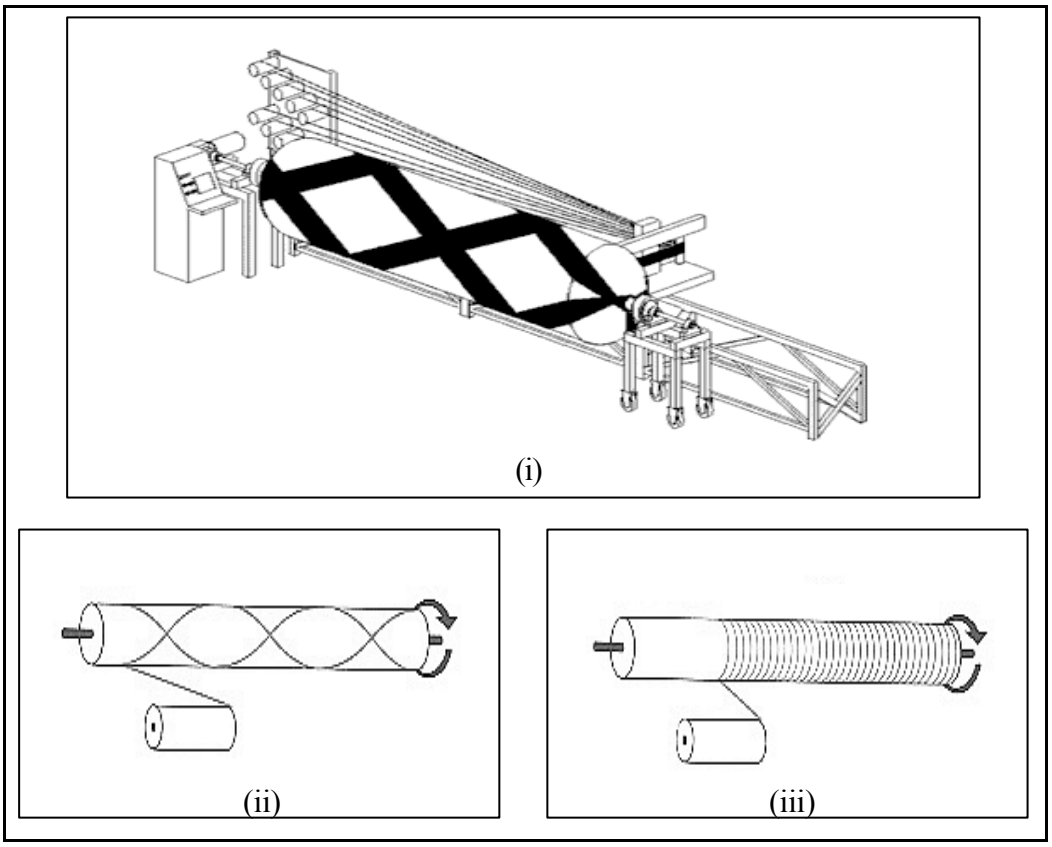

Figure 1.1 Filament-winding Technique. (i) Schematic representation of the process. (ii) Presentation of coupled helical winding of layers. (iii) Presentation of hoop winding of layers.

Each layer of reinforcement can vary in winding tension, winding angle, or resin content. By varying the winding angle with respect to the mandrel axis, directional strength can be obtained by considering the loads, which will operate on the finished product. Coupled helical winding of layers ($\pm\theta$) are usually preferred (Figure 1.1(ii)), whereas hoop winding (winding angle, very close to 90°, Figure 1.1(iii)) can also be used in combination with the helical layers. Other advantages of filament winding technique are high specific strength, specific modulus and fiber volume percentage of the finished products and high repeatability of the process. (Production can be repeated successively, to obtain the same properties of the finished products)

The main limitation of filament winding technique is the difficulty in production of complex shapes due to the requirement of very complex mandrel designs. In addition, production of reverse curvature parts is not possible by using this technique. These limitations restrict the application area of this technique to the production of mainly cylindrical, usually axisymmetric, hollow parts. Main application areas of this technique are pipelines, shafts, pressure vessels, rocket motor cases, rocket launch tubes, and gas tanks.

1.1.1 Material Selection

Mainly, glass, carbon, and aramid reinforcements are preferred for filament winding. Glass fibers are preferred for less critical applications due to their low cost. Carbon fibers have better mechanical and thermal properties, and due to this reason, are usually selected as the reinforcement material for filament winding technique in the aerospace and defense industry. Aramid fibers have also comparable, mechanical and thermal properties with the carbon fibers. However, both carbon and aramid fibers have the common disadvantage of high cost in compare to glass fibers. A comparison of mechanical properties of commercially available continuous fibers is given in Table 1.1.

Thermoset or thermoplastic resin systems are usually used for impregnation of the continuous fibers in filament winding. Most commonly, epoxy resins are used due to their wide range of thermal and mechanical properties. Polyester and vinyl ester resin systems are also used due to their lower cost compared to epoxy resin systems, in commercial applications.

Table 1.1 A comparison of mechanical properties of commercially available continuous fibers, adapted from Ref [1].

Fiber	Elastic Modulus (GPa)	Tensile Strength (MPa)	Tensile Strain (%)
S - Glass	72.5	3447	4.80
R - Glass	86.2	2068	2.4
Carbon	248.0	4550	1.64
Aramid	186.0	3445	1.8

The curing temperature of the wound products is determined by the resin system selected for an application. The main factor controlling the curing temperature is the glass transition temperature (T_g) of the resin system selected. As a function of T_g, curing can be performed either in an oven or at room temperature. However, oven curing is usually preferred due to the much shorter curing time.

1.1.2 Winding and Impregnation Methods in Filament Winding

Joining of reinforcement and the resin system is termed as impregnation. In filament winding, mainly two impregnation methods are used, namely; dry winding and wet winding. In dry winding method, preimpregnated fibers are directly wounded on the mandrel surface. This technique is also termed as prepreg winding. The application of this technique causes the manufacturer to obtain better mechanical properties of the finished products. However, due to

the high prepreg material costs, this method is usually only preferred for high performance applications.

In wet winding method, passing the fibers from a resin bath before the winding operation performs the impregnation of fibers. This impregnation method is commercially the most common and involves additional process variables compared to dry winding technique, such as, resin viscosity and fiber tension. Resin viscosity has a great importance in filament winding technique. If the viscosity is too high, unevenly coating of fibers with resin can occur, whereas in the other extreme, if the resin viscosity is too low, resin may flow out of the part during winding, which can cause a relatively lower weight percent of resin in the finished product.

Since the continuous fiber reinforcements are packaged on the form of rolls in wet winding technique, the tension setting of the fibers should be controlled before the impregnation process. This can be achieved by introducing tension at the roll, with the aid of a tensioning device. Tension setting can also have an effect on mechanical performance of the finished product, and therefore has to be accepted as a design variable in wet winding technique.

Winding of fibers in filament winding can be performed by using either helical or polar winding technique. In helical winding technique, the mandrel rotates continuously while the fiber feed carriage moves unidirectionaly along the mandrel axis. In polar winding, different from the helical winding, the mandrel remains stationary, while the fiber feed carriage both rotates along the longitudinal axis of the mandrel and moves unidirectionally along the mandrel axis.

1.2 Analysis of Filament-Wound Composite Tubes

The application areas, stated in Section 1.1, involve various loading conditions, mainly, axial loads, torsion, internal and external pressure, and bending. For an application, the thickness (number of windings), and the winding angle of the fibers are defined by taking into account the loading conditions, under which the finished product will operate. In Figure 1.2, a schematic representation of these loads is presented on a filament-wound composite tubular structure.

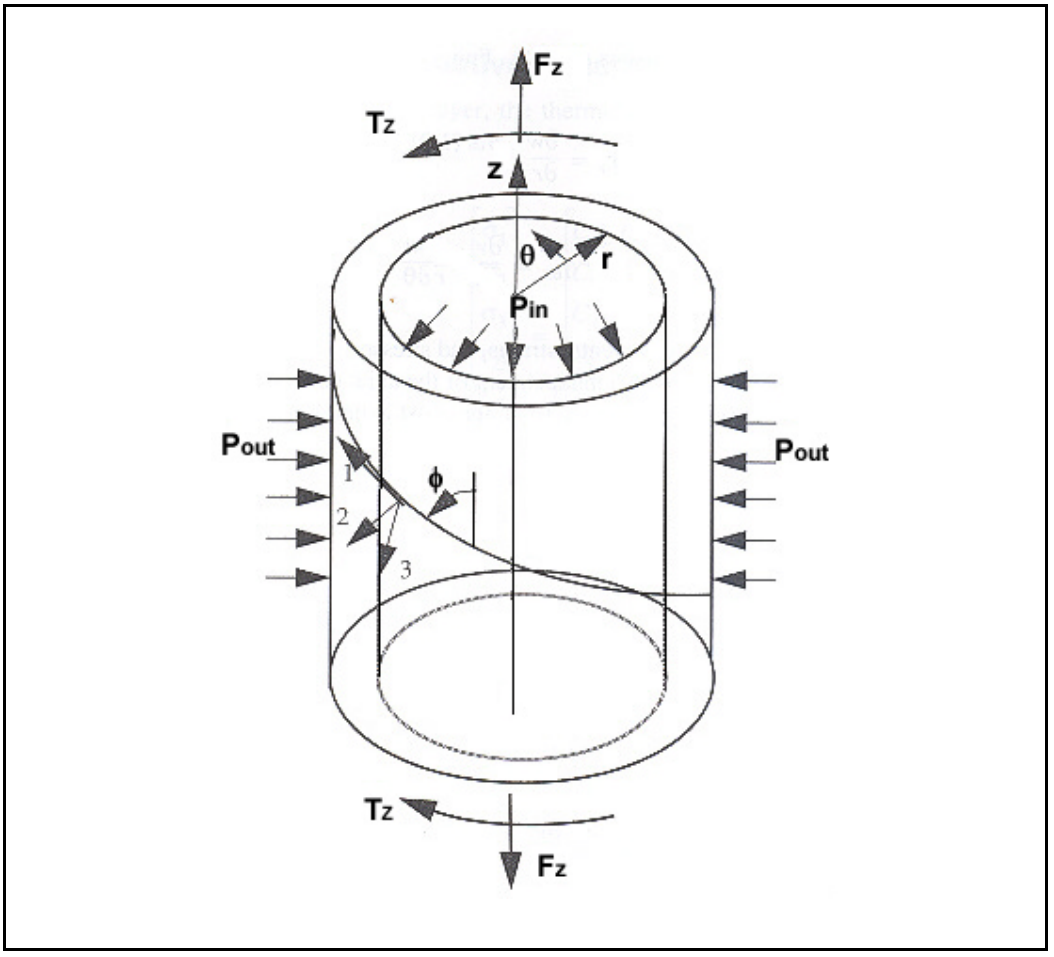

Figure 1.2 Schematic representation of the possible service loads, for a filament-wound composite tubular structure.

In the next section, the methodologies, which are commonly used for the theoretical analysis of the mechanical performance of the filament-wound composite structures and some illustrations of the related literature review, will be presented. The following section involves a review of past experimental studies, performed to characterize filament wound composite tubes.

1.2.1 Theoretical Analysis of Mechanical Performance of Filament-Wound Composite Structures

In most of the studies performed to determine the mechanical properties of filament-wound composite tubes, these structures are modeled as a combination of layers, each having a winding direction with respect to the longitudional axis of the tubular composite part and each having a finite thickness. This assumption simplifies the model, such that; with the aid of this assumption, the single layer solution can be successively extended to laminated tube geometry, and therefore to filament-wound composite structure. The assumption however can cause a negligible error for helical layers, that is; the helical layers, having plus and minus winding angles are not forming two totally distinct layers since the fiber bands criss-cross by creating a weaving effect.

On the basis of the above assumption, several analytical analyses for multilayered filament-wound composite structures were performed so as to determine the stresses and displacements, arising from the loads, presented in Figure 1.2 [2–8], based on the solution of Lekhnitskii [9] for anisotropic tubes composed of single layer. Solutions were also obtained for filament-wound composite structures, under combined loading conditions, such as the study of P. M. Wild and G. W. Vickers [10]. They developed an analytical procedure to assess the stress and deformations of a filament-wound cylindrical shell comprising a number of sublayers, each of which is cylindrically orthotropic.

Radial body force due to rotation about the cylinder axis, internal and external pressures and axial force was considered during the study.

A similar study was performed by C. S. Chouchaoui and O. O. Ochoa [11] to determine the stresses and displacements of an assembly of several coaxial hollow circular cylinders, made of orthotropic materials. Differently, torsion and bending loads are considered in addition to internal-external pressure and axial loading.

C. T. Sun and Sijian Li [12] obtained an analytical solution for thick laminates, consisting of large numbers of repeating sublaminates/layers. The laminate was modeled as a three-dimensional homogenous anisotropic solid, based on the assumption, stated above. Reduced expressions for the effective moduli were derived in each lamina by using constant stress and constant strain boundary conditions.

In the study of Aleçakir [13], analytical solutions for stresses and displacements in each orthotropic layer of a multi-layered filament-wound composite tube, subjected to axisymmetric and bending loads were obtained, by developing a method based on the governing equations for a homogenous body having cylindrical anisotropy [9]. The results were verified by performing experiments, concerning the bending behavior of composite tubes.

K. Chandrashekhara and P. Gopalakrishnan [14] obtained a three-dimensional elasticity solution for a long multilayered cylindrical shell of transversely isotropic layers, which are subjected to axisymmetric radial load. Numerical results were also presented for cylindrical shells, having different thickness – to – outer radius ratios and for different ratios of the modulus of elasticity in the radial direction of layers.

A partially different approach was also developed so as to obtain an analytical solution for the stress and deformations of filament-wound structures under various loading conditions, based on classical laminated plate theory. In this approach, a rectangular section was taken from the wall of a filament-wound tube and modeled as an angle – ply laminate, by using the classical lamination theory. A schematic presentation of this model is presented in Figure 1.3.

This approach can be illustrated by the study of M. F. S. Al-Khalil and P. D. Soden [15], such that; they developed a solution to calculate the three-dimensional effective elastic constants for filament-wound fiber-reinforced composite tubes with the aid of the above assumption. They presented the winding angle dependence of all of the elastic constants for E-glass, carbon, and epoxy reinforced filament-wound tubes.

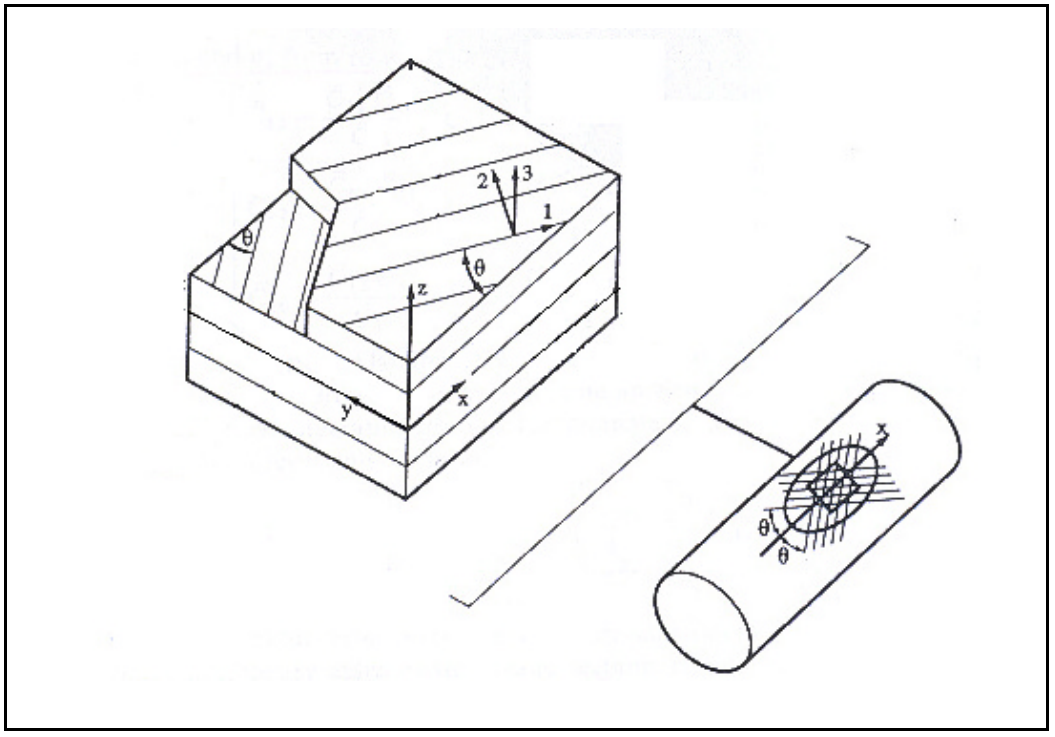

Figure 1.3 Angle-ply models for an element from the wall of a filament-wound tube. [15]

The structures, produced by the filament-winding technique are becoming more complicated in terms of geometry and loading. This factor necessitates the usage of computational methods in the analysis of filament-wound structures. Finite element method is being widely used for the analysis of continuous fiber reinforced composite structures, especially for the determination of stresses and displacements under various loading conditions, failure prediction and damage determination [16-19].

In the study of Ilhan [20], the response of filament-wound composite tubes and pressure vessels under various loading conditions was investigated by the finite element method. Internal pressure, axial force, torsion, bending moment, and combination of these loads were considered during the study and the development of a computer program was performed for design and analysis purposes. Both solid and shell elements were used in the study. Maximum tolerable values for a certain loading condition and geometry of tubes, and the optimum winding angle, were aimed to be calculated by utilizing the maximum stress, maximum strain, and Tsai-Wu failure criteria.

In the study of Monika G. Garrell, Albert J. Shis, Edgar Lara-Curzio, and Ronald O. Scattergood [21], finite element method was used to investigate the effect of stress concentration in ASTM D 638 Tensile test specimens. Two-dimensional, plane stress, six-node and twelve degree-of-freedom triangular linear elastic element was selected to model the tensile test specimens. Different from the study of Ilhan, the commercially available ANSYS finite element analysis software and its mesh generator were used for modeling. Nodal Von-Misses and principle stresses were obtained from the analysis, which were then used to calculate the stress concentration factor.

S. Arsene, and J. Bai [22], developed a new approach to measure the transverse properties of structural tubing, by using finite element method. Three-dimensional finite element modeling with contact was performed to

analyze the stress and strain distribution in the ring specimens, to optimize the ring testing system. By performing a series of analysis, a new design of a holding device was proposed in order to determine the transverse behavior of tubular products.

1.2.2 Mechanical Testing of Filament-Wound Composite Structures

Filament-wound composite structures have been tested extensively, mainly to fulfill two main requirements:

- To provide the necessary material and strength data for the design purposes

- To verify the accuracy of the completed design studies

For the purposes stated above, a test specimen configuration must be selected, on the basis that, test results should provide material properties useful in the design stage. Three types of testing geometry are commonly used in testing of filament-wound composite structures, namely; flat specimens (coupon specimens), ring specimens (Figure 1.4), and tubular specimens. Axial (tension/compression), shear, and bending response of each testing geometry can be determined by applying a suitable loading to the specimen. In addition to these tests, internal pressure and torsion tests can be applied to the tubular specimens. Tests, involving biaxial/combined loading of test specimen can also be performed.

D. Cohen [23] performed an experimental study to investigate the effect of winding tension, stacking sequence, winding tension gradient, and winding time on hoop stress, hoop stiffness, fiber and void volume fraction distribution through thickness, and interlaminar shear strength of carbon fiber reinforced filament wound ring specimens. Hoop strength and hoop stiffness of the

specimens were obtained by performing pressurized ring tests [24] on the filament-wound ring specimens. The interlaminar shear strength of composites were determined by performing short-beam shear (SBS) tests, according to ASTM D2344-88. It was shown that composite strength increases for cylinders, wound without winding gradient, wound in short time, with high winding tension. However, it was also stated that the effect of these variables on strength were relatively small, with effect of winding tension being the largest.

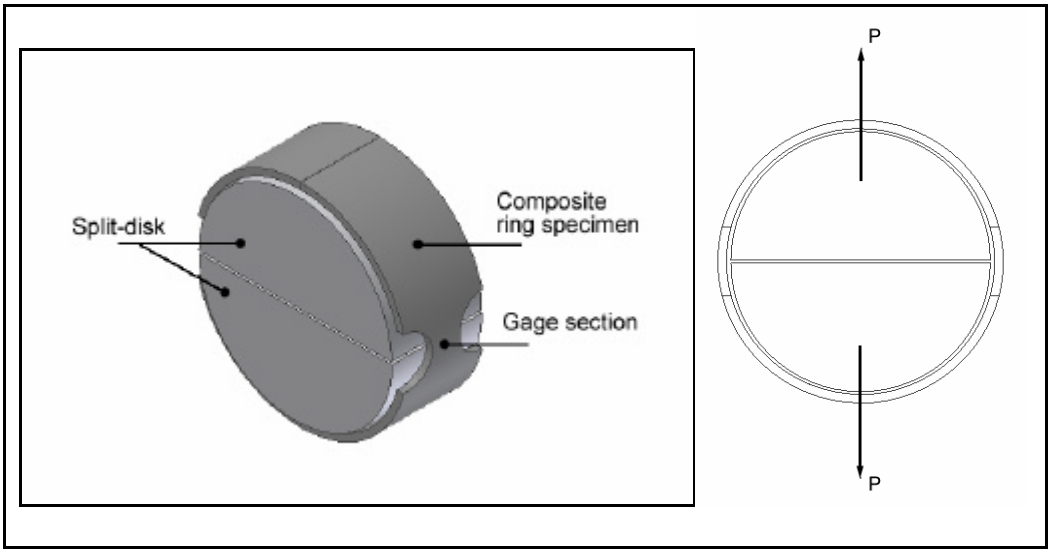

Figure 1.4 Ring specimen geometry and schematic of ring test

H. Wang, R. Bouchard, R. Eagleson, P. Martin, and W. R. Tyson, performed ring hoop tension tests to ring samples [25], having a single reduced section of area. The paper involves an improved modification of the test, to determine the hoop stress – strain curve, and it was concluded that ring hoop tension test is an accurate method to measure transverse tensile properties of tubular specimens.

C. S. Lee, W. Hwang, H.C Park, and K. S. Han [26] performed biaxial tests on cross-ply carbon/epoxy composite tubes under combined torsion and axial tension/compression up to failure to investigate the effect of biaxial loading ratios on failure strength and failure mechanism. In that study, it was concluded that there is a strong interaction between the axial stress and the shear stress at failure.

Jinbo Bai, Philippe Seeleuthner, and P. Bompard [27] performed an experimental study to investigate the mechanical behavior of ±55° filament-wound glass fiber reinforced epoxy resin tubes. Series of tests were carried out under various combinations of hoop and axial stress to evaluate the filament-wound tubes mechanical behavior under pure axial tensile load, pure internal pressure, and under combined loading. Observations on specimens, loaded to twenty to fifty percent of the ultimate tensile strength, showed that the main damage initiation mechanisms are microcracking and delamination. Depending on the loading conditions, one of the mechanisms dominates over the other.

Another experimental study, concerning ±55° filament-wound composite tubes, was performed by M. Caroll, F. Ellyin, D. Kujawski, and A. S. Chiu [28]. Glass fiber/epoxy tubes, having ±55° winding angle were tested in a biaxial testing machine with various ratios of axial stress to hoop stress. The resulting stress/strain curves were analyzed and biaxial failure envelopes in terms of stress and strain were constructed, demonstrating the complexity of the behavior of the tubes. It was shown that the rate and ratio of biaxial loading affect the monotonic failure strength, damage accumulation and the mode of failure.

In the study of Ayral [29], the influence of fiber directions on the mechanical properties of carbon fiber reinforced polyether-ether-ketone (PEEK) thermoplastic matrix composites was investigated by conducting tension,

flexural, impact, and in plane shear tests. In addition, physico-chemical tests were also performed to obtain the fiber and matrix mass percentages, density and void content of test panels. The test specimens were prepared by using autoclave and vacuum bag molding process. Tests were performed with 0° and 90° fiber directions.

In Reference [30], filament-wound composite tubes, produced by four different fiber materials (carbon, aramid, E-glass, S2-glass) and two different resin systems were tested. Axial (tensile/compressive), internal pressure, impact, and torsion response of test specimens, having 25°, 45°, and 54° winding angle were determined separately. In addition thermal analysis technique was used so as to obtain fiber and matrix mass percentages, and the glass transition temperatures of the matrix phase. Under the scope of the study, coupon tests were also performed in order to define the material properties of the selected composite materials.

1.3 Scope of the Thesis

The thesis includes five chapters. A brief introduction about the subject, thesis objective, and the related literature is presented in Chapter 1. The second chapter involves information about the specimen details, its designations, and experimental technique. General aspects of the modeling study is given in Chapter 3. The fourth chapter includes the results of the experimental work and the simulation study, and their comprehensive discussion. The conclusions obtained from the study, is summarized in the last chapter.

CHAPTER 2

SAMPLE PREPERATION AND EXPERIMENTAL TECHNIQUE

2.1 Introduction

This chapter involves material selection of specimens, their fabrication and designation procedure, and the experimental technique. In the following two sections, brief information about the selected resin systems and reinforcements will be presented. This will be followed by test specimen fabrication procedure in Section 2.4. In Section 2.5, the methodology used in identification of specimens will be presented. In the last section, experimental technique (test specimen geometries, test equipments, test procedure, and calculations) will be presented for split-disk and tube tensile tests separately.

2.2 Material Selection

Test specimens were fabricated from five different fibers and two different epoxy resin systems. In the following two sections, descriptions of these materials are given.

2.2.1 Resin Systems

Epoxy resins have been the major matrix material of polymer-matrix composites, especially for aircraft applications, due to their ease of processing, good mechanical properties, and moderate cost. They are thermosetting and inert resin systems that a good combination of high mechanical and electrical properties can be obtained. They can be used for service temperatures up to

180–270 °C. Their tensile strength may be up to 83 MPa, hardness to Rockwell M 110, with elongations up to 2–5%. They also have high resistance to common solvents, oils, and chemicals [31].

In this study, two different, epoxy resin systems were used in manufacturing of test specimens. These are HUNTSMAN product, LY556 (Epoxy Resin)/ HY917 (Hardener)/ DY070 (Accelerator) and MY740 (Epoxy Resin)/ HY918 (Hardener)/ DY062 (accelerator) systems. The former is a hot-curing, low viscosity resin system that exhibits good wetting properties and is easy to process. It has good chemical resistance, especially to acids at temperatures up to about 80 C^{o}. It is a suitable resin system for production of composites with filament winding, tape winding, pultrusion, and injection moulding processes. The latter resin system (MY740 / HY918 / DY062) is also a hot-curing, low-viscosity impregnating resin system, also suitable for filament winding, wet laminating, and pultrusion processes. It has good mechanical and dielectric properties at elevated temperatures and it has good aging resistance. It has relatively higher resin viscosity compared to the former resin system. In addition, it has relatively shorter minimum curing time, and pot life. The properties of these resin systems, supplied by the manufacturer are tabulated in Table 2.1 and Table 2.2, respectively.

2.2.2 Reinforcements

The fibers used in this study are PPG product, Roving 1084 600 TEX and Roving 1084 2400 TEX glass fibers, CAMELYAF Product, WR3 2400 TEX glass fiber, FORTAFIL product, 503, 2190 TEX carbon fiber and Tenax product , HTA 5331 800 TEX carbon fiber. For CAMELYAF Product, WR3 2400 TEX glass fiber, fiber feed is from the inner of the rolls. For the rest of the fibers, fiber feed is from the outer of the rolls. In Table 2.3 and Table 2.4, the properties of these reinforcements, supplied by the manufacturer are tabulated.

Table 2.1 Properties of HUNTSMAN product, LY556/ HY917/ DY070 resin + hardener system.

Property	Units	Value		
Tensile Strength	**(MPa)**	80 – 90		
Tensile Modulus	**(GPa)**	3.2 – 3.6		
Elongation at break	**(%)**	3 – 7		
Glass Trans. Temp.	**(°C)**	135 - 150 (for curing at 120 °C)	145 – 155 (for curing at 140 °C)	150 – 155 (for curing at 160 °C)
Viscocity	**(mPa.s)**	700 - 900 (at 25 C°)	200 – 300 (at 40 C°)	< 75 (at 60 C°)
Thermal Exp. Coeff.	**(1/K)**	10^{-6}		
Poisson's Ratio		0.35		
Pot life, isotherm. 15 g	**(min)**	420 – 460 (at 60 C°, and 1500 mPa.s)		
Nom. Curing Schedule	**(h/ °C)**	4/80 + 4/140		

Table 2.2 Properties of HUNTSMAN product, MY740 /HY918/ DY062 resin + hardener system.

Property	Units	Value	
Tensile Strength	**(MPa)**		
Tensile Modulus	**(GPa)**		
Elongation at break	**(%)**		
Glass Trans. Temp.	**(°C)**	123 (with min. curing schedule)	
Viscosity (average)	**(mPa.s)**	950 (at 25 °C)	70 (at 60 °C)
Thermal Exp. Coeff.	**(1/K)**	10^{-6}	
Poisson's Ratio		0.35	
Pot life, isotherm. 15 g	**(min)**	210	
Min. Curing Schedule	**(h/ °C)**	2/80 + 2/120	

Table 2.3 Properties of Tenax product, HTA 5331 800 TEX carbon fiber and FORTAFIL product, 503, 2190 TEX carbon fiber.

Property	Units	TENAX, HTA 5331	FORTAFIL, 503
Linear Density	(tex)	800	2190
Tensile Strength	(MPa)	3796	3800
Tensile Modulus	(GPa)	240.8	231
Elongation at break	(%)	1.51	1.64
Filament Diameter	(μm)	7	6
Spec. Density	(g/cm^3)	1.76	1.80

Table 2.4 Properties of CAMELYAF Product, WR3 2400 TEX glass fiber, and PPG product, Roving 1084, 2400 and 600 TEX glass fibers.

Property	Units	CAMELYAF WR3	PPG Roving 1084 - 2400	PPG Roving 1084 – 600
Linear Density	(tex)	2400	2400	600
Tensile Strength	(MPa)		2250	2070
Tensile Modulus	(GPa)		75	72.45
Elongation at break	(%)		3	3 – 4
Filament Diameter	(μm)	22.5	15	15
Spec. Density	(g/cm^3)		2.6	2.63

2.3 Micromechanics

From the micromechanical point of view, the properties of a multicomponent composite material can be raughly obtained by the properties of its indivudial constituents and their relative fractions in composite (weight or volume fractions). Even though the results obtained with this assumption is deficient in predicting the mechanical properties of filament-wound tubular composites (since it is not considering the effect of shape, orientation, distribution, and size of reinforcement, relative strength of fiber/matrix interface etc.), it can be a good tool for discussing the reliability of the experimental studies, performed under the scope of the thesis. Therefore, the results of calculations, performed by considering this assumption will be presented in here.

Accordingly, the longitudinal and transverse modulus of a composite can be approximated as follows:

$$E_L = v_f.E_f + v_m.E_m \tag{2.1}$$

$$\frac{1}{E_T} = \frac{v_f}{E_f} + \frac{v_m}{E_m} \tag{2.2}$$

where:

E_L : Longitudinal Young's modulus

E_T : Transverse Young's modulus

E_f : Modulus of fiber reinforcement

E_m : Modulus of matrix phase

v_f, v_m : Volume frasctions of reinforcement and matrix phase respectivelly.

By using the data, presented in Tables 2.1-2.4 and given in [30], longitudinal and transverse modulus of elasticity was obtained and is presented in Table 2.5 for each fiber type. For all calculations, the data for first resin system (HUNTSMAN product, LY556/ HY917/ DY070) was used.

Table 2.5 Longitudinal/transverse modulus data, calculated by rule of mixtures.

Reinforcement	**E_x (GPa)**	**E_y (GPa)**
PPG Glass Fiber, 2400 TEX	44.08	7.43
PPG Glass Fiber, 600 TEX	42.03	7.45
TENAX Carbon Fiber, 800 TEX	143.73	7.72
FORTAFIL Carbon Fiber, 2190 TEX	137.68	8.12

2.4 Test Specimen Fabrication

By using five different reinforcements, two different resin systems, two different tension settings (during the production of the specimens) and five different winding angles, 100 different test groups were obtained. These variables and their identification numbers used in determination of testing groups are tabulated in Table 2.6.

Table 2.6 The variables, used in determination of testing groups.

Id. Number	Reinforcements	Winding Angles
1	PPG Glass Fiber, 2400 TEX (Outer fiber feed)	0°
2	CAMELYAF Glass Fiber, 2400 TEX (Inner fiber feed)	±25°
3	TENAX Carbon Fiber, 800 TEX (Outer fiber feed)	±45°
4	PPG Glass Fiber, 600 TEX (Outer fiber feed)	±65°
5	FORTAFIL Carbon Fiber, 2190 TEX (Outer fiber feed)	90°
Id. Number	**Resin Systems**	**Tension Settings**
1	MY740 / HY918 / DY062	Normal (without using weight)
2	LY556 / HY917 / DY070	With tension (with weight)

Under the scope of the thesis, 100 tubular specimens were produced by using wet winding technique in filament-winding facilities of Baris Elektrik Endüstrisi A. S., Ankara. Winding operations were performed on a 60 mm diameter steel mandrel with a three axial, computer controlled Bolenz & Schafer filament-winding machine. These wound tubes, together with the mandrel, were then placed into temperature-controlled furnaces, for curing operation. By considering the resin system used, two different, two-step curing program were determined, and these programmes were as follows:

For specimens, fabricated with Resin System 1 (MY740 / HY918 / DY062):

- Curing at 80°C, for two hours.
- Curing at 120°C, for two hours.

For specimens, fabricated with Resin System 2 (LY556 / HY917 / DY070):

- Curing at 80°C, for four hours.
- Curing at 140°C, for four hours.

After the curing operation, the removal of the mandrel from the specimens was performed. Each specimen was then cut so as to obtain five split-disk test specimens and a tensile test specimen (Figure 2.1). Production details of each specimen, including their dimensions, number of wounded layers and their configurations will be given in Appendix A.

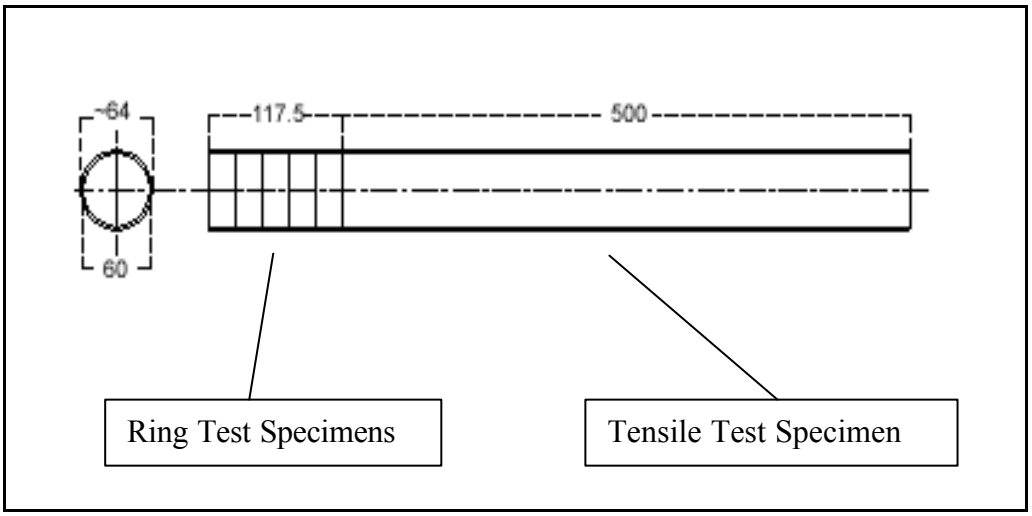

Figure 2.1 Drawing of filament-wound tube and method of cutting.

2.5 Test Specimen Designations

To identify the fiber and resin system, winding angle, and tension setting of each specimen, a specimen number was designated to each specimen. Each number represents a variable in this designation. In Figure 2.2, a schematic representation of this designation is presented. Each number in this designation is determined in correlation with Table 2.6. As an illustration, the third specimen, produced with fiber 1 (PPG glass fiber, 2400 TEX), resin system 2 (LY556 / HY917 / DY070), tension setting 1 (with tension), and winding angle 3 (±45° winding angle), was designated as 1231-3, whereas the

second specimen, produced with fiber 3 (TENAX Carbon Fiber, 800 TEX), resin system 1 (LY556 / HY917 / DY070), tension setting 2 (without tension), and winding angle 1 (0° winding angle), was designated as 3112-2.

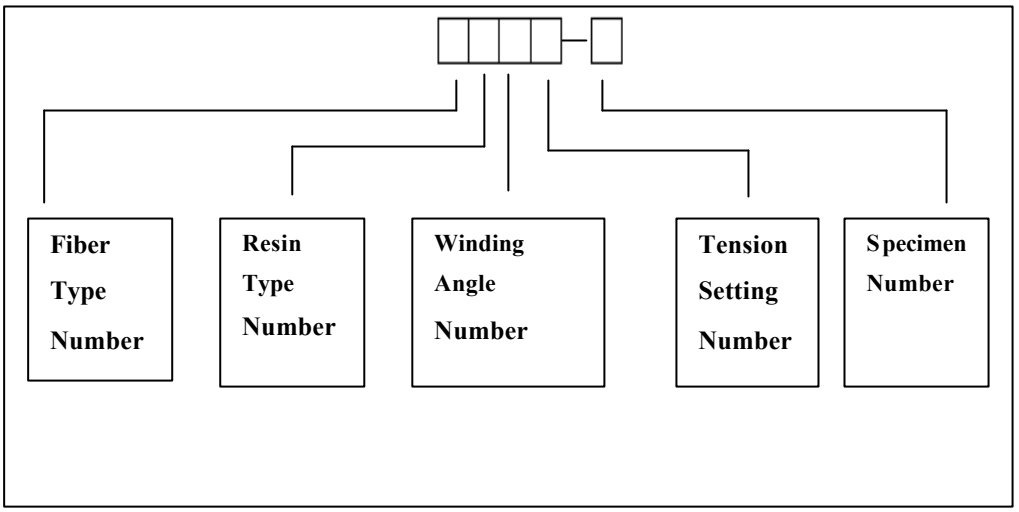

Figure 2.2 Specimen number designation procedure

2.6 Experimental Technique

2.6.1 Split-disk Test

2.6.1.1 Introduction

Determination of hoop tensile properties of filament-wound composite tubular specimens by split disk method is the main objective of this test. The tests were performed according to ASTM D 2290, "Apparent Hoop Tensile Strength of Plastic or Reinforced Plastic Pipe by Split Disk Method" [33]. The standard covers the determination of the comparative apparent tensile strength of most plastic products utilizing a split disk test fixture, when tested under

defined conditions of pre-treatment, temperature, humidity, and test machine speed. The test is also suitable for resin matrix composites reinforced by continuous fibers, and utilizing a split disk test fixture.

Tests were performed with specimens having 0° (unidirectional), ± 25°, ± 45°, ± 65° and 90° (unidirectional) winding angles. Five specimens were tested from each testing group, two of which are tested by the assembling of strain gages, to obtain strain data. Mainly, the ultimate hoop tensile strength and hoop tensile modulus of elasticity of the specimens were determined. In addition, mean average of these results were calculated for each group, and with the aid of this data, the general behavior of the specimens were aimed to be discussed comprehensively.

2.6.1.2 Test Specimen Geometry

Test specimens were full-diameter, full-wall thickness rings, with an inner radius of 60 mm, and an average outer radius of 64 mm. Each specimen involves two sections of reduced area, which were located 180° apart from each other. The specimens were produced free of machining marks, and each were uniform in cross-section. Drawings of specimens are shown in Figure 2.3.

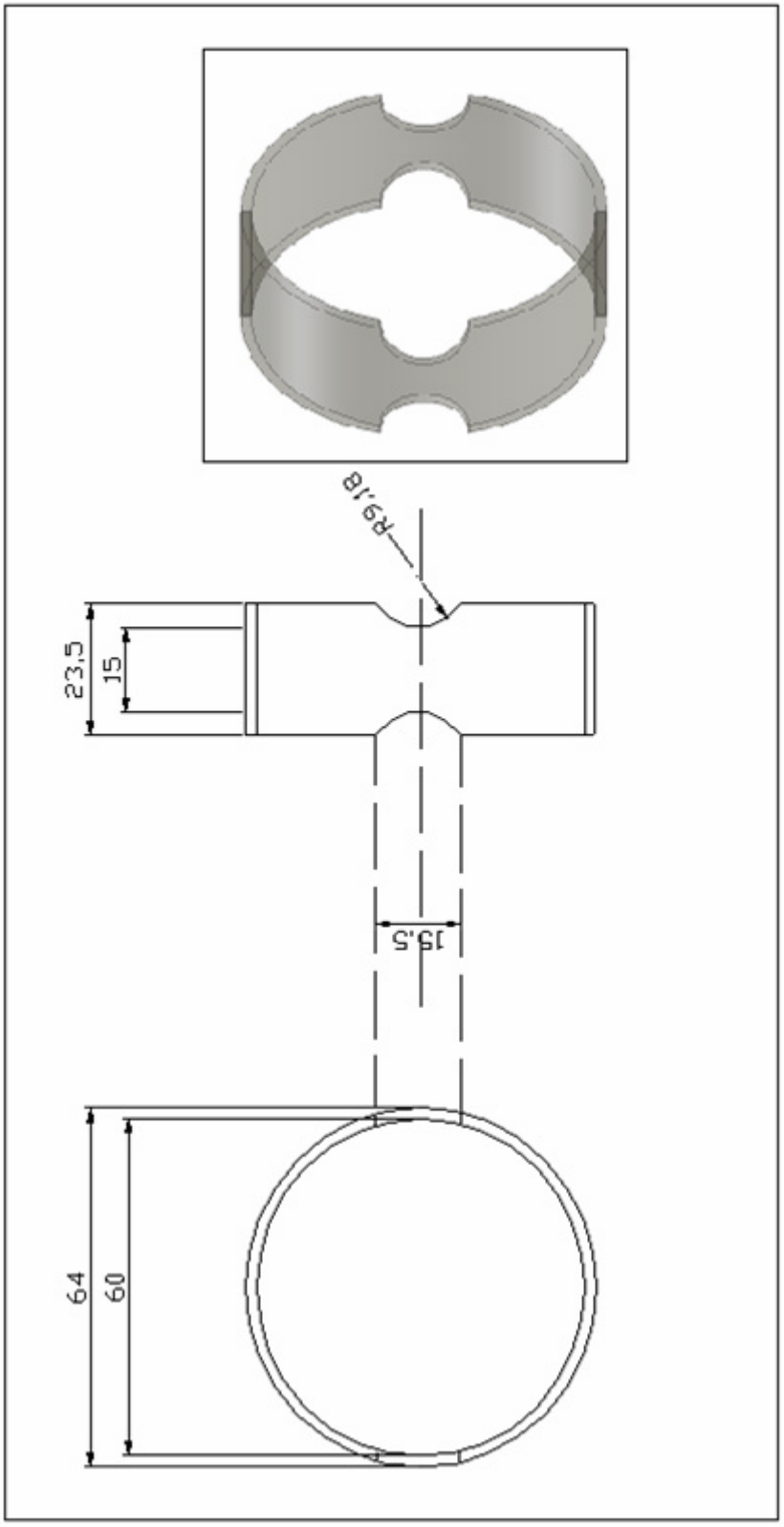

Figure 2.3 Drawing of split disk test specimen

2.6.1.3 Test Equipments

The test fixture involves two half, disk shape components, which were combined to the upper and lower connecting arms of the test fixture, with a mill. Split-disk test specimens were located between the two half disk shape components and the upper and lower connecting arms, with the reduced sections aligned perpendicular to the plane of separation of the two half disk shape components. An apparent tensile strength rather than a true tensile strength can be obtained in the test because of a bending moment imposed during the test at the split between the split disk test fixtures [33]. The test fixture was therefore designed to minimize the effect of this bending moment. The drawing and a photograph of the split-disk test fixture are presented in Figure 2.4 and Figure 2.5, respectively.

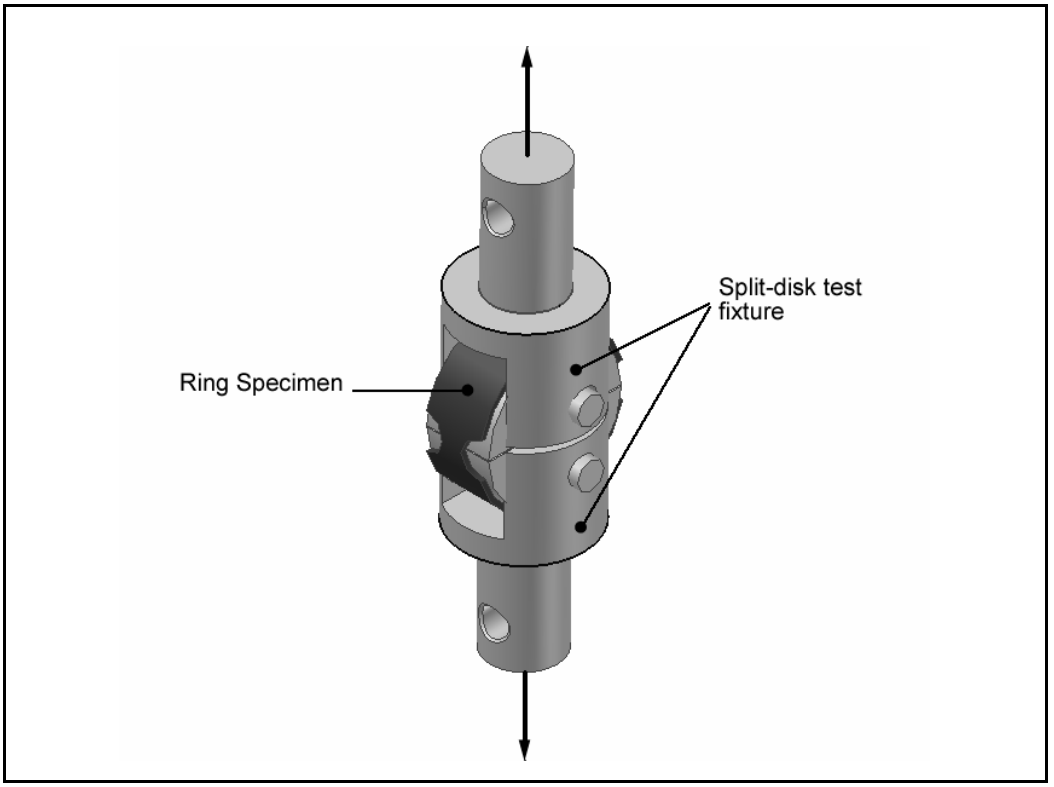

Figure 2.4 Test fixture used in split-disk tests.

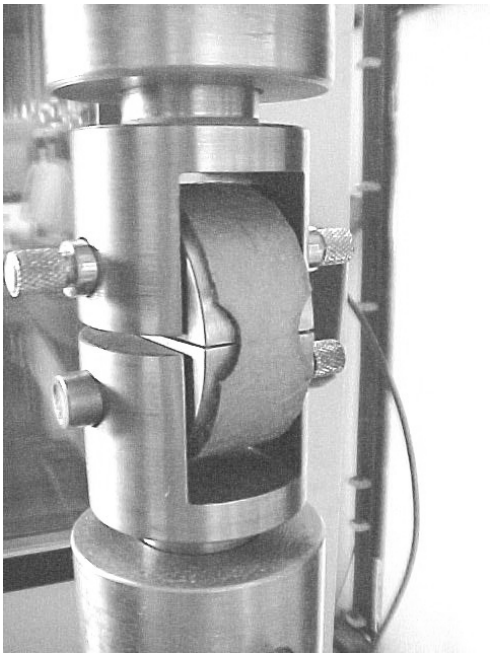

Figure 2.5 Photograph of the split-disk test fixture, assembled on the tensile testing machine.

The apparatus, used in split disk tests were as follows:

- Universal Testing Instrument, INSTRON 4206: for testing metallic and composite materials in either tension or compression. The specifications are; testing capacity of 150 kN (33.750 lbs), crosshead speed range of 0.005 to 500 mm/min with an accuracy of 0.2% over 100 mm, operating temperatures at –150 to 300 °C.
- Split-disk test fixture.
- Load indicator; with an accuracy of ±1 % of reading to 1/50 of load cell capacity.
- Digital calipers
- Data acquisition system
- TML strain gages, type YFLA - 5

The properties of the strain gages, supplied by the manufacturer are given in Table 2.7.

Table 2.7 Properties of the strain gages, used in experiments.

TML Strain Gage – YFLA – 5	
Gage Resistance	120 ± 3 Ω
Gage Factor	2.12
Temperature Compensation Factor	–
Transverse Sensitivity	0.2

2.6.1.4 Test Procedure

The procedure followed during the tests were as follows:

- Reduced section dimensions of the specimens were measured with digital calipers. For each specimen, thickness measurements were made at four places, two of which is from the gage sections. Width of both of the reduced sections was also recorded. Specimen reduced section areas were then calculated by using the minimum thickness and minimum width measurements.

- The specimens were mounted on the split disk test fixture with the reduced sections located at the split in the fixture, taking care to align the test specimen on the split disk specimen holder so that it was centered along the line joining the points of attachment of the fixture to the test machine.

- Speed of testing (velocity of separation of the two members of the testing machine) was set to a constant speed and the test was started.

- Load and strain data were taken until the failure of the specimen.

- For each test group, arithmetic mean of the measured ultimate hoop tensile strength and hoop tensile modulus were calculated and reported as the average value.

- Standard deviations for each group of specimens were calculated.

2.6.1.5 Calculations

The apparent hoop tensile strength of the specimens were calculated by using the following equation:

$$\sigma_{htu} = \frac{P_{max}}{2.A_m} \tag{2.3}$$

where:

σ_{htu} : Ultimate hoop tensile strength, MPa

P_{max} : Maximum load prior to failure, N

A_m : Minimum cross-sectional area of the two reduced sections, d x b, mm^2

Obtained strain and calculated stress data were then used to plot stress – strain graphs of the specimens. These graphs were used so as to obtain the hoop tensile modulus of elasticity of the specimens. For this purpose, slope of the linear portion of the graphs were determined, by fitting a straight line to the linear portion of the graphs, with the least square method. Therefore:

$$E_h = \frac{d\sigma}{d\varepsilon} \qquad (2.4)$$

where:

E_h : Hoop tensile modulus of elasticity, GPa.

$d\sigma / d\varepsilon$: Slope of the linear portion of the stress – strain curve.

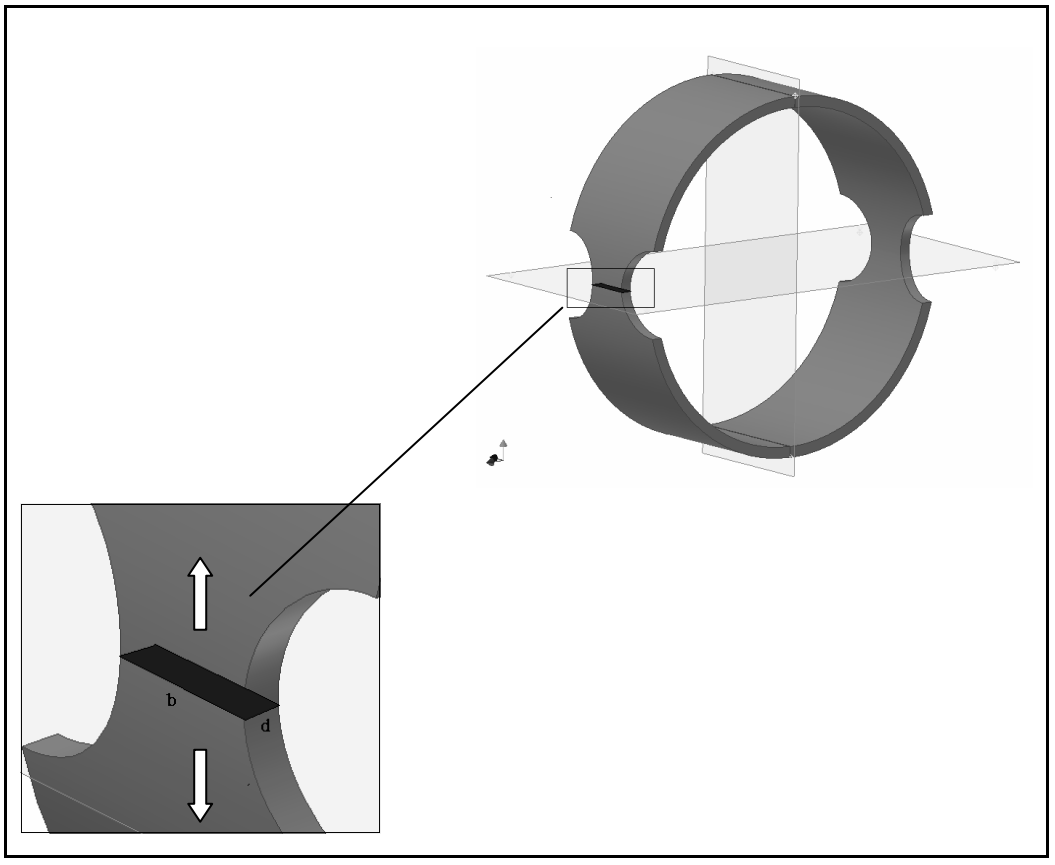

Figure 2.6 Cross-sectional area on which hoop tensile stress is applied.

After calculating hoop tensile strength and hoop tensile modulus of elasticity of each specimen, the arithmetic mean of these results, standard deviations, and coefficient of variations were calculated with the following equations:

$$\bar{X} = \frac{1}{n}.\left(\sum_{i=1}^{n} X_i\right) \tag{2.5}$$

$$S = \sqrt{\frac{\sum_{i=1}^{n} X_i - n.X_i^2}{n-1}} \tag{2.6}$$

$$CV = \left(\frac{S}{\bar{X}}\right)100 \tag{2.7}$$

where:

S : Estimated standard deviation

CV : Sample Coefficient of variation, in percent

$\bar{X}$: Arithmetic mean of the set of observations

X : Value of single observation

n : Number of observations

2.6.2 Tube Tensile Test

2.6.2.1 Introduction

The objective of this test is to determine longitudinal tensile properties of filament-wound composite tubular specimens. The tests were performed according to ASTM D 2105, "Standard Test Method for Longitudinal Tensile Properties of "Fiberglass" (Glass-Fiber-Reinforced Thermosetting-Resin) Pipe and Tube" [34]. The standard covers the determination of the comparative longitudinal tensile properties of fiberglass pipe when tested under defined conditions of pretreatment, temperature, and testing machine speed. The test is also suitable for resin matrix composites reinforced by continuous carbon fibers and PPG fibers.

Under the scope of these tests, specimens, having 90°, ±65°, and ±45° winding angles were tested. Strain gages were assembled on each specimen in longitudinal direction, to obtain strain data. The properties of interest include mainly, the ultimate tensile strength, ultimate tensile strain, and the tensile modulus of elasticity of each specimen. The results of these tests were then evaluated with the results of the coupon tests to investigate the general behavior of the specimens.

2.6.2.2 Test Specimen Geometry

Test specimens were sections of 500 mm length continuous fiber reinforced pipe or tubing, having an inner radius of 60 mm, an average outer radius of 64 mm with a gage length of 450 mm between the grips. The specimens were produced free of machining marks, and each were uniform in cross-section. Geometry of tensile test specimens is presented in Figure 2.7.

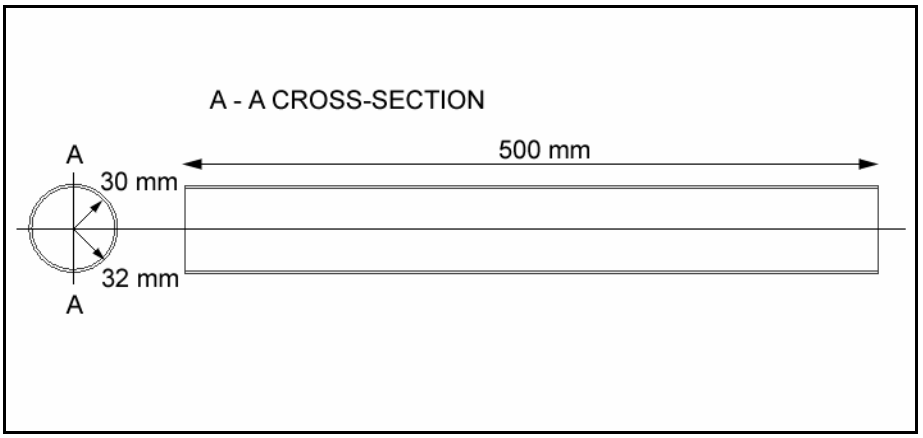

Figure 2.7 Drawing of tensile test specimen

2.6.2.3 Test Equipments

For the tensile test, the design and production of a test fixture was performed. The test fixture involves various components, as shown in Figure 2.8. Design of the fixture is performed so that no crushing load was applied to the pipe and a pure tensile loading is obtained. A photograph of tube tensile test, test set up is presented in Figure 2.9.

To make the strain measurement, a strain gage was assembled on each of the test specimens. Strain gages were assembled on the middle section of the specimens, parallel to the pipe axis to measure the longitudinal tensile strain.

The apparatus, used in tensile tests were as follows:

- Universal Testing Instrument, INSTRON 4206
- Tensile test, test fixture
- Load indicator; with an accuracy of ±1 % of reading to 1/50 of load cell capacity.
- Data acquisition system
- Digital calipers
- TML strain gages, type YFLA - 5

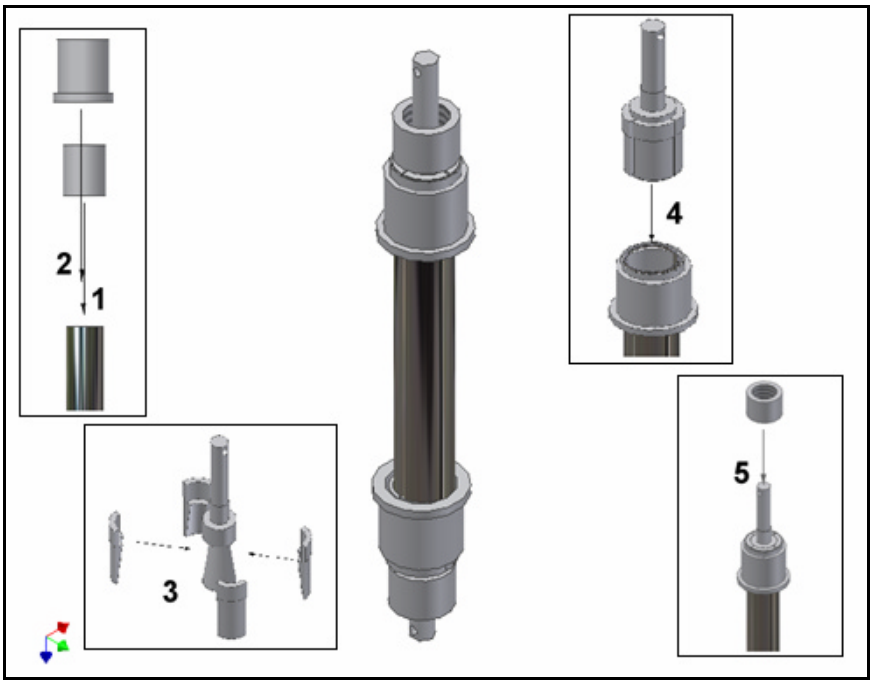

Figure 2.8 Schematic of tensile test fixture.

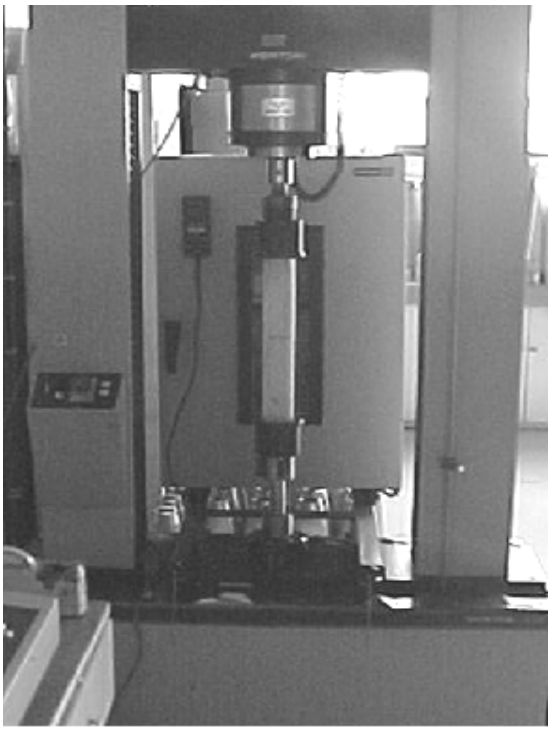

Figure 2.9 Tube tensile test and test setup.

2.6.2.4 Test Procedure

The procedure followed during the tests were as follows:

- A strain gage was assembled on the middle section of each of the specimens, along the pipe axis. Care was taken not to cause a measurement error due to gage misalignment.

- Inner and outer diameters of the specimens were measured from two perpendicular sections of the specimens, by using digital calipers. The cross-sectional area of each tube was then determined by using the average of these measurements.

- The specimens were mounted on the tube tensile test fixture by taking care to align the tube axis parallel to the symmetry axis of upper and lower parts of the fixture.

- Speed of testing (velocity of separation of the two members of the testing machine) was set to a constant speed and the test was started.

- Load and strain data were taken until the failure of the specimen.

2.6.2.5 Calculations

The cross-sectional area of the specimens were calculated with the following equation:

$$A_t = \frac{\pi}{4}(d_{out}{}^2 - d_{in}{}^2) \qquad (2.8)$$

where:

A_t : Average cross-sectional area of tube, mm^2.

d_{out} : Average outer radius of the specimen, mm.

d_{in} : Average inner radius of the specimen, mm.

The axial tensile strength of the specimens were then calculated by using the following equation:

$$\sigma_{ltu} = \frac{P_{max}}{A_t} \tag{2.9}$$

where:

σ_{ltu} : Ultimate longitudinal tensile strength, MPa.

P_{max} : Maximum load prior to failure, N.

Percent elongation of the specimens can be calculated with the following equation:

$$\varepsilon_{ult} = \left(\frac{\Delta l_f}{l_0} \right) 100 \tag{2.10}$$

where:

e_{ult} : Strain to failure, (%).

Δl_f : Extension at the moment of rupture, mm.

l_0 : Original gage length, mm.

Obtained strain and calculated stress data were then used to plot stress – strain graphs of the specimens. These graphs were used so as to obtain the longitudinal tensile modulus of elasticity of the specimens. For this purpose, slope of the linear portion of the graphs were determined, by fitting a straight

line to the linear portion of the graphs, with the least square method. Therefore,

$$E_l = d\sigma / d\varepsilon \tag{2.11}$$

where:

E_l : Longitudinal tensile modulus of elasticity, GPa.

$d\sigma / d\varepsilon$: Slope of the linear portion of the stress – train curve.

CHAPTER 3

MODELING OF SPLIT-DISK TESTS BY FINITE ELEMENT METHOD

3.1 Introduction

This chapter involves the basic theory of simulation of split-disk testing of the selected composite specimens by using the finite element method. "ANSYS Workbench 7.1" finite element program was used for this purpose. Results were obtained for both carbon fiber reinforced and glass fiber reinforced specimens, and having winding angles of 25^o, 45^o, and 65^o. Therefore, a comprehensive discussion of the experimental results with the analysis was performed.

In the next section, basic theoretical aspects of this study will be presented. This will be followed by the specifications of the problem, including the geometrical aspects, element selection, mesh attributes, material data used in the analysis and the boundary conditions, in Section 3.3.

3.2 Theoretical Aspects

3.2.1 Finite Element Method

The finite element method (FEM) is a numerical procedure that can be applied to obtain solutions to a variety of problems in engineering, including steady, transient, linear, or non-linear problems in stress analysis, heat transfer, fluid flow etc. The basic steps involved in any FEM consist of the following steps:

- Creating and discretizing the solution domain into finite elements.
- Assuming an approximate continuous function to represent the solution of an element.
- Developing equations for an element.
- Constructing the global stiffness matrix.
- Applying boundary conditions, initial conditions, and loading.
- Solving a set of linear/non-linear algebraic equations simultaneously to obtain nodal results.
- Postprocessing of the solution, to obtain other necessary data.

3.2.2 Finite Element Modeling of Laminated Composites

As stated in Chapter 1, laminated composites are usually represented by a series of equivalent laminated homogenous plates or shells. This definition necessitates the determination of elastic constants of the composite and the configuration of the lamination. Therefore, different from an isotropic material, only the material properties change when the element stiffness matrices are formed, in finite element modeling of composites.

Laminated thin shell elements, both linear and quadratic, are usually used in modeling of laminated composites. In addition, solid elements can also be preferred. In this study modeling of composite structure with shell elements was performed. Once nodal displacements have been calculated, stresses and strains in individual layers can be recovered and resolved into an appropriate material axes.

3.2.3 Finite Element Analysis of Curved, Thin Walled Structures

A structural shell is a body bounded by two curved surfaces, with the behavior of the shell, being governed by the behavior of an appropriate reference surface. In a shell, the membrane and the bending behavior are coupled. Therefore, the coupled deformations in the form of stretching and curvature change of the reference surface are required in predicting the strains existing throughout the shell space.

When an elastic structure is loaded by some external forces or moments, its potential energy increases. This potential energy is made up of the internal strain energy due to deformation and the potential of the loads that act within the structure or on its surface. By using this principle, and with the aid of Rayleigh – Ritz Method, the element stiffness matrix (K_{EL}) can be given by [35]:

$$K_{EL} = \int_{Vol} [B]^T . [D] . [B] . d(vol) \tag{3.1}$$

where, $[D]$ is the elasticity or elastic stiffness matrix, defined by the equation:

$$\{s\} = [D] . \{e\} \tag{3.2}$$

and, [B] is the strain – displacement matrix, based on the element shape functions, and defined by the equation:

$$\{e\} = [B] . \{u\} \tag{3.3}$$

The remaining terms in the above equations are:

vol : Volume of element.

$\{e\}$: Strain vector

$\{s\}$: Stress vector

$\{u\}$: Nodal displacement vector.

In a two dimensional model, one can write:

$$d(vol) = dt.dA \tag{3.4}$$

where t is the shell thickness and A is the shell surface area. Therefore, Equation (3.5) takes the form:

$$K_{EL} = \int_A \left[\iint_t [B]^T .[D][B] dt \right] dA \tag{3.5}$$

Accordingly, the formulation of two dimensional shell model involves the following steps:

- Definition of coordinate systems. (Different coordinate systems have to be used, including global, nodal, and local coordinate systems).
- Formulation of strain – displacement matrix ([B]).
- Formulation of stress – strain matrix ([D])
- Formulation of element stiffness matrix (K_{EL}), in correlation with Equation 3.5.

3.3 Problem Specifications

3.3.1 Geometry

In Figure 3.1, the model geometry is presented. As seen in the figure, the geometry of the model involves two half, disk-shape volumes and an outer shell, superimposed on the outer surfaces of the inner volumes.

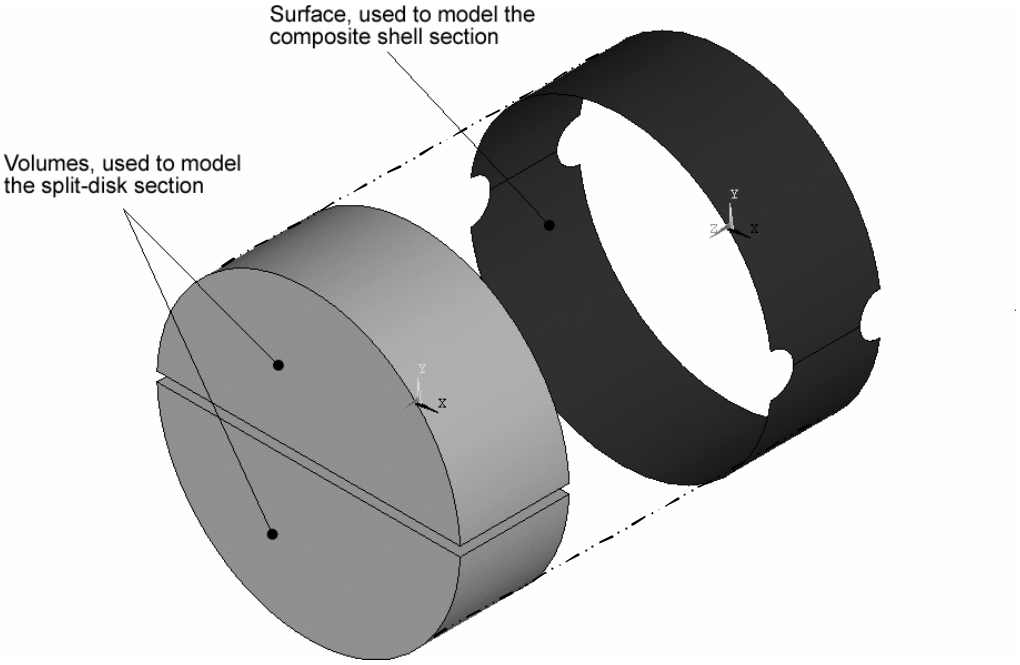

Figure 3.1 The geometry of the model

Due to the orthotropic nature of the composite section and the necessity of simultaneous bidirectional loading of the inner split-disks, modeling of full geometry was preferred in place of half/quarter symmetrical model. To specify the material properties and layer configurations, a local cylindrical coordinate system was defined.

3.3.2 Element Selection

Four element types were used in modeling of split-disk testing of composites. These are SOLID185 3-D 8-node structural solid element (for modeling the split disk test fixture), SHELL99 linear layered structural shell element (for modeling of filament-wound composite specimen), and TARGE170, 3-D target segment - CONTA 174, 3-D, 8-node, surface-to-surface contact elements (for modeling of the contact surface between the composite section and the split-disk test fixture).

3.3.2.1 SOLID185 3-D 8-Node Structural Solid Element

SOLID185 is an 8-node structural solid element, capable for the three-dimensional modeling of solid structures. The element has three degrees of freedom at each node: translations in the nodal x, y, and z directions. The element has plasticity, hyperelasticity, stress stiffening, creep, large deflection, and large strain capabilities. It also has mixed formulation capability for simulating deformations of nearly incompressible elastoplastic materials, and fully incompressible hyperelastic materials.

A schematic view of the element, including its geometry, node locations, and the coordinate system is presented in Figure 3.2. Element is defined by eight nodes and the orthotropic material properties. In this study, these elements's, element coordinate systems was defined in global directions, since the split-disk test fixture material properties are isotropic.

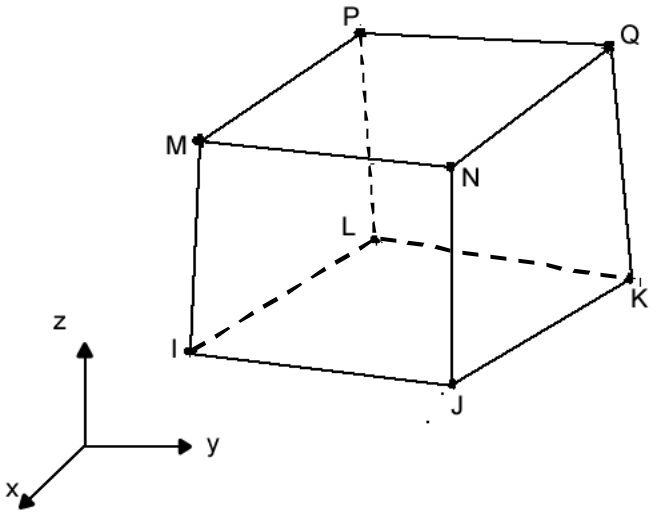

Figure 3.2 Description of SOLID185 structural shell element. [36]

3.3.2.2 SHELL99 Linear Layered Structural Shell Element

SHELL99 is an eight-node structural shell element, capable for layered applications of a structural shell model. The element has six degrees of freedom at each node: translations in the nodal x, y, and z directions and rotations about the nodal x, y, and z-axes. Up to 250 layers can be specified with the usage of this element.

A schematic view of the element, including its geometry, node location and element coordinate system is presented in Figure 3.3. The element is defined by eight nodes, average or corner layer thicknesses, layer material direction angles, and orthotropic material properties.

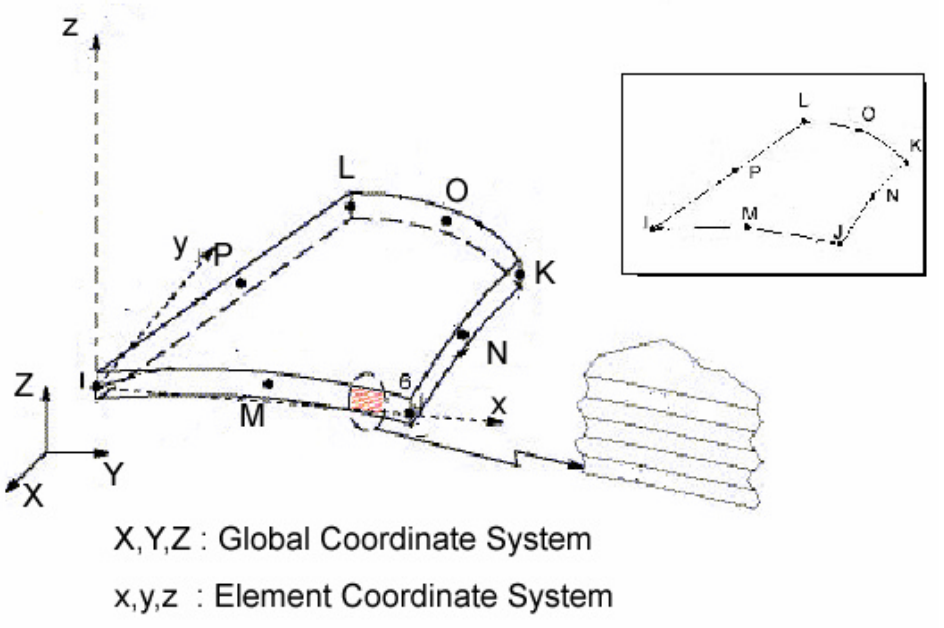

Figure 3.3 Description of SHELL99 structural shell element. [36]

3.3.2.3 TARGE170, 3-D Target Segment - CONTA 174, 3-D, Surface-to-Surface Contact Elements

CONTA 174 is an eight node, surface to surface contact element, which is used to represent contact and sliding between 3-D "target" surfaces and a deformable surface. The element is applicable to three-dimensional structural and coupled thermal-structural contact analysis.

This element can be located on the surfaces of 3-D solids or shell elements with midside nodes. (In this study, it was located on the outer surfaces of the split-disk test fixture). It has the same geometric characteristics as the solid or shell element face with which it is connected. Contact occurs when the element surface penetrates one of the target segment elements (for our case, TARGE170) on a specified target surface. Coulomb and shear stress friction can be allowed.

The geometry and node locations of CONTA174 surface-to-surface contact element is presented in Figure 3.4. The element is defined by eight nodes. It can degenerate to a six node element depending on the shape of the underlying solid or shell elements.

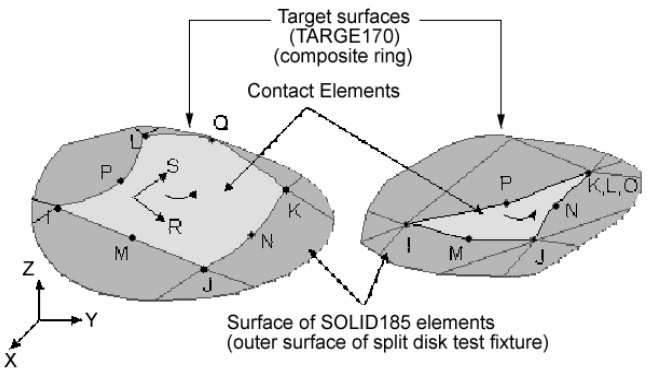

Figure 3.4 Description of CONTA174 3-D surface-to-surface contact element.

In this study, TARGE170, 3-D target segment elements was used to represent the target surfaces for the associated contact elements. These elements are paired with its associated contact surface via a shared real constant set. Any translational or rotational displacement, forces and moments can be imposed on these elements. For rigid target surfaces, these elements can easily model complex target shapes. For flexible targets, these elements will overlay the solid elements describing the boundary of the deformable target body. In this study, these elements were located on the inner surface of the composite ring specimen.

3.3.3 Mesh Attributes

The mesh pattern of the model is presented in Figure 3.5. The composite section was modeled with quadirilateral elements. The mesh pattern of the split-disk section involves only brick type elements, with quadrilateral surfaces.

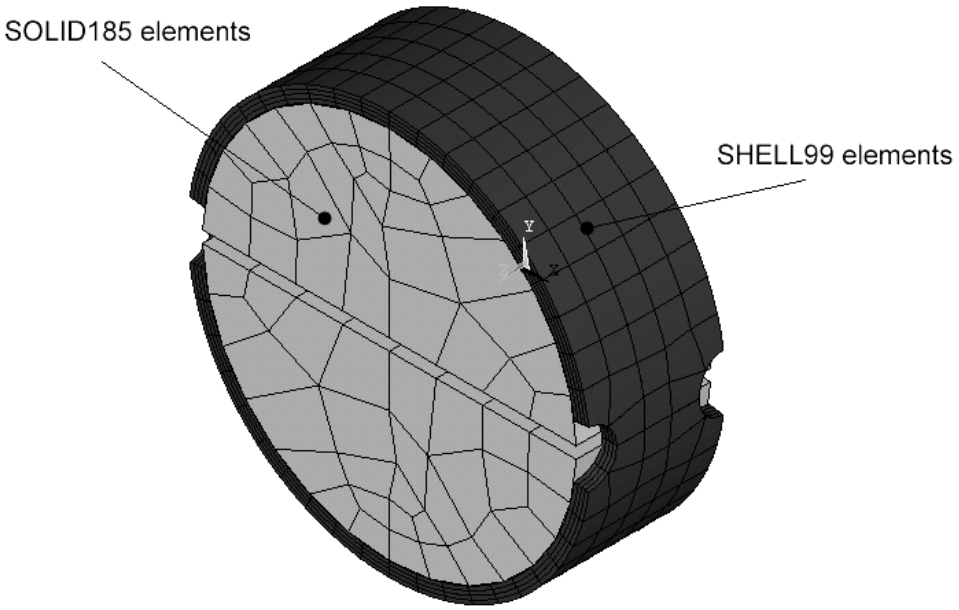

Figure 3.5 Mesh pattern of the split disk section of the model.

3.3.4 Constants and Material Properties

As it is stated in the beginning of this chapter, results were obtained for both carbon fiber reinforced and glass fiber reinforced specimen, having winding angles of 25^o, 45^o, and 65^o. Some part of the necessary data, required to perform the analysis (layer thicknesses, layer configurations, and in-plane stiffness values in primary material coordinates; E_1, E_2) were obtained from real specimens, tested under the scope of the thesis. These specimens' identification numbers and the related data are summarized in Tables 3.1 and 3.2.

Table 3.1 Layer configurations, layer thicknesses and in-plane stiffness (E1, E2) of the specimens, used in the analysis.

Specimen Name	**Layer Configuration**	**Thickness (mm)**	**E_1 (GPa)**	**E_2 (GPa)**
3221	$(\pm 25)_3$	0.350	148.76	8.57
3231	$(\pm 45)_2$	0.213		
3241	$(\pm 65)_4$	0.200		

Table 3.2 Layer configurations, layer thicknesses and in-plane stiffness (E1, E2) of the specimens, used in the analysis.

Specimen Name	**Layer Configuration**	**Thickness (mm)**	**E_1 (GPa)**	**E_2 (GPa)**
1221	$(\pm 25)_2$	0.480	70.02	10.78
1231	$(\pm 45)_2$	0.385		
1241	$(\pm 65)_2$	0.375		

The configurations of layers in the above tables are presented in usual abbreviation, to designate stacking sequence of layers, for multilayered composites. The rest of the necessary data (remaining in – plane elastic properties, and through-thickness elastic constants) for modeling of composite ring section were obtained from [30].

For calculations, referring to inner, steel, split-disk section of the model, isotropic material constants were taken as follows [31]:

E = 207 GPa

υ (Poisson's Ratio) = 0.3

3.3.5 Boundary Conditions

As stated in Section 3.3.1, modeling of full geometry was preferred in place of half/quarter symmetrical model. Therefore no symmetry boundary conditions was used upon modeling of split-disk tests.

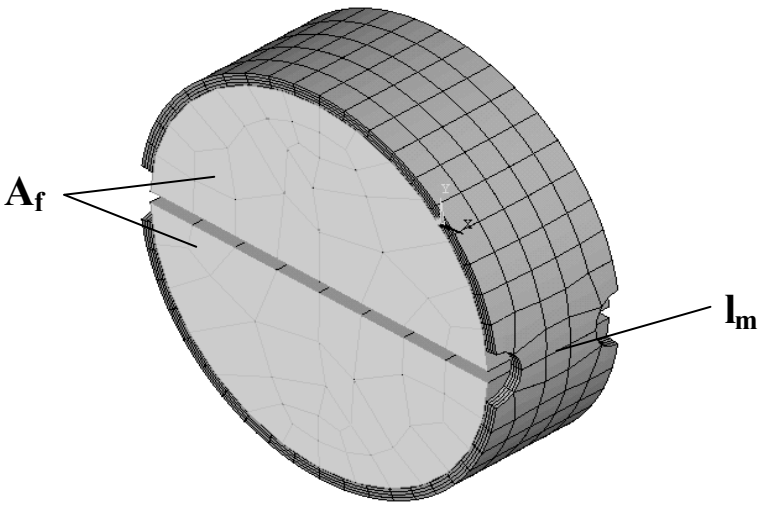

Figure 3.6 The area/line on which the boundary conditions are defined.

The nodes on one face of the inner split-disk section (A_f) was constrained in two transverse directions, perpendicular to the direction of loading (x and z directions), to prevent the motion of the entire model due to the effect of normal-shear coupling (Figure 3.6). In addition, nodes on the line (l_m), located in the middle of the gage section were fixed to prevent the symmetry of the model upon loading.

CHAPTER 4

RESULTS AND DISCUSSIONS

4.1 Introduction

This chapter involves the results and discussion of experimental and simulation studies performed under the scope of the thesis. In the next section, tabulated results of experimental work will be presented. Comprehensive discussions of these results will be given in the following section. In Section 4.4, the results of the simulation study will be given and evaluated with the results of the experimental work.

4.2 Experimental Results

4.2.1 Split-disk Test Results

In correlation with ASTM D 2290, load and strain data were taken until the failure of the specimens. In addition, failure types and their locations on the specimens were also recorded. These data were used so as to calculate the hoop tensile strength of the specimens, and at the same time, converted into stress – strain graphs, as stated in Section 2.4.1.5. These graphs were then used in determination of hoop tensile modulus of elasticity of the specimens. For this purpose, the slope of the linear portion of these curves was determined by fitting a straight line, with the least-square method. These graphs were plotted in Microsoft Excel Program. By using the equations stated in Section 2.4.1.5, arithmetic mean of the measured ultimate hoop tensile strength and hoop

tensile modulus, standard deviation, and percent coefficient of variation were calculated for each testing groups.

In Tables 4.1 through 4.12, the tabulated strength results of split-disk test specimens are presented. In the first column of the tables, the specimen designation numbers are tabulated. Second and third columns involve the maximum load, and the calculated apparent composite hoop tensile strength of each specimen. In the next three columns, the mean average tensile strength of each testing group (including five specimens for a single group), their standard deviation, and their percent sample coefficient of variation are tabulated respectively.

Table 4.1 Hoop tensile strength results of split-disk tests and the related statistical results for specimens 1111-1 through 1132-5.

Specimen Designation	P_{max} (N)	s_{htu} (Mpa)	$s_{htu}^{(average)}$ (MPa)	Standard Deviation	CV (%)
1111-1	260.4	8.9	**11.56**	**2.52**	**21.81**
1111-2	252.7	8.9			
1111-3	402.5	14.5			
1111-4	364.3	12.7			
1111-5	375.2	12.8			
1121-1	2017	37.8	**36.54**	**1.55**	**4.25**
1121-2	2013	37.5			
1121-3	2131	36.8			
1121-4	1997	33.9			
1121-5	2044	36.6			
1131-1	7671	169.2	**152.02**	**11.69**	**7.69**
1131-2	7332	148.4			
1131-3	7146	158.1			
1131-4	6258	144.3			
1131-5	6937	140.1			
1141-1	25470	566.3	**584.30**	**36.47**	**6.24**
1141-2	24820	556.6			
1141-3	27330	634.2			
1141-4	25840	611.6			
1141-5	24150	552.8			
1151-1	35010	805.8	**788.82**	**24.17**	**3.06**
1151-2	35140	768.2			
1151-3	35180	780.2			
1151-4	37070	822.1			
1151-5	35120	767.8			
1112-1	254.7	8.8	**11.46**	**2.42**	**21.15**
1112-2	252.7	8.9			
1112-3	388.2	13.9			
1112-4	364.3	12.7			
1112-5	381.2	13			
1122-1	2399	45.5	**41.62**	**3.07**	**7.39**
1122-2	2317	44.3			
1122-3	2119	39.1			
1122-4	2241	40.4			
1122-5	2103	38.9			
1132-1	7802	169.5	**159.26**	**14.60**	**9.17**
1132-2	7707	178.9			
1132-3	6704	155.6			
1132-4	6827	147.7			
1132-5	6669	144.6			

Table 4.2 Hoop tensile strength results of split-disk tests and the related statistical results for specimens 1142-1 through 1222-5.

Specimen Designation	P_{max} (N)	s_{htu} (MPa)	$s_{htu}^{(average)}$ (MPa)	Standard Deviation	CV (%)
1142-1	25490	563.0	**588.54**	**50.61**	**8.60**
1142-2	26530	638.6			
1142-3	26010	601.7			
1142-4	22610	514.0			
1142-5	25730	625.4			
1152-1	37170	863.6	**835.60**	**30.82**	**3.69**
1152-2	34450	794.4			
1152-3	37830	864.2			
1152-4	36520	841.7			
1152-5	36920	814.1			
1211-1	1689	39.1	**37.96**	**1.97**	**5.19**
1211-2	1685	34.8			
1211-3	1890	39.6			
1211-4	1756	39.0			
1211-5	1634	37.4			
1221-1	2017	37.8	**36.54**	**1.55**	**4.25**
1221-2	2013	37.5			
1221-3	2131	36.8			
1221-4	1997	33.9			
1221-5	2044	36.6			
1231-1	5446	124.4	**150.74**	**15.30**	**10.15**
1231-2	7415	158.8			
1231-3	7446	157.2			
1231-4	7087	162.4			
1231-5	7068	150.9			
1241-1	25530	566.0	**582.36**	**34.54**	**5.93**
1241-2	26580	591.2			
1241-3	25750	608.6			
1241-4	27470	615.2			
1241-5	22970	530.8			
1251-1	37520	813.0	**809.36**	**55.04**	**6.80**
1251-2	38180	826.5			
1251-3	34990	738.7			
1251-4	40010	887.1			
1251-5	36410	781.5			
1212-1	98.59	3.5	**4.03**	**0.61**	**15.01**
1212-2	145.9	4.9			
1212-3	95.25	3.5			
1212-4	121.2	4.4			
1212-5	102.7	3.9			
1222-1	1831	38.7	**36.95**	**1.20**	**3.24**
1222-2	1791	35.3			
1222-3	1756	37.3			
1222-4	1922	36.9			
1222-5	1890	36.7			

Table 4.3 Hoop tensile strength results of split-disk tests and the related statistical results for specimens 1232-1 through 2112-5.

Specimen Designation	P_{max} (N)	S_{htu} (MPa)	$S_{htu}^{(average)}$ (MPa)	Standard Deviation	CV (%)
1232-1	7471	155.9	**156.88**	**8.06**	**5.14**
1232-2	7277	157.6			
1232-3	7529	164.5			
1232-4	6791	143.9			
1232-5	7652	162.5			
1242-1	25980	581.3	**618.42**	**31.97**	**5.17**
1242-2	26860	616.5			
1242-3	29340	669.4			
1242-4	26840	608.2			
1242-5	26740	616.7			
1252-1	37170	863.6	**835.60**	**30.82**	**3.69**
1252-2	34450	794.4			
1252-3	37830	864.2			
1252-4	36520	841.7			
1252-5	36920	814.1			
2111-1	276	10.8	**9.65**	**0.88**	**9.15**
2111-2	193	10.2			
2111-3	185	8.8			
2111-4	233	9.6			
2111-5	185	8.8			
2121-1	1673	29.2	**28.44**	**1.25**	**4.41**
2121-2	1555	27.6			
2121-3	1669	30.1			
2121-4	1559	26.9			
2121-5	1622	28.4			
2131-1	7229	136.9	**146.94**	**9.68**	**6.59**
2131-2	7853	160.5			
2131-3	7734	144.4			
2131-4	7829	152.9			
2131-5	6945	140.0			
2141-1	20940	443.0	**482.10**	**37.96**	**7.87**
2141-2	21100	454.1			
2141-3	25000	522.4			
2141-4	22400	468.4			
2141-5	24870	522.6			
2151-1	35610	788.5	**742.84**	**38.11**	**5.13**
2151-2	33450	701.3			
2151-3	35530	776.3			
2151-4	33620	714.7			
2151-5	34110	733.4			
2112-1	276	10.8	**9.65**	**0.88**	**9.15**
2112-2	193	10.2			
2112-3	185	8.8			
2112-4	233	9.6			
2112-5	185	8.8			

Table 4.4 Hoop tensile strength results of split-disk tests and the related statistical results for specimens 2122-1 through 2251-5.

Specimen Designation	P_{max} (N)	S_{htu} (MPa)	$S_{htu}^{(average)}$ (MPa)	Standard Deviation	CV (%)
2122-1	2147	34.6	**34.73**	**2.50**	**7.20**
2122-2	2036	31.5			
2122-3	2155	34.2			
2122-4	2175	34.8			
2122-5	2395	38.5			
2132-1	7703	152.2	**141.18**	**13.25**	**9.39**
2132-2	7644	147.8			
2132-3	7150	140.0			
2132-4	6227	118.8			
2132-5	7403	147.1			
2142-1	22770	475.0	**482.36**	**21.29**	**4.41**
2142-2	23590	485.2			
2142-3	22500	494.0			
2142-4	22680	507.0			
2142-5	22300	450.6			
2152-1	35340	732.0	**720.34**	**11.92**	**1.65**
2152-2	34810	725.4			
2152-3	34110	710.3			
2152-4	35460	705.1			
2152-5	35440	728.9			
2211-1	276	10.8	**9.65**	**0.88**	**9.15**
2211-2	193	10.2			
2211-3	185	8.8			
2211-4	233	9.6			
2211-5	185	8.8			
2221-1	2017	34.8	**32.47**	**1.69**	**5.21**
2221-2	1875	30.4			
2221-3	1819	31.3			
2221-4	1827	32.7			
2221-5	1910	33.1			
2231-1	8180	162.2	**148.02**	**12.76**	**8.62**
2231-2	8047	145.1			
2231-3	7853	147.5			
2231-4	6850	128.8			
2231-5	8310	156.5			
2241-1	17510	501.6	**517.94**	**48.39**	**9.34**
2241-2	19690	597.8			
2241-3	16940	469.8			
2241-4	18350	522.2			
2241-5	18810	498.3			
2251-1	34210	730.3	**706.72**	**24.06**	**3.40**
2251-2	35040	700.7			
2251-3	33140	670.0			
2251-4	36310	726.1			
2251-5	34710	706.5			

Table 4.5 Hoop tensile strength results of split-disk tests and the related statistical results for specimens 2212-1 through 3141-5.

Specimen Designation	P_{max} (N)	S_{htu} (MPa)	$S_{htu}^{(average)}$ (MPa)	Standard Deviation	CV (%)
2212-1	276	10.8	**9.65**	**0.88**	**9.15**
2212-2	193	10.2			
2212-3	185	8.8			
2212-4	233	9.6			
2212-5	185	8.8			
2222-1	2179	35.8	**33.66**	**1.24**	**3.68**
2222-2	1981	33.2			
2222-3	2009	33.4			
2222-4	2009	32.9			
2222-5	1993	32.9			
2232-1	8544	174.7	**155.48**	**13.41**	**8.62**
2232-2	7411	143.2			
2232-3	8125	147.3			
2232-4	8752	164.2			
2232-5	7715	148.0			
2242-1	23290	484.4	**481.60**	**36.16**	**7.51**
2242-2	22420	496.8			
2242-3	20710	430.0			
2242-4	22850	528.1			
2242-5	22520	468.7			
2252-1	32830	699.6	**701.94**	**6.56**	**0.93**
2252-2	34910	693.6			
2252-3	34130	710.3			
2252-4	34550	699.6			
2252-5	34770	706.6			
3111-1	205.1	6.5	**4.61**	**0.55**	**11.94**
3111-2	272.2	7.8			
3111-3	39.4	1.3			
3111-4	31.56	0.9			
3111-5	205.6	6.5			
3121-1	2005	39.7	**39.46**	**2.30**	**5.83**
3121-2	2159	43.1			
3121-3	1922	39.4			
3121-4	1965	38.0			
3121-5	1910	37.1			
3131-1	6231	165.3	**156.80**	**8.28**	**5.28**
3131-2	6429	163.9			
3131-3	6437	158.2			
3131-4	5860	149.9			
3131-5	5615	146.7			
3141-1	32690	717.2	**667.92**	**44.22**	**6.62**
3141-2	29750	681.1			
3141-3	29340	607.7			
3141-4	30140	638.6			
3141-5	30980	695.0			

Table 4.6 Hoop tensile strength results of split-disk tests and the related statistical results for specimens 3151-1 through 3221-5.

Specimen Designation	P_{max} (N)	S_{htu} (MPa)	$S_{htu}^{(average)}$ (MPa)	Standard Deviation	CV (%)
3151-1	42330	1224.0	**1187.40**	**89.21**	**7.51**
3151-2	39190	1080.0			
3151-3	39090	1109.0			
3151-4	44550	1291.0			
3151-5	42110	1233.0			
3112-1	205.1	6.5	**4.61**	**0.58**	**12.59**
3112-2	272.2	7.8			
3112-3	39.4	1.3			
3112-4	31.56	0.9			
3112-5	205.6	6.5			
3122-1	1855	41.0	**39.91**	**2.46**	**6.16**
3122-2	1842	37.6			
3122-3	1756	37.6			
3122-4	1953	43.4			
3122-5	1871	40.1			
3132-1	6930	160.9	**172.48**	**8.16**	**4.73**
3132-2	7155	173.8			
3132-3	6764	173.4			
3132-4	6850	170.6			
3132-5	6886	183.7			
3142-1	30570	733.5	**691.84**	**44.24**	**6.39**
3142-2	30030	694.4			
3142-3	34350	734.8			
3142-4	28970	663.1			
3142-5	29340	633.4			
3152-1	48130	1372.0	**1201.20**	**103.72**	**8.63**
3152-2	42310	1212.0			
3152-3	39290	1105.0			
3152-4	39880	1138.0			
3152-5	40940	1179.0			
3211-1	205.1	6.5	**4.61**	**0.74**	**16.07**
3211-2	272.2	7.8			
3211-3	39.4	1.3			
3211-4	31.56	0.9			
3211-5	205.6	6.5			
3221-1	1634	34.1	**34.79**	**2.78**	**8.00**
3221-2	1914	37.4			
3221-3	1748	37.8			
3221-4	1591	33.4			
3221-5	1507	31.2			

Table 4.7 Hoop tensile strength results of split-disk tests and the related statistical results for specimens 3231-1 through 3252-5.

Specimen Designation	P_{max} (N)	S_{htu} (MPa)	$S_{htu}^{(average)}$ (MPa)	Standard Deviation	CV (%)
3231-1	6295	151.7	**153.26**	**4.80**	**3.13**
3231-2	6587	157.1			
3231-3	6104	145.9			
3231-4	6247	153.8			
3231-5	6283	157.8			
3241-1	32650	638.8	**627.46**	**22.32**	**3.56**
3241-2	31510	654.8			
3241-3	32160	620.9			
3241-4	30220	594.7			
3241-5	31210	628.1			
3251-1	40670	1128.0	**1157.60**	**30.13**	**2.60**
3251-2	42440	1167.0			
3251-3	40790	1157.0			
3251-4	42700	1203.0			
3251-5	41060	1133.0			
3212-1	205.1	6.5	**4.61**	**0.65**	**14.11**
3212-2	272.2	7.8			
3212-3	39.4	1.3			
3212-4	31.56	0.9			
3212-5	205.6	6.5			
3222-1	2115	41.4	**41.68**	**1.97**	**4.73**
3222-2	2029	43.6			
3222-3	1926	42.2			
3222-4	1879	38.5			
3222-5	1910	42.8			
3232-1	6815	155.9	**150.10**	**13.12**	**8.74**
3232-2	6192	148.0			
3232-3	6756	167.9			
3232-4	5454	132.2			
3232-5	6665	146.5			
3242-1	29690	598.7	**623.36**	**56.64**	**9.09**
3242-2	32180	659.0			
3242-3	32810	694.6			
3242-4	27210	546.9			
3242-5	28990	617.6			
3252-1	44900	1289.0	**1185.20**	**92.93**	**7.84**
3252-2	40650	1104.0			
3252-3	42560	1266.0			
3252-4	40870	1185.0			
3252-5	38360	1082.0			

Table 4.8 Hoop tensile strength results of split-disk tests and the related statistical results for specimens 4111-1 through 4132-5.

Specimen Designation	P_{max} (N)	S_{htu} (MPa)	$S_{htu}^{(average)}$ (MPa)	Standard Deviation	CV (%)
4111-1	165.7	5.5	**5.86**	**0.52**	**8.88**
4111-2	43.32	1.5			
4111-3	248.5	8.9			
4111-4	59.19	2.1			
4111-5	319.6	11.2			
4121-1	2190	50.6	**50.36**	**1.40**	**2.78**
4121-2	2182	51.3			
4121-3	2005	48.1			
4121-4	2159	50.1			
4121-5	2147	51.7			
4131-1	7825	193.0	**200.96**	**4.79**	**2.38**
4131-2	7928	201.0			
4131-3	8263	202.3			
4131-4	8236	205.8			
4131-5	8310	202.7			
4141-1	21950	487.3	**496.34**	**30.39**	**6.12**
4141-2	20650	466.0			
4141-3	23800	501.5			
4141-4	23540	545.7			
4141-5	22170	481.2			
4151-1	30330	747.5	**778.70**	**24.51**	**3.15**
4151-2	30700	797.2			
4151-3	30290	765.3			
4151-4	30900	774.9			
4151-5	31450	808.6			
4112-1	165.7	5.5	**5.86**	**0.87**	**14.85**
4112-2	43.32	1.5			
4112-3	248.5	8.9			
4112-4	59.19	2.1			
4112-5	319.6	11.2			
4122-1	2280	52.7	**50.82**	**2.50**	**4.91**
4122-2	2198	51.9			
4122-3	2099	47.0			
4122-4	2269	52.8			
4122-5	2222	49.6			
4132-1	7703	196.3	**205.18**	**6.23**	**3.04**
4132-2	8279	203.1			
4132-3	8236	204.9			
4132-4	8417	208.7			
4132-5	8437	212.9			

Table 4.9 Hoop tensile strength results of split-disk tests and the related statistical results for specimens 4142-1 through 4212-5.

Specimen Designation	P_{max} (N)	S_{htu} (MPa)	$S_{htu}^{(average)}$ (MPa)	Standard Deviation	CV (%)
4142-1	16560	452.7	**554.08**	**83.57**	**15.08**
4142-2	16530	483.5			
4142-3	21120	651.6			
4142-4	19680	605.4			
4142-5	19930	577.2			
4152-1	31890	880.1	**895.22**	**32.20**	**3.60**
4152-2	32030	846.7			
4152-3	33140	927.8			
4152-4	33430	914			
4152-5	33530	907.5			
4211-1	165.7	5.5	**5.86**	**0.92**	**15.70**
4211-2	43.32	1.5			
4211-3	248.5	8.9			
4211-4	59.19	2.1			
4211-5	319.6	11.2			
4221-1	1827	41.89	**42.99**	**1.64**	**3.81**
4221-2	1705	41.31			
4221-3	1851	43.25			
4221-4	1847	42.92			
4221-5	1930	45.56			
4231-1	7668	201.3	**198.14**	**5.13**	**2.59**
4231-2	7802	193.3			
4231-3	7691	196.2			
4231-4	7502	194.4			
4231-5	8094	205.5			
4241-1	20060	601.5	**594.05**	**24.60**	**4.14**
4241-2	19330	552.5			
4241-3	20170	613.3			
4241-4	20280	610.3			
4241-5	20410	592.7			
4251-1	33700	890.6	**862.92**	**55.99**	**6.49**
4251-2	32670	894.1			
4251-3	30570	768.1			
4251-4	33760	905.0			
4251-5	32320	856.8			
4212-1	165.7	5.5	**5.86**	**4.22**	**72.03**
4212-2	43.32	1.5			
4212-3	248.5	8.9			
4212-4	59.19	2.1			
4212-5	319.6	11.2			

Table 4.10 Hoop tensile strength results of split-disk tests and the related statistical results for specimens 4222-1 through 5141-5.

Specimen Designation	P_{max} (N)	S_{htu} (MPa)	$S_{htu}^{(average)}$ (MPa)	Standard Deviation	CV (%)
4222-1	1930	45.0	**42.49**	**2.73**	**6.43**
4222-2	1875	44.1			
4222-3	1772	40.5			
4222-4	1752	38.7			
4222-5	1902	44.1			
4232-1	18550	502.4	**565.24**	**51.19**	**9.06**
4232-2	18100	522.5			
4232-3	21170	575.3			
4232-4	21020	608.4			
4232-5	21120	617.6			
4242-1	20060	601.5	**594.05**	**24.60**	**4.14**
4242-2	19330	552.5			
4242-3	20170	613.3			
4242-4	20280	610.3			
4242-5	20410	592.7			
4252-1	33100	942.2	**880.12**	**45.23**	**5.14**
4252-2	29890	814.4			
4252-3	31810	879.2			
4252-4	32340	882.3			
4252-5	33310	882.5			
5111-1	67.03	1.5	**1.46**	**0.14**	**9.62**
5111-2	42.65	1.1			
5111-3	63.21	1.5			
5111-4	41.17	1.1			
5111-5	94.67	2.1			
5121-1	1867	38.7	**38.75**	**0.41**	**1.06**
5121-2	1871	39.3			
5121-3	1760	38.3			
5121-4	1772	39.1			
5121-5	1737	38.4			
5131-1	5228	132.0	**142.94**	**13.89**	**9.71**
5131-2	5608	156.2			
5131-3	6101	159.3			
5131-4	5505	137.7			
5131-5	5477	129.5			
5141-1	40870	734.4	**656.30**	**61.11**	**9.31**
5141-2	31530	571.6			
5141-3	39860	691.0			
5141-4	36640	636.5			
5141-5	36600	648.0			

Table 4.11 Hoop tensile strength results of split-disk tests and the related statistical results for specimens 5151-1 through 5221-5.

Specimen Designation	P_{max} (N)	S_{htu} (MPa)	$S_{htu}^{(average)}$ (MPa)	Standard Deviation	CV (%)
5151-1	49940	1053.0	**1009.62**	**41.10**	**4.07**
5151-2	45780	946.1			
5151-3	49260	1038.0			
5151-4	46820	1006.0			
5151-5	46050	1005.0			
5112-1	580.1	16.4	**10.36**	**1.54**	**14.86**
5112-2	370.9	9.4			
5112-3	430.1	10.3			
5112-4	370.9	9.5			
5112-5	240.7	6.2			
5122-1	1748	34.6	**40.57**	**3.49**	**8.61**
5122-2	1918	43.5			
5122-3	1788	41.2			
5122-4	1883	41.1			
5122-5	1851	42.5			
5132-1	5430	142.9	**145.04**	**6.92**	**4.77**
5132-2	5481	152.9			
5132-3	5055	134.5			
5132-4	5074	146.4			
5132-5	5465	148.5			
5142-1	34390	577.6	**616.08**	**34.11**	**5.54**
5142-2	36150	607.6			
5142-3	35100	594.9			
5142-4	38220	663.0			
5142-5	37390	637.3			
5152-1	48380	1010.0	**1014.20**	**19.37**	**1.91**
5152-2	49880	1029.0			
5152-3	49320	1039.0			
5152-4	48440	999.9			
5152-5	47950	993.1			
5211-1	67.03	1.5	**1.85**	**0.33**	**17.69**
5211-2	87.87	2.1			
5211-3	90.75	2.1			
5211-4	90.45	2.1			
5211-5	69.27	1.5			
5221-1	193.4	6.4	**6.76**	**0.65**	**9.59**
5221-2	197.3	7.1			
5221-3	196.2	7.1			
5221-4	178.45	5.8			
5221-5	203.25	7.4			

Table 4.12 Hoop tensile strength results of split-disk tests and the related statistical results for specimens 5231-1 through 5252-5.

Specimen Designation	P_{max} (N)	S_{htu} (MPa)	$S_{htu}^{(average)}$ (MPa)	Standard Deviation	CV (%)
5231-1	5670	139.1	**138.24**	**6.90**	**4.99**
5231-2	5615	143.5			
5231-3	5224	127.4			
5231-4	5592	136.5			
5231-5	5746	144.7			
5241-1	35200	628.9	**616.44**	**44.47**	**7.21**
5241-2	31790	548.7			
5241-3	36310	656.9			
5241-4	33900	597.2			
5241-5	35260	650.5			
5251-1	50970	1093.0	**1033.38**	**60.55**	**5.86**
5251-2	48380	1004.0			
5251-3	52110	1102.0			
5251-4	49300	965.9			
5251-5	50080	1002.0			
5212-1	220.9	5.3	**4.12**	**0.48**	**11.66**
5212-2	165.7	3.8			
5212-3	90.75	2.1			
5212-4	193.4	4.3			
5212-5	224.9	5.0			
5222-1	1673	35.6	**34.73**	**2.46**	**7.08**
5222-2	1709	38.6			
5222-3	1559	33.9			
5222-4	1452	32.7			
5222-5	1546	32.9			
5232-1	3591	88.9	**107.18**	**12.62**	**11.77**
5232-2	4657	121.7			
5232-3	4321	108.9			
5232-4	4250	101.6			
5232-5	4601	114.8			
5242-1	36510	613.7	**645.34**	**31.77**	**4.92**
5242-2	37830	650.9			
5242-3	38220	652.8			
5242-4	34020	617.4			
5242-5	39860	691.9			
5252-1	47280	970.6	**964.46**	**51.37**	**5.33**
5252-2	48230	995.5			
5252-3	50330	1003.0			
5252-4	48890	977.6			
5252-5	44590	875.6			

In Figures 4.1 and 4.3, stress-strain curves of two split-disk test specimens (1251 – 1, 1251 – 2) are presented as an illustration. As seen in the figures, the stress-strain graphs of the split-disk test specimens involve an initial decrease in strain, followed by a linear increase in both stress and strain. This unusual behavior (sharp decrease in strain) was observed in split-disk tests due to the effect of a bending moment, imposed during test at the split, between the split-disk test fixtures. This moment was induced by the change in contour of the rings between the two disk sections as they separate [33]. Due to this reason, an effective hoop tensile modulus of elasticity was obtained for each specimen, by fitting a line to the linear region of the stress-strain graphs. This is illustrated in Figures 4.2 and 4.4, which involve the least-square fitted lines and their equations for the specimens 1251–1, and 1251–2, respectively.

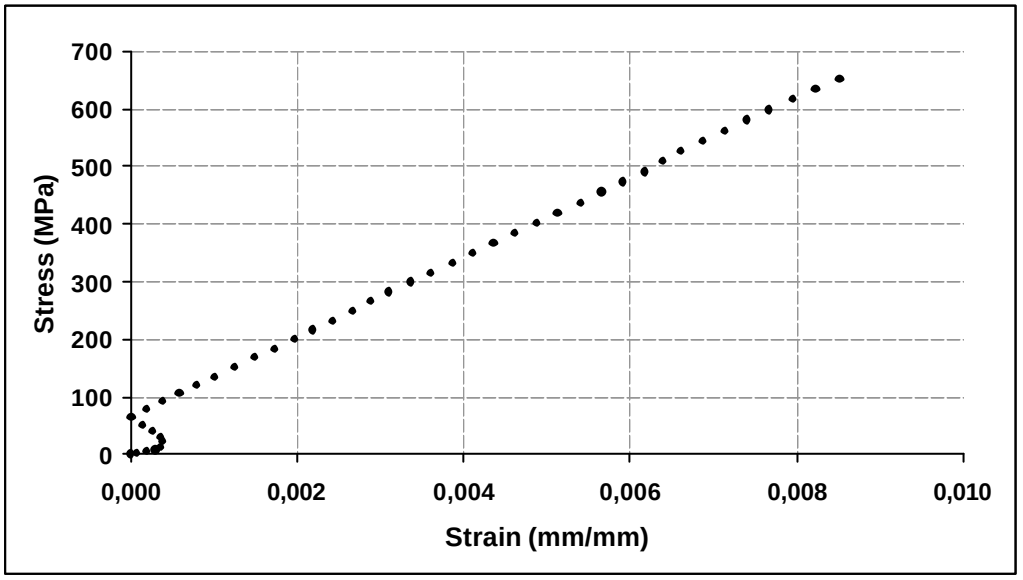

Figure 4.1 Stress – strain curve of 1251-1 split-disk test specimen.

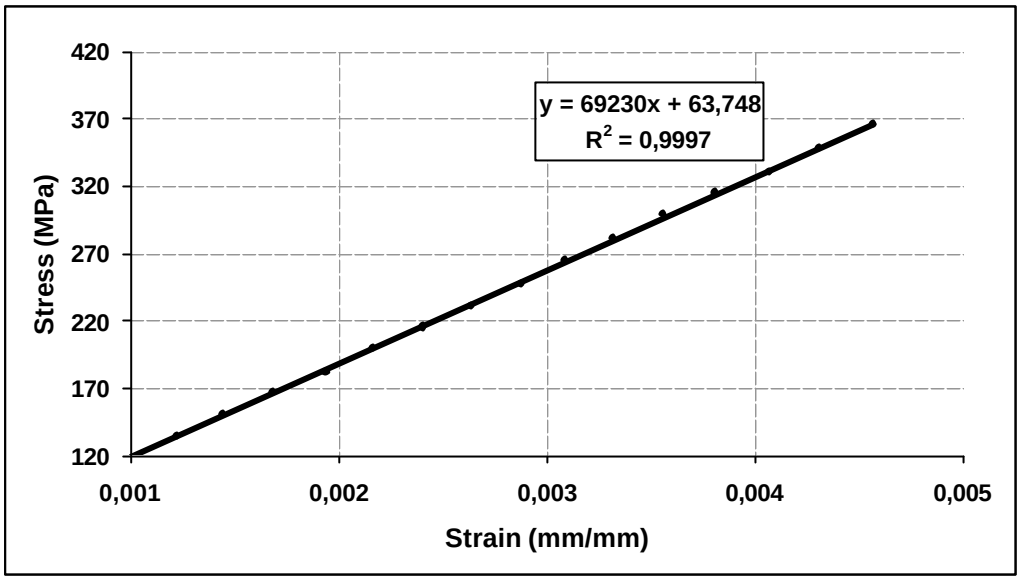

Figure 4.2 Least-square fitted stress-strain curve of 1251-1 ring test specimen.

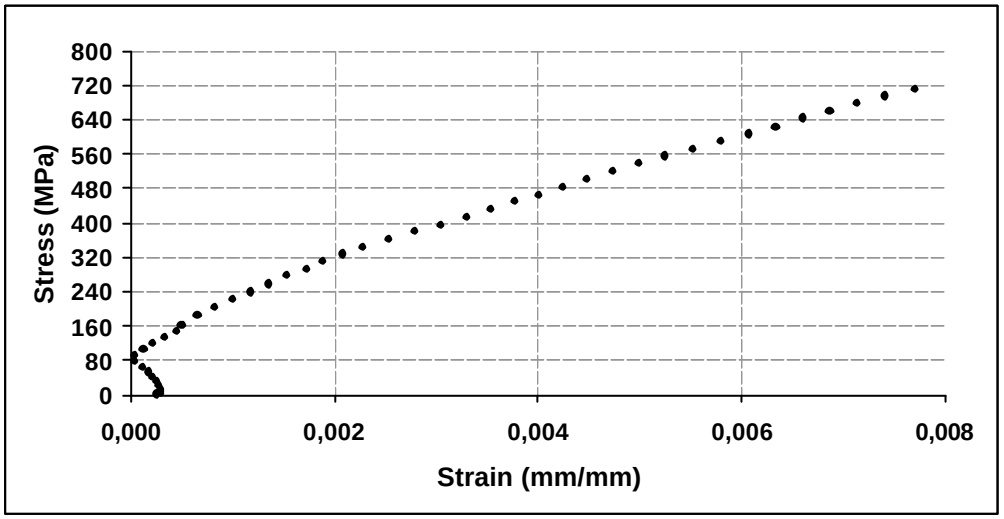

Figure 4.3 Stress –Strain curve of 1251-2 ring test specimen.

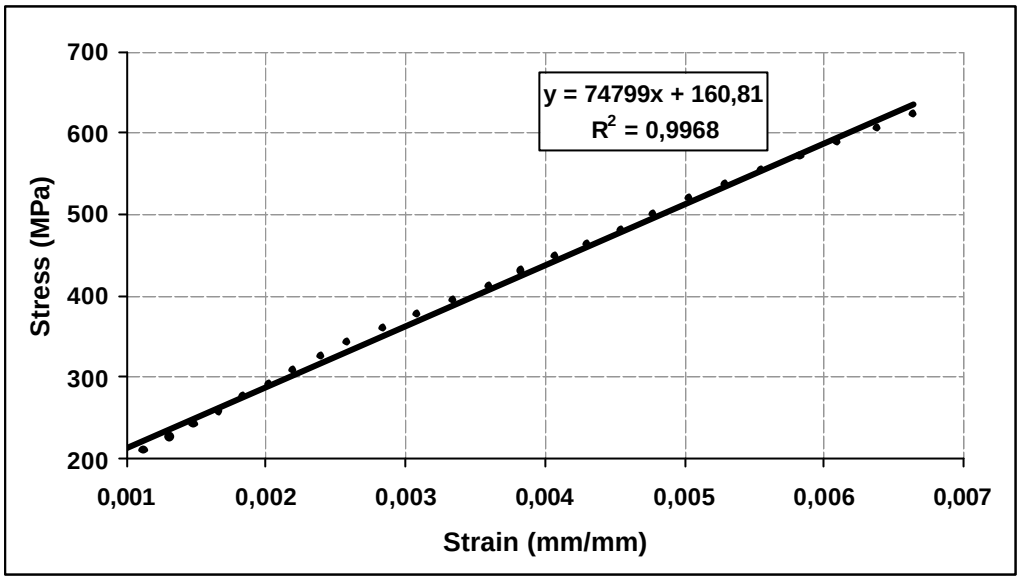

Figure 4.4 Least-square fitted stress-strain curve of 1251-2 ring test specimen.

As illustrated in Figures 4.1 - 4.4, hoop tensile modulus of elasticity was determined for each of the split-disk test specimens. These results are tabulated in Tables 4.13 through 4.17. Similar to the strength results, the first column involves the specimen designation numbers. In the second column, the obtained hoop tensile modulus of elasticity of each specimen is presented. The next three columns, involves the statistical data (mean average hoop tensile modulus of elasticity, their standard deviation, and their percent sample coefficient of variation).

Table 4.13 Hoop tensile modulus of elasticity results of split-disk tests and related statistical results for specimens 1111-1 through 1252-2.

Specimen Designation	E_h (GPa)	$E_h^{(average)}$ (GPa)	Standard Deviation	CV (%)
1111-1	11.88	12.090	0.297	2.456
1111-2	12.3			
1121-1	13.81	13.585	0.318	2.342
1121-2	13.36			
1131-1	21.55	21.030	0.735	3.497
1131-2	20.51			
1141-1	45.02	47.380	3.338	7.044
1141-2	49.74			
1151-1	56.87	56.560	0.438	0.775
1151-2	56.25			
1112-1	11.21	11.730	0.735	6.269
1112-2	12.25			
1122-1	14.49	14.440	0.071	0.490
1122-2	14.39			
1132-1	29.09	29.975	1.252	4.175
1132-2	30.86			
1142-1	54.77	55.215	0.629	1.140
1142-2	55.66			
1152-1	63.53	70.680	10.112	14.306
1152-2	77.83			
1211-1	11.56	10.780	1.103	10.233
1211-2	10			
1221-1	10.53	12.125	2.256	18.603
1221-2	13.72			
1231-1	19.48	18.070	1.994	11.035
1231-2	16.66			
1241-1	50.33	49.900	0.608	1.219
1241-2	49.47			
1251-1	72.8	70.015	3.939	5.625
1251-2	67.23			
1212-1	13.43	14.090	0.933	6.624
1212-2	14.75			
1222-1	14.3	13.965	0.474	3.392
1222-2	13.63			
1232-1	17.81	18.315	0.714	3.899
1232-2	18.82			
1242-1	45.88	46.820	1.329	2.839
1242-2	47.76			
1252-1	62.25	64.190	2.744	4.274
1252-2	66.13			

Table 4.14 Hoop tensile modulus of elasticity results of split-disk tests and related statistical results for specimens 2111-1 through 2252-2.

Specimen Designation	E_h (GPa)	$E_h^{(average)}$ (GPa)	Standard Deviation	CV (%)
2111-1	12.11	11.675	0.615	5.269
2111-2	11.24			
2121-1	12.15	12.695	0.771	6.071
2121-2	13.24			
2131-1	19.05	19.425	0.530	2.730
2131-2	19.8			
2141-1	45.83	45.260	0.806	1.781
2141-2	44.69			
2151-1	57.92	59.560	2.319	3.894
2151-2	61.2			
2112-1	11.56	11.155	0.573	5.135
2112-2	10.75			
2122-1	11.74	12.625	1.252	9.913
2122-2	13.51			
2132-1	16.71	17.195	0.686	3.989
2132-2	17.68			
2142-1	49.2	48.805	0.559	1.145
2142-2	48.41			
2152-1	62.36	62.945	0.827	1.314
2152-2	63.53			
2211-1	13.86	13.215	0.912	6.903
2211-2	12.57			
2221-1	13.46	12.805	0.926	7.234
2221-2	12.15			
2231-1	18.89	19.365	0.672	3.469
2231-2	19.84			
2241-1	49.89	49.370	0.735	1.490
2241-2	48.85			
2251-1	59.47	61.850	3.366	5.442
2251-2	64.23			
2212-1	11.21	11.665	0.643	5.516
2212-2	12.12			
2222-1	11.58	11.260	0.453	4.019
2222-2	10.94			
2232-1	16.84	17.505	0.940	5.372
2232-2	18.17			
2242-1	56.43	57.605	1.662	2.885
2242-2	58.78			
2252-1	65.07	66.910	2.602	3.889
2252-2	68.75			

Table 4.15 Hoop tensile modulus of elasticity results of split-disk tests and related statistical results for specimens 3111-1 through 3252-2.

Specimen Designation	E_h (GPa)	$E_h^{(average)}$ (GPa)	Standard Deviation	CV (%)
3111-1	10.25	9.950	0.424	4.264
3111-2	9.65			
3121-1	13.88	13.045	1.181	9.052
3121-2	12.21			
3131-1	25.71	25.145	0.799	3.178
3131-2	24.58			
3141-1	97.42	96.715	0.997	1.031
3141-2	96.01			
3151-1	144.07	140.750	4.695	3.336
3151-2	137.43			
3112-1	9.56	9.050	0.721	7.970
3112-2	8.54			
3122-1	13.78	13.010	1.089	8.370
3122-2	12.24			
3132-1	22.89	21.165	2.440	11.526
3132-2	19.44			
3142-1	102.77	102.030	1.047	1.026
3142-2	101.29			
3152-1	170.23	169.395	1.181	0.697
3152-2	168.56			
3211-1	8.99	8.555	0.615	7.191
3211-2	8.12			
3221-1	9.22	8.750	0.665	7.596
3221-2	8.28			
3231-1	16.73	16.830	0.141	0.840
3231-2	16.93			
3241-1	93.27	93.980	1.004	1.068
3241-2	94.69			
3251-1	141.65	148.700	9.970	6.705
3251-2	155.75			
3212-1	9.56	9.050	0.721	7.970
3212-2	8.54			
3222-1	10.91	9.745	1.648	16.907
3222-2	8.58			
3232-1	18.02	19.200	1.669	8.692
3232-2	20.38			
3242-1	97.62	99.655	2.878	2.888
3242-2	101.69			
3252-1	160.01	159.215	1.124	0.706
3252-2	158.42			

Table 4.16 Hoop tensile modulus of elasticity results of split-disk tests and related statistical results for specimens 4111-1 through 4252-2.

Specimen Designation	E_h (GPa)	$E_h^{(average)}$ (GPa)	Standard Deviation	CV (%)
4111-1	13.16	12.850	0.438	3.412
4111-2	12.54			
4121-1	12.89	12.845	0.064	0.495
4121-2	12.8			
4131-1	18.91	17.005	2.694	15.843
4131-2	15.1			
4141-1	45.88	45.990	0.156	0.338
4141-2	46.1			
4151-1	60.35	59.625	1.025	1.720
4151-2	58.9			
4112-1	8.99	9.275	0.403	4.346
4112-2	9.56			
4122-1	11.5	10.515	1.393	13.248
4122-2	9.53			
4132-1	18.9	18.615	0.403	2.165
4132-2	18.33			
4142-1	52.72	52.800	0.113	0.214
4142-2	52.88			
4152-1	76.91	77.420	0.721	0.932
4152-2	77.93			
4211-1	12.21	12.780	0.806	6.308
4211-2	13.35			
4221-1	15.7	14.445	1.775	12.287
4221-2	13.19			
4231-1	21.3	21.910	0.863	3.937
4231-2	22.52			
4241-1	51.51	50.120	1.966	3.922
4241-2	48.73			
4251-1	60.77	60.895	0.177	0.290
4251-2	61.02			
4212-1	12.24	12.795	0.785	6.134
4212-2	13.35			
4222-1	14.51	14.155	0.502	3.547
4222-2	13.8			
4232-1	19.78	19.820	0.057	0.285
4232-2	19.86			
4242-1	51.91	51.620	0.410	0.795
4242-2	51.33			
4252-1	71.44	70.095	1.902	2.714
4252-2	68.75			

Table 4.17 Hoop tensile modulus of elasticity results of split-disk tests and related statistical results for specimens 5111-1 through 5252-2.

Specimen Designation	E_h (GPa)	$E_h^{(average)}$ (GPa)	Standard Deviation	CV (%)
5111-1	10.89	10.390	0.707	6.806
5111-2	9.89			
5121-1	10.19	11.200	1.428	12.753
5121-2	12.21			
5131-1	24.72	24.745	0.035	0.143
5131-2	24.77			
5141-1	120.8	120.300	0.707	0.588
5141-2	119.8			
5151-1	178.71	179.960	1.768	0.982
5151-2	181.21			
5112-1	9.34	10.060	1.018	10.122
5112-2	10.78			
5122-1	15.95	14.340	2.277	15.878
5122-2	12.73			
5132-1	20.45	20.810	0.509	2.447
5132-2	21.17			
5142-1	105.61	104.920	0.976	0.930
5142-2	104.23			
5152-1	184.53	190.670	8.683	4.554
5152-2	196.81			
5211-1	8.85	8.420	0.608	7.222
5211-2	7.99			
5221-1	14.357	13.284	1.518	11.429
5221-2	12.21			
5231-1	25.1	26.035	1.322	5.079
5231-2	26.97			
5241-1	109.3	108.975	0.460	0.422
5241-2	108.65			
5251-1	176.65	169.630	9.928	5.853
5251-2	162.61			
5212-1	7.56	8.070	0.721	8.937
5212-2	8.58			
5222-1	9.02	9.780	1.075	10.990
5222-2	10.54			
5232-1	25.68	24.240	2.036	8.401
5232-2	22.8			
5242-1	102.81	104.150	1.895	1.820
5242-2	105.49			
5252-1	191.53	190.190	1.895	0.996
5252-2	188.85			

4.2.2 Tube Tensile Test Results

Load and strain data were taken until the failure of the specimens as specified in ASTM D 210. Type of failure of each specimen, and its location were also recorded. These data were then used so as to calculate the longitudinal tensile strength of the specimens, and at the same time, converted into stress – strain graphs, as stated in Section 2.4.2.5, to determine the longitudinal tensile modulus of elasticity of the specimens. For this purpose, the slope of the linear portion of these curves was determined by fitting a straight line, with the least-square method.

Tables 4.18 and 4.19 involve the tabulated results of tube tensile test specimens. In these tables, the specimen designation number, the cross-sectional area, the maximum load observed during the test, the elongation recorded at the instant of observation of maximum load, and the percent elongation data are presented in each column, respectively.

Determination of longitudinal tensile modulus of elasticity is illustrated in Figures 4.5–4.10. In Figures 4.5, 4.7, and 4.9, obtained stress-strain curves of 1211 – 1221 – 1231 tube tensile test specimens are presented, respectively. The least square fitted curves and their equations are plotted for these specimens in Figures 4.6, 4.8, and 4.10.

Longitudinal tensile modulus of elasticity of the remaining specimens are tabulated in Tables 4.20 and 4.21. The maximum stress observed during the tests, and the strains, recorded at the instant of observation of maximum stress are also tabulated in these tables.

Table 4.18 Load and elongation results of tube tensile tests for specimens 1131 through 3152.

Specimen Designation	Cross. Area (mm^2)	Max. Load (N)	Elongation at Max. Load (mm)	Elongation (%)
1131	294.76	34470.0	39.9	8.876
1141	272.72	9692.0	1.2	0.273
1151	285.85	3777.0	0.4	0.100
1132	289.80	34433.1	51.4	11.422
1142	265.11	9669.0	1.2	0.269
1152	285.85	3018.0	0.4	0.091
1231	307.64	32549.6	44.2	9.822
1241	270.04	8441.0	1.9	0.423
1251	279.92	3781.0	0.5	0.105
1232	294.76	33834.7	41.3	9.176
1242	270.04	8405.0	1.1	0.243
1252	283.27	3662.0	0.4	0.094
2131	314.59	35257.1	44.2	9.824
2141	309.63	7825.0	1.6	0.351
2151	313.60	1760.0	1.5	0.344
2132	309.25	36621.0	43.8	9.729
2142	301.69	7317.0	1.2	0.257
2152	308.64	3409.0	0.4	0.099
2231	319.56	37729.3	41.5	9.222
2241	220.92	8867.0	1.5	0.330
2251	310.62	2301.0	0.3	0.077
2232	329.51	40466.3	40.4	8.984
2242	295.75	7901.0	1.2	0.270
2252	311.61	3602.0	0.4	0.096
3131	260.19	28861.0	36.7	8.144
3141	293.76	13220.0	2.7	0.597
3151	224.83	1973.0	0.5	0.118
3132	240.52	30950.6	40.1	8.907
3142	297.73	11820.0	2.3	0.519
3152	236.60	3197.0	0.9	0.190

Table 4.19 Load and elongation results of tube tensile tests for specimens 3231 through 5252.

Specimen Designation	Cross. Area (mm^2)	Max. Load (N)	Elongation at Max. Load (mm)	Elongation (%)
3231	262.16	30030.0	30.2	6.716
3241	274.98	11590.0	2.5	0.562
3251	218.96	2175.0	0.7	0.159
3232	252.31	32569.2	43.4	9.633
3242	305.66	13260.0	2.7	0.610
3252	226.79	1815.0	0.5	0.122
4131	256.25	36679.6	45.1	10.024
4141	295.75	7995.0	1.2	0.263
4151	244.45	4155.0	0.5	0.119
4132	277.94	34442.9	44.8	9.949
4142	216.03	8306.0	1.4	0.303
4152	240.52	2893.0	0.4	0.079
4231	260.19	30930.9	52.2	11.609
4241	220.92	8347.0	1.2	0.263
4251	236.60	954.9	0.2	0.046
4232	220.92	30570.0	39.3	8.733
4242	226.79	6247.0	1.9	0.427
4252	224.83	966.8	1.3	0.287
5131	299.71	29640.0	17.0	3.778
5141	353.46	17940.0	3.0	0.671
5151	309.63	4404.0	0.9	0.210
5132	228.75	26967.7	16.7	3.700
5142	364.47	15740.0	2.9	0.637
5152	307.64	5662.0	1.8	0.400
5231	270.04	26220.0	18.7	4.149
5241	355.46	16180.0	2.8	0.612
5251	293.76	4190.0	1.0	0.215
5232	248.38	24550.0	17.1	3.800
5242	365.47	15570.0	2.8	0.627
5252	317.58	4029.0	0.9	0.207

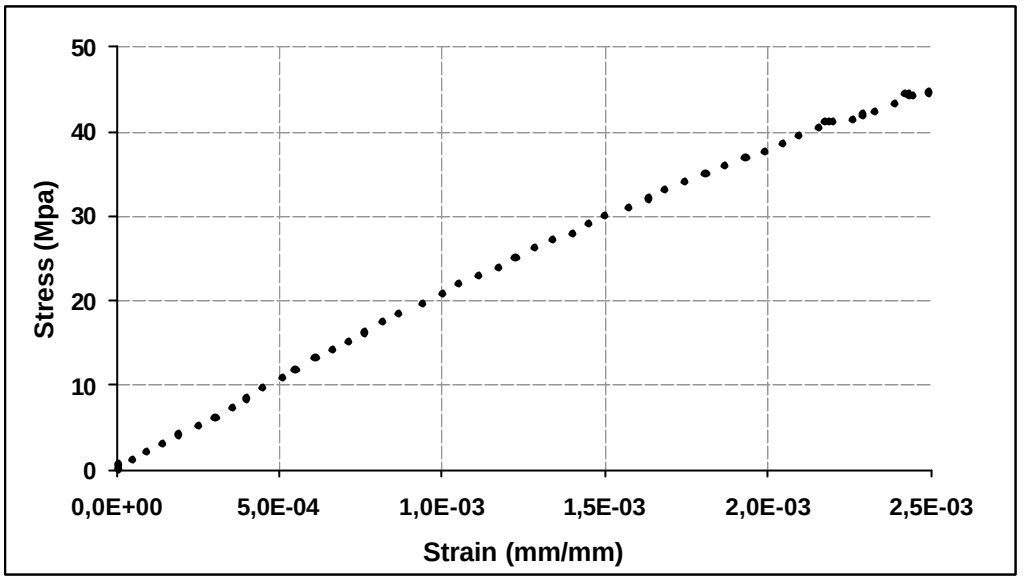

Figure 4.5 Stress–strain curve of 1131 tube tensile test specimen.

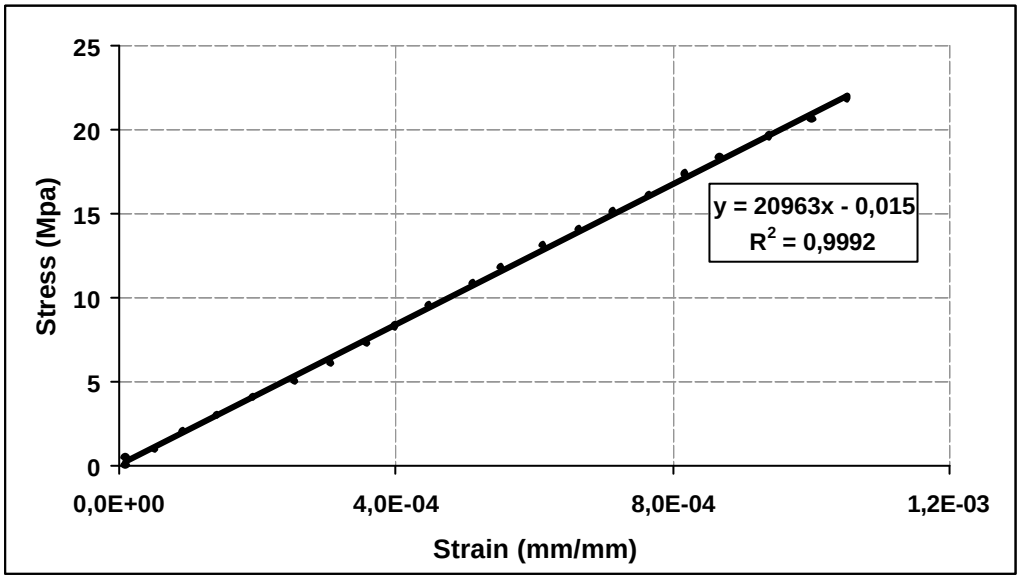

Figure 4.6 Least-square fitted stress-strain curve of 1131 tube tensile test specimen.

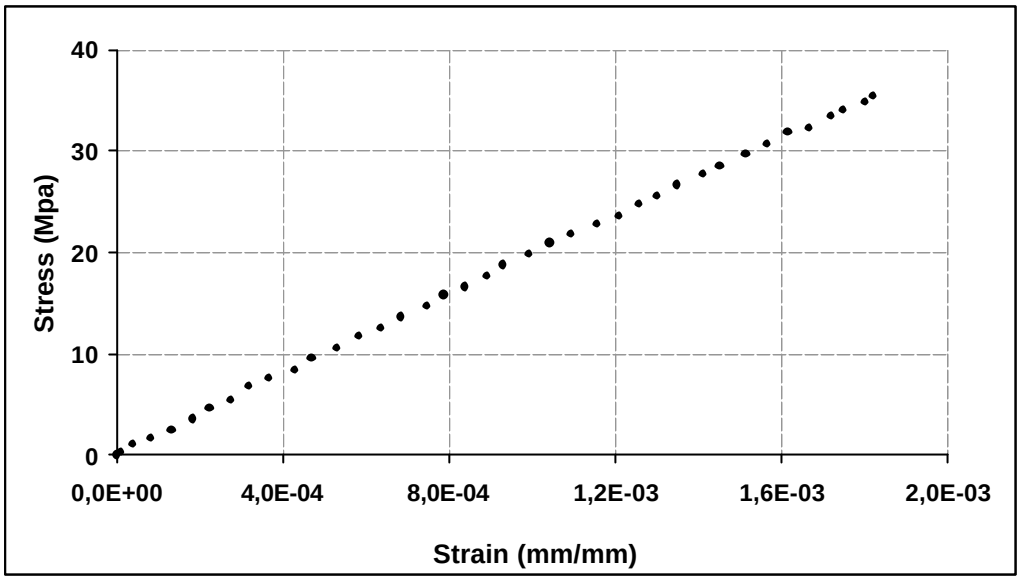

Figure 4.7 Stress – Strain curve of 1141 tube tensile test specimen.

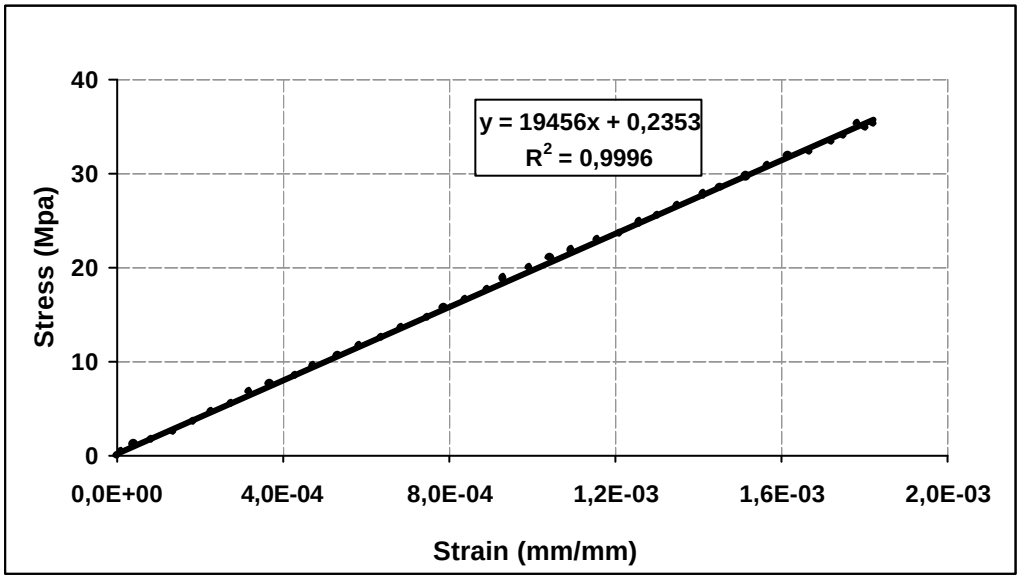

Figure 4.8 Least-square fitted stress-strain curve of 1141 tube tensile test specimen.

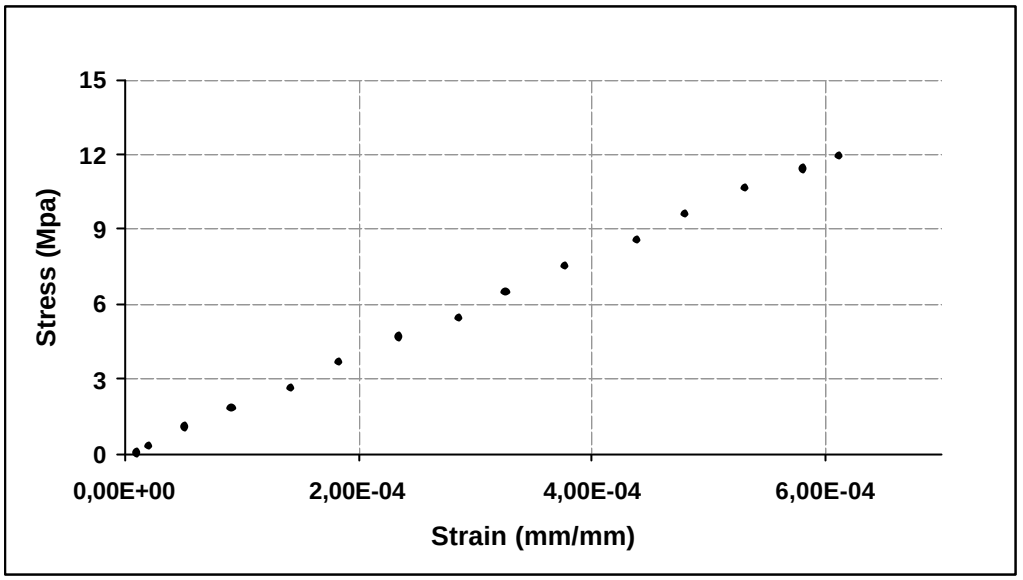

Figure 4.9 Stress – Strain curve of 1151 tube tensile test specimen.

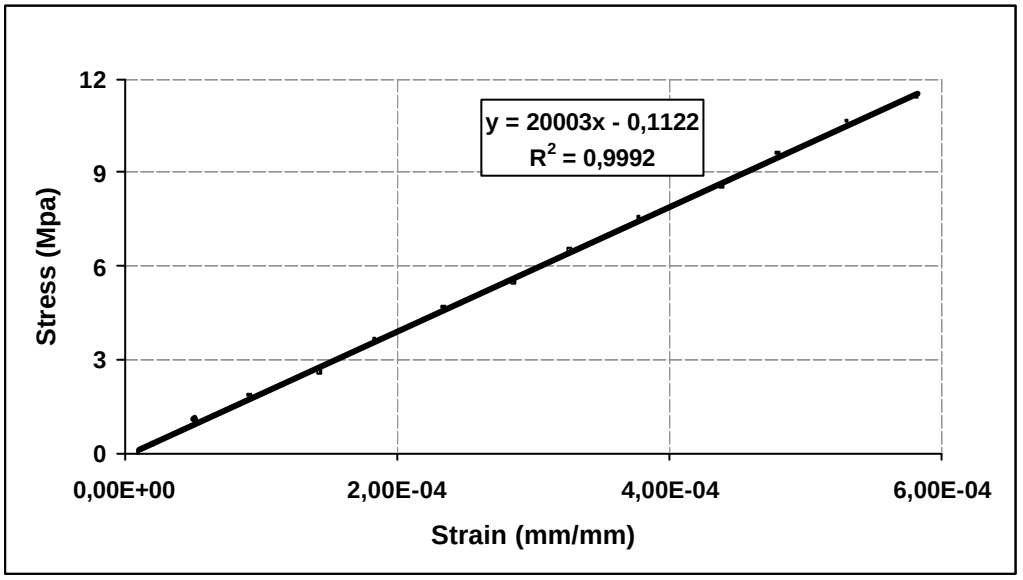

Figure 4.10 Least-square fitted stress-strain curve of 1151 tube tensile test specimen.

Table 4.20 Longitudinal tensile strength/tensile modulus of elasticity results of tube tensile tests for specimens 1131 through 3152.

Specimen Designation	s_{ltu} (MPa)	e_{ult} (mm/mm)	E_L (GPa)
1131	116.90	0.0998	20.96
1141	35.54	0.0031	19.46
1151	13.21	0.0011	20.00
1132	118.82	0.1285	27.56
1142	36.47	0.0030	17.84
1152	10.56	0.0010	19.12
1231	105.80	0.1105	24.07
1241	31.25	0.0048	19.45
1251	13.51	0.0012	20.92
1232	114.79	0.1032	22.23
1242	31.12	0.0027	17.38
1252	12.93	0.0011	16.74
2131	112.07	0.1105	20.43
2141	25.27	0.0039	17.40
2151	5.61	0.0039	18.08
2132	118.42	0.1079	16.13
2142	24.25	0.0029	14.57
2152	11.05	0.0011	15.95
2231	118.07	0.1037	26.00
2241	40.13	0.0037	22.09
2251	7.41	0.0009	14.63
2232	122.81	0.1011	23.45
2242	26.71	0.0030	17.63
2252	11.56	0.0011	18.61
3131	110.92	0.0814	16.95
3141	35.54	0.0670	9.49
3151	8.77	0.0013	10.37
3132	128.68	0.0891	19.17
3142	39.69	0.0058	16.83
3152	13.51	0.0021	8.59

Table 4.21 Longitudinal tensile strength/tensile modulus of elasticity results of tube tensile tests for specimens 3231 through 5252.

Specimen Designation	s_{ltu} (MPa)	e_{ult} (mm/mm)	E_L (GPa)
3231	114.50	0.0755	21.68
3241	42.16	0.0063	12.97
3251	9.93	0.0018	9.56
3232	129.08	0.0963	18.83
3242	43.38	0.0069	11.63
3252	8.00	0.0014	10.94
4131	143.14	0.1128	23.66
4141	27.03	0.0030	20.29
4151	17.00	0.0013	22.51
4132	123.92	0.1119	25.59
4142	38.45	0.0034	19.15
4152	12.03	0.0009	17.22
4231	118.88	0.1306	24.79
4241	37.78	0.0030	21.68
4251	4.04	0.0005	21.68
4232	138.30	0.0983	20.95
4242	27.54	0.0048	18.15
4252	4.30	0.0032	20.12
5131	98.87	0.4250	17.64
5141	50.76	0.0075	14.78
5151	14.22	0.0024	12.57
5132	117.89	0.4030	15.57
5142	43.18	0.0072	10.70
5152	18.40	0.0158	8.19
5231	97.07	0.0467	20.05
5241	45.51	0.0069	10.96
5251	14.26	0.0024	9.83
5232	98.83	0.0427	26.59
5242	42.60	0.0071	18.63
5252	12.68	0.0023	10.36

4.3 Discussion of Experimental Work

4.3.1 Split Disk Tests

In this section, the effect of winding angle, tension setting, and type of fiber and resin on the hoop tensile properties of the specimens will be evaluated independently by using the tabulated results given in the previous sections.

In Figure 4.11, dominant failure mechanisms observed during the tests and their locations on specimens, having 90^o (2151, 4151), 65° (4141, 2141), 45^o (4231, 2132), and 25^o (2221, 2222) winding angles are compared. As seen from the photographs, failure of specimens occurred in the gage section whatever the winding angle is. For specimens, having 90^o winding angle (Figure 4.11(a)), fiber-matrix debonding, parallel to the fibers and loading axis, was followed by rupture of fibers. For specimens, having $\pm 65^o$ winding angle (Figure 4.11(b)), the progress of failure was occurred in a similar manner. In addition, delamination of $\pm 65^o$ layers was observed. The outer layer was observed to be totally damaged.

For $\pm 45^o$ winding angle specimens (Figure 4.11(c)), different from $\pm 65^o$ winding angle specimens, fiber-matrix debonding occurred more dominantly. Delamination of $\pm 45^o$ layers was also observed for these specimens. Finally, for 25^o winding angle specimens (Figure 4.11 (d)), fiber breakage was very limited, and the specimen failed with the rupture of the matrix phase, which causes the formation of less macroscopic damage on the specimens, and low failure strength.

In Figures 4.12–4.16, winding angle dependence of hoop tensile strength of specimens were represented by a continuous curve, fit by least square method, by using the experimental data. These curves were obtained by using the

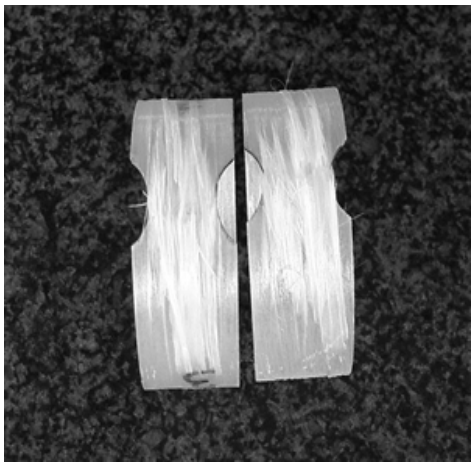

(a) ($\theta = 90^o$)

Fiber fracture, fiber-matrix debonding

(b) ($\theta = 65^o$)

Fiber failure, fiber-matrix debonding, delamination

(c) ($\theta = 45^o$)

Delamination, fiber-matrix debonding

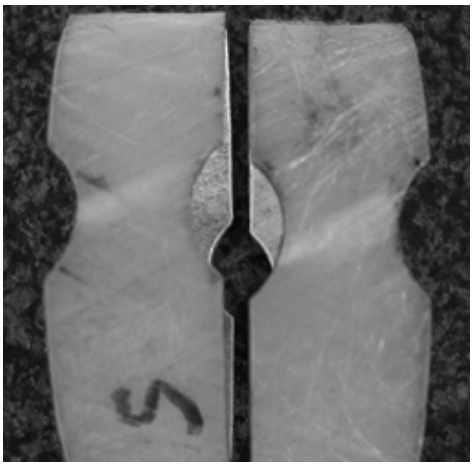

(d) ($\theta = 25^o$)

Matrix cracking

Figure 4.11 Dominant failure mechanisms and their locations on split-disk specimens.

results of the tests performed with the specimens 1211, 1221, 1231, 1241, 1251 (Figure 4.12); 2211, 2221, 2231, 2241, 2251 (Figure 4.13); 3211, 3221, 3231, 3241, 3251 (Figure 4.14); 4211, 4221, 4231, 4241, 4251 (Figure 4.15); and 5211, 5221, 5231, 5241, 5251 (Figure 4.16). The figures involve both the variation of hoop tensile strength of the specimens tested and also the error bars, representing the range of expected strength values. These data were obtained by using the calculated standard deviations for the specimens tested.

As it is expected, the highest strength values were obtained for the specimens, having the winding angle of 90^0, since the fiber direction is parallel to the direction of loading. The lowest strength values were obtained for the specimens, having the winding angle of 0^0, where the fiber direction is perpendicular to the direction of loading. The results for the specimens, having 25^0, 45^0, and 65^0 winding angles exhibited intermediate performance between these two extremes as expected.

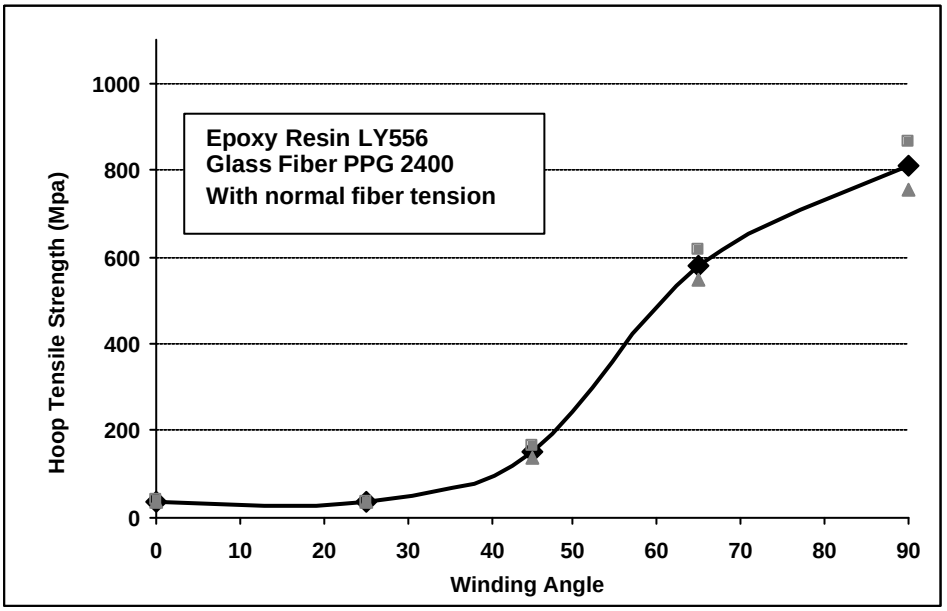

Figure 4.12 Hoop tensile strength vs. winding angle for specimens (fiber 1, resin 2, tension setting 1).

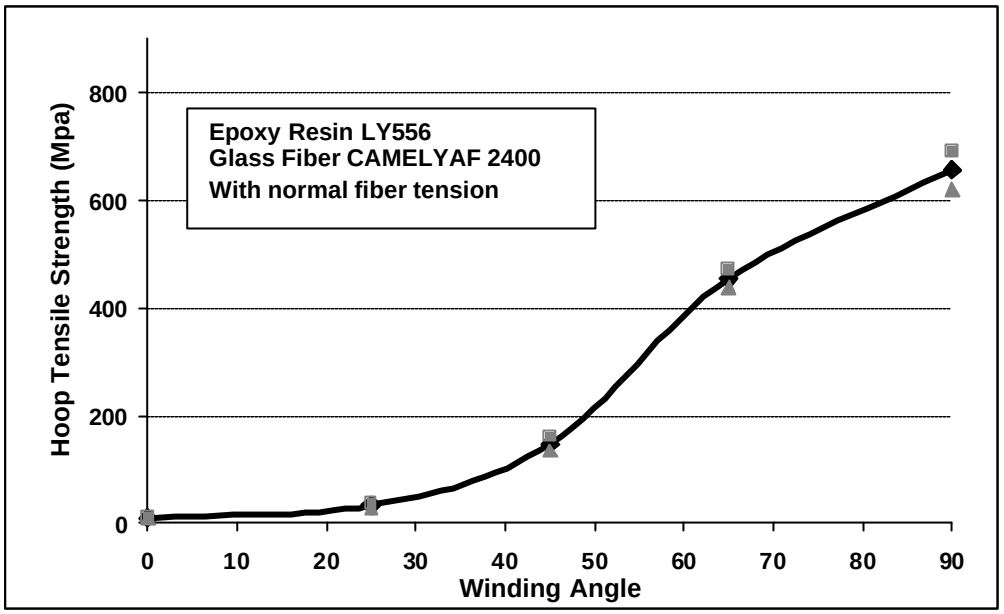

Figure 4.13 Hoop tensile strength vs. winding angle for specimens (fiber 2, resin 2, tension setting 1).

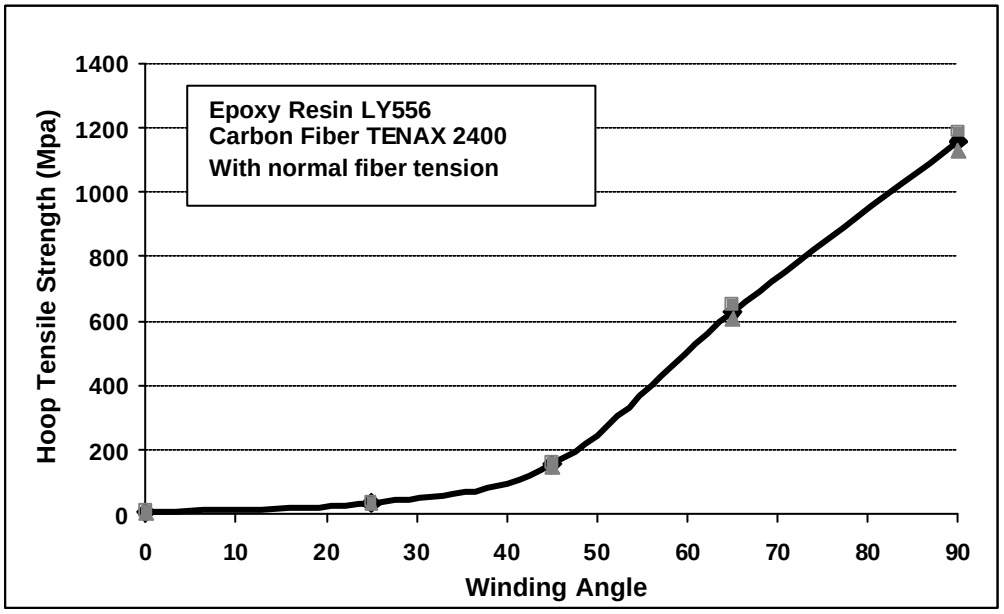

Figure 4.14 Hoop tensile strength vs. winding angle for specimens (fiber3, resin 2, tension setting 1).

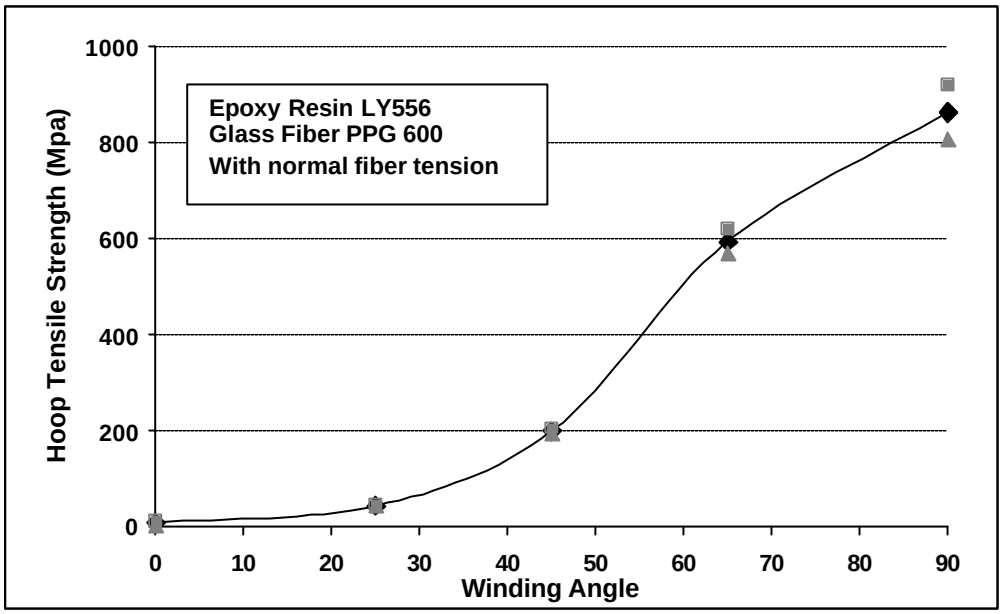

Figure 4.15 Hoop tensile strength vs. winding angle for specimens (fiber 4, resin 2, tension setting 1).

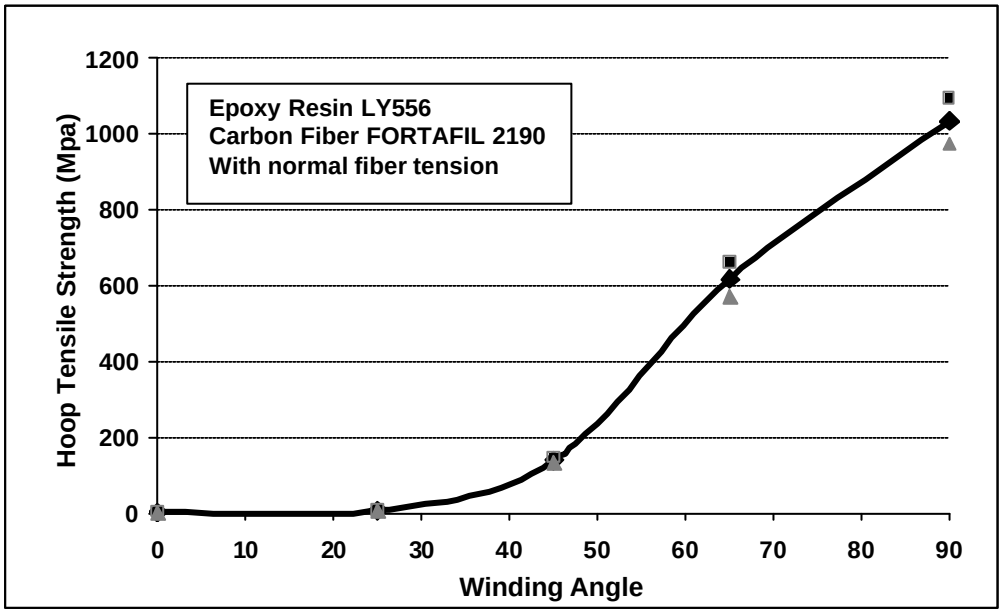

Figure 4.16 Hoop tensile strength vs. winding angle for specimens (fiber 5, resin 2, tension setting 1).

In Figure 4.17, hoop tensile strengths of specimens, having different fibers are compared as a function of winding angle. The specimens having the same resin system (resin 2) and tension setting (tension setting 1) are compared so as to visualize the effect of fiber type on mechanical performance of specimens. According to this figure, it can be stated that the specimens produced by carbon fibers showed better mechanical performance compared to the ones reinforced with glass fibers. This result became more dominant as the winding angle of specimens approached to the direction of loading (90^o). In addition, highly anisotropic behavior of the carbon fiber system can also be seen in the same figure, such that, a sharp decrease of hoop tensile strength was detected when the winding direction of the fibers were altered from the direction of loading.

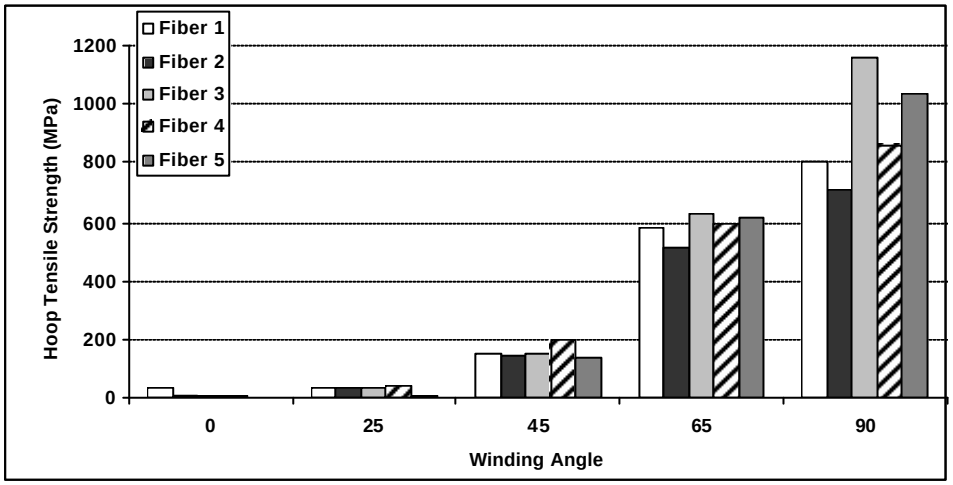

Figure 4.17 Comparison of hoop tensile strengths of specimens having different fiber types, as a function of winding angle.

From the specimens, reinforced with glass fibers, the one reinforced with PPG 600 TEX glass fiber (Fiber 4) showed better performance. This result can be explained by the effect of low linear density of Fiber 4. As the linear density of fibers decreases, the diameters of the fiber bundles, used during the winding operation, decreases, which causes the fiber bands to criss-cross more

efficiently, by creating a weaving effect. The same result can also be seen by comparing the strength results of carbon fiber reinforced specimens. The specimen produced with low linear density carbon fibers (fiber 3) showed better mechanical performance compared to the one produced with high linear density carbon fibers (fiber 5).

In Figure 4.18, hoop tensile strengths of specimens, having different resin systems are compared for each fiber type. The specimens having the same winding angle ($\pm 65^{o}$) and tension setting (tension setting 1) are compared so as to visualize the effect of resin system on mechanical performance of specimens. According to this figure, it can be stated that the effect of resin system on hoop tensile properties of specimens is negligible.

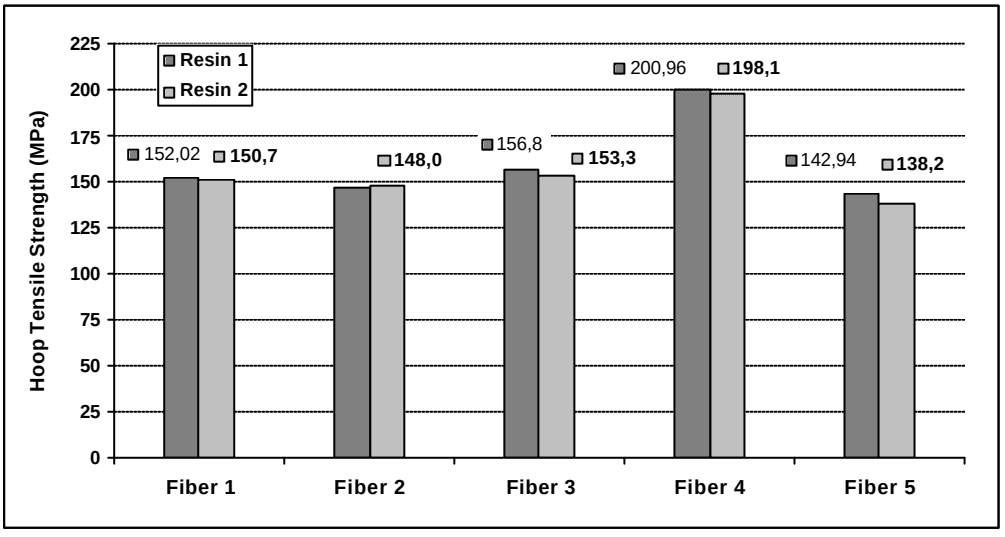

Figure 4.18 Comparison of hoop tensile strengths of specimens having different resin systems, as a function of fiber type.

The effect of tension setting on hoop tensile properties of the specimens can be understood by inspecting Figures 4.19–4.23. In these figures, the variation of hoop tensile strength is plotted for two cases, with tension and without tension, as a function of winding angle. According to these figures, no significant differences were detected in terms of hoop tensile strength of the specimens. However, a slight increase in strength was detected for the specimens, produced with PPG glass fibers (Fiber 1, Fiber 4), and wounded with tension for winding angles greater than 60^0. For CAMELYAF Product, WR3 2400 TEX glass fiber, fiber feed was from the inner of the rolls, which made the control of fiber tension more difficult. Therefore, the same effect was not observed for the specimens, reinforced with CAMELYAF glass fiber (Fiber 2)

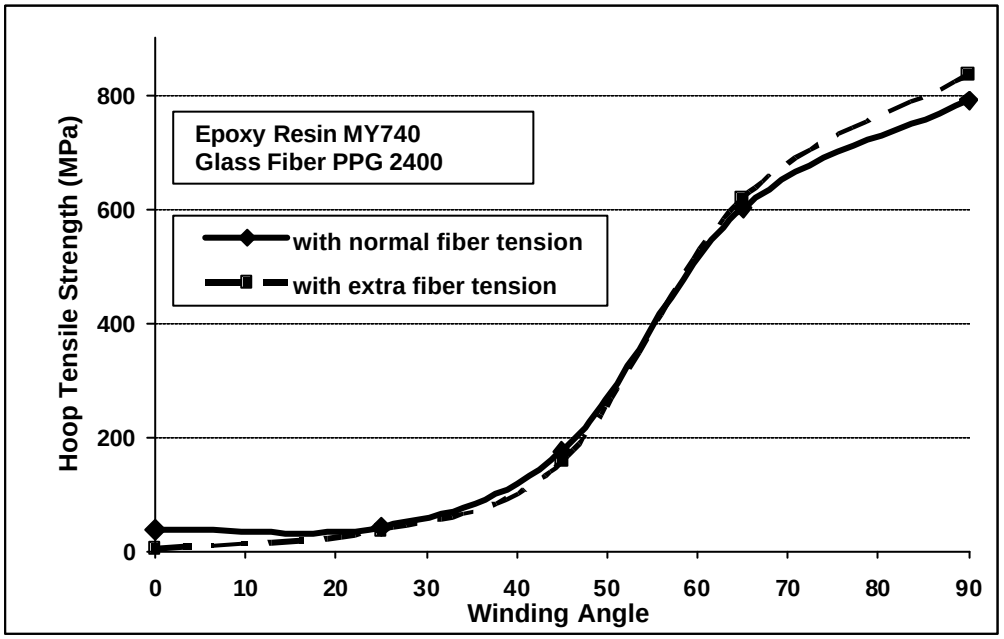

Figure 4.19 Hoop tensile strength vs. winding angle for specimens (fiber 1, resin 1, tension settings 1-2).

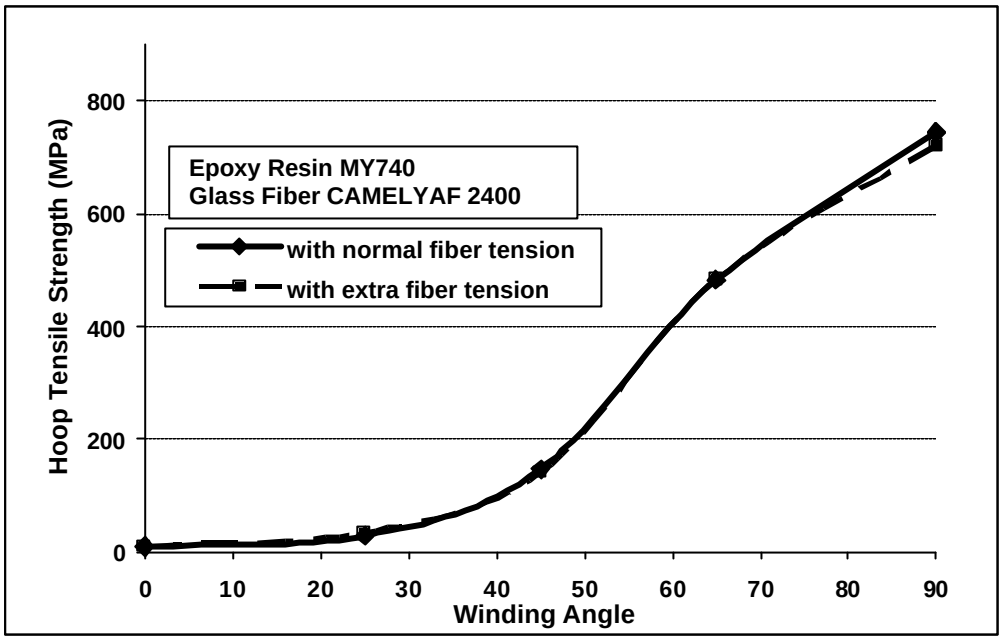

Figure 4.20 Hoop tensile strength vs. winding angle for specimens (fiber 2, resin 1, tension setting 1-2).

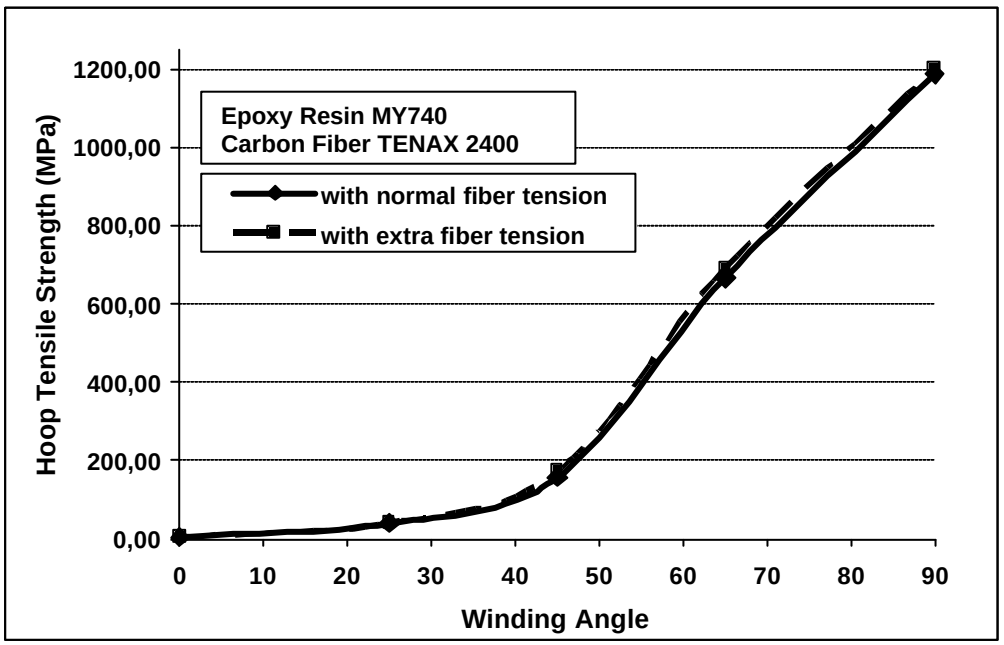

Figure 4.21 Hoop tensile strength vs. winding angle for specimens (fiber 3, resin 1, tension setting 1-2).

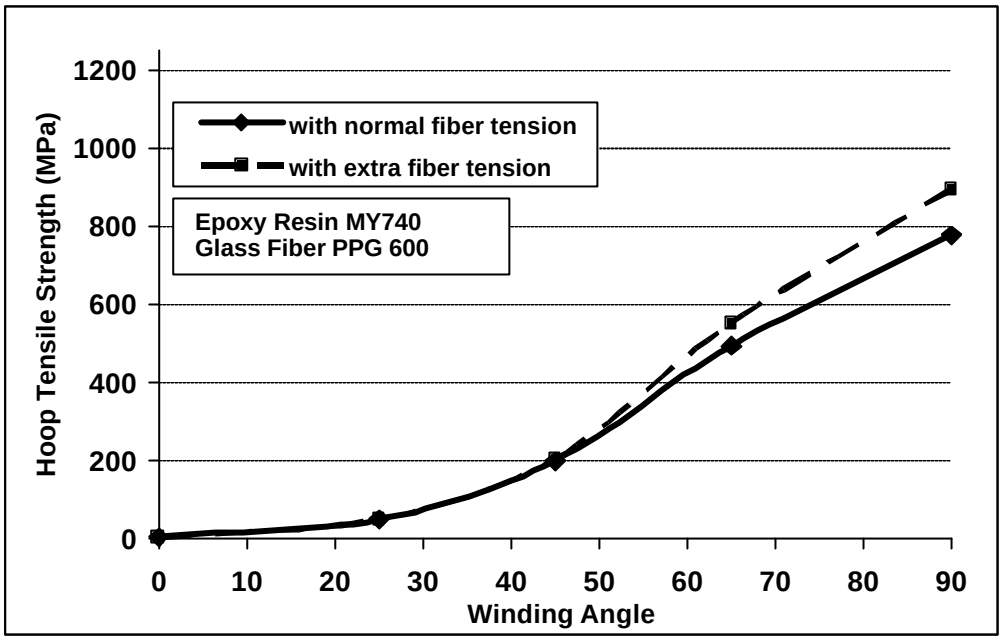

Figure 4.22 Hoop tensile strength vs. winding angle for specimens (fiber 4, resin 1, tension setting 1-2).

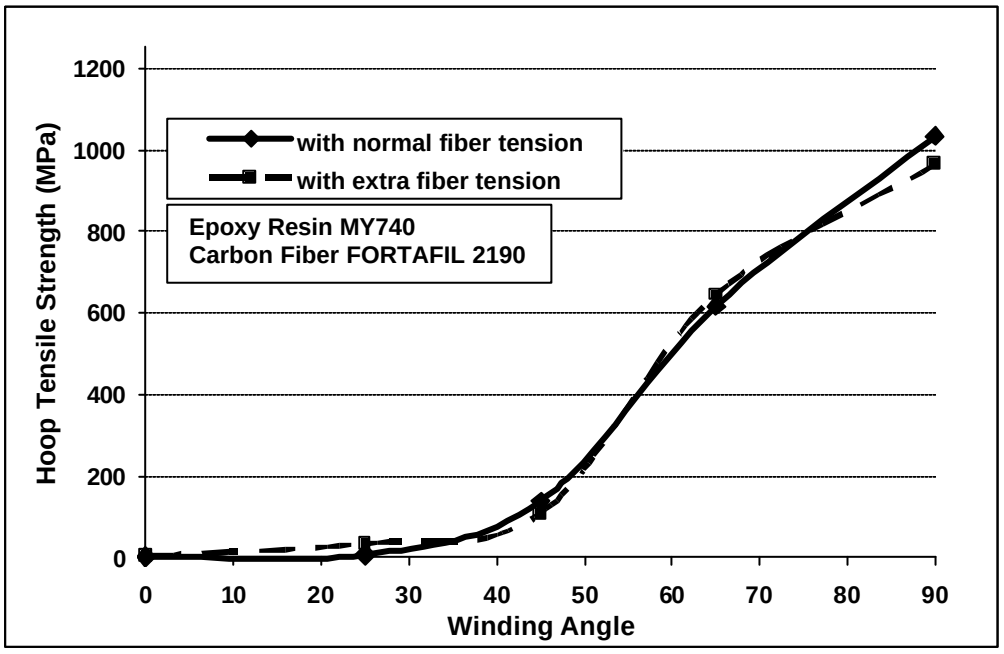

Figure 4.23 Hoop tensile strength vs. winding angle for specimens (fiber 5, resin 1, tension setting 1-2).

Similar to the strength results of split-disk tests, winding angle dependence of hoop tensile modulus of elasticity of specimens are represented by a continuous curve, fit by least square method. These curves were obtained by using the results of the tests performed with the specimens 1111, 1121, 1131, 1141, 1151 (Figure 4.24); 2111, 2121, 2131, 2141, 2151 (Figure 4.25); 3111, 3121, 3131, 3141, 3151 (Figure 4.26); 4111, 4121, 4131, 4141, 4151 (Figure 4.27); and 5111, 5121, 5131, 5141, 5151 (Figure 4.28) The error bars are also plotted, by using the calculated standard deviations.

In Figures 4.24–4.28, a similar distribution of hoop tensile modulus of elasticity is obtained with the strength results, presented in Figures 4.12 – 4.16. Differently, the advanced properties of carbon fiber reinforced specimens (Figure 4.26, Figure 4.28) became more dominant, such that, the calculated hoop tensile modulus of elasticity of carbon fiber reinforced specimens is almost 2–3 times greater than the ones reinforced with glass

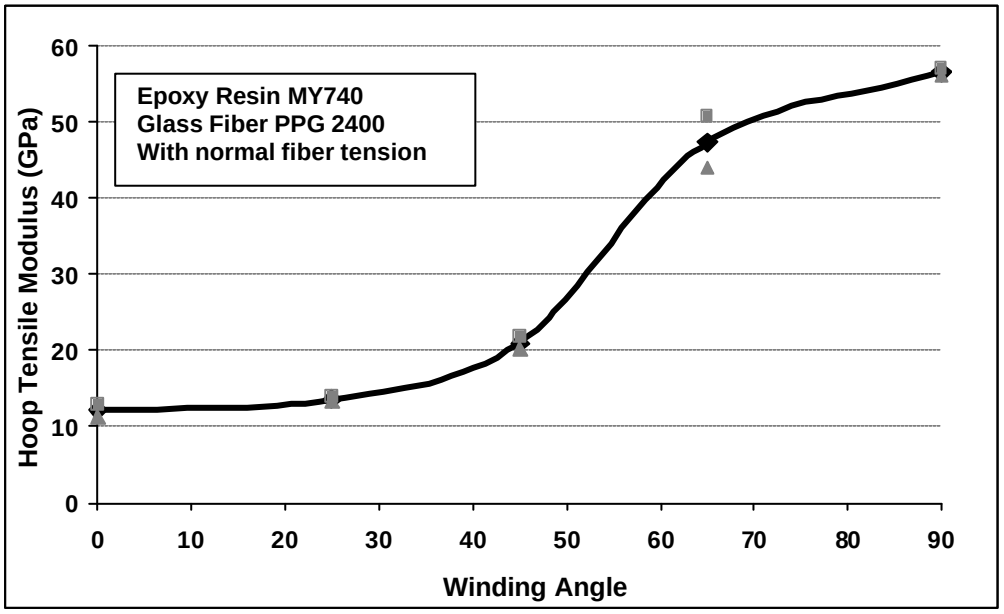

Figure 4.24 Hoop tensile modulus of elasticity vs. winding angle for specimens (fiber 1, resin 1, tension setting 1).

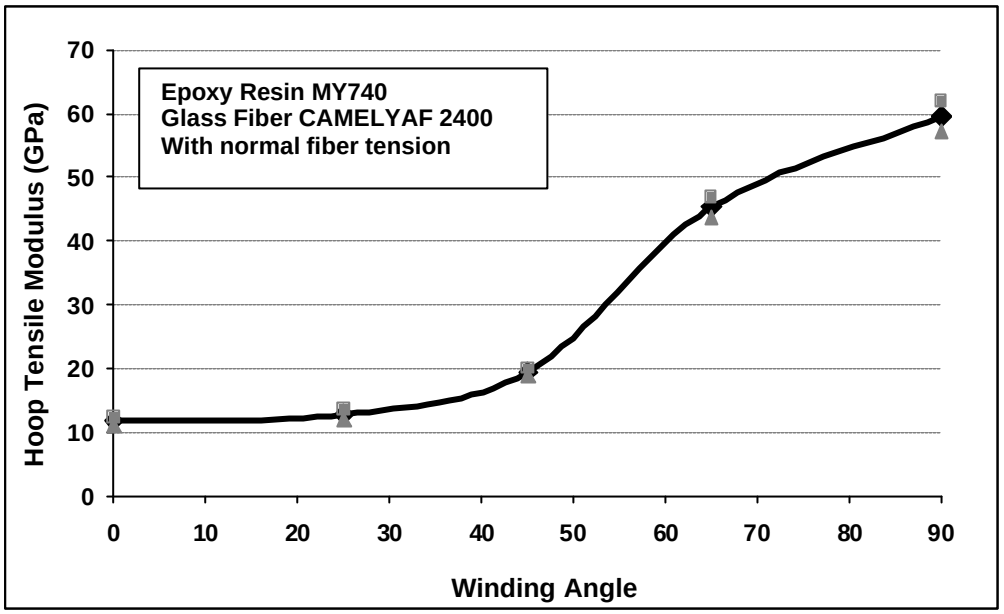

Figure 4.25 Hoop tensile modulus of elasticity vs. winding angle for specimens (fiber 2, resin 1, tension setting 1).

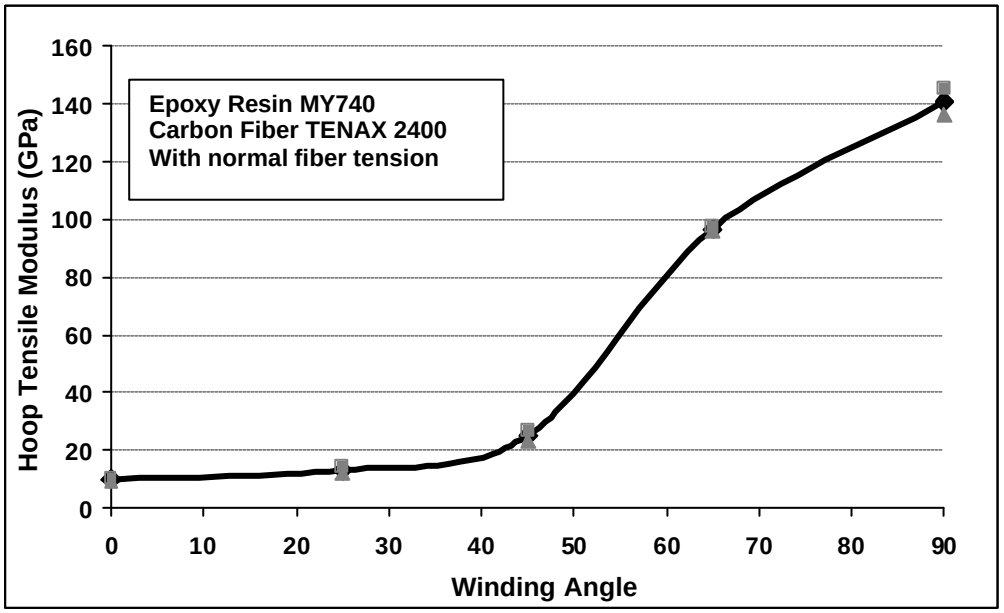

Figure 4.26 Hoop tensile modulus of elasticity vs. winding angle for specimens (fiber 3, resin 1, tension setting 1).

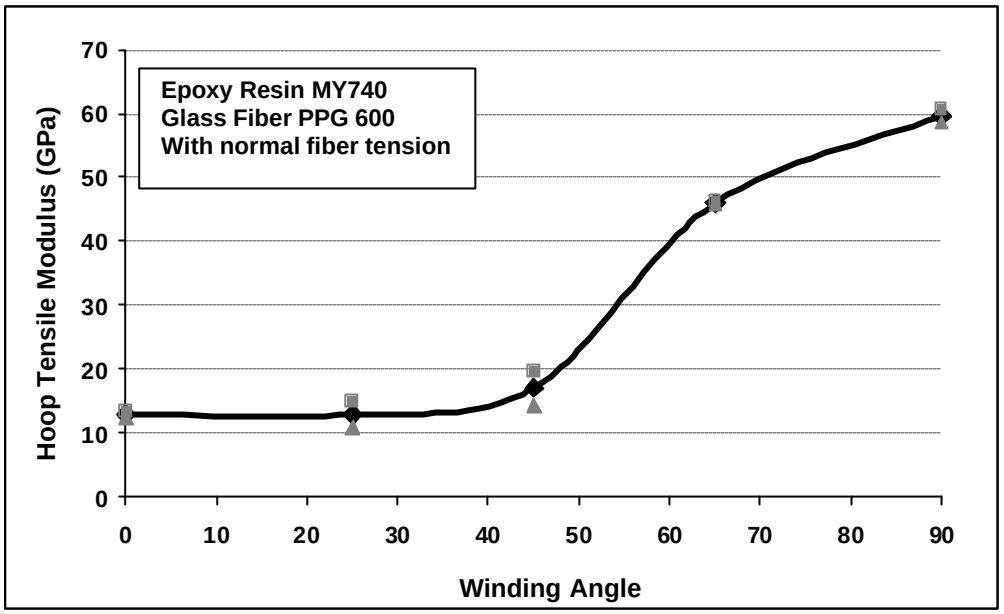

Figure 4.27 Hoop tensile modulus of elasticity vs. winding angle for specimens (fiber 4, resin 1, tension setting 1).

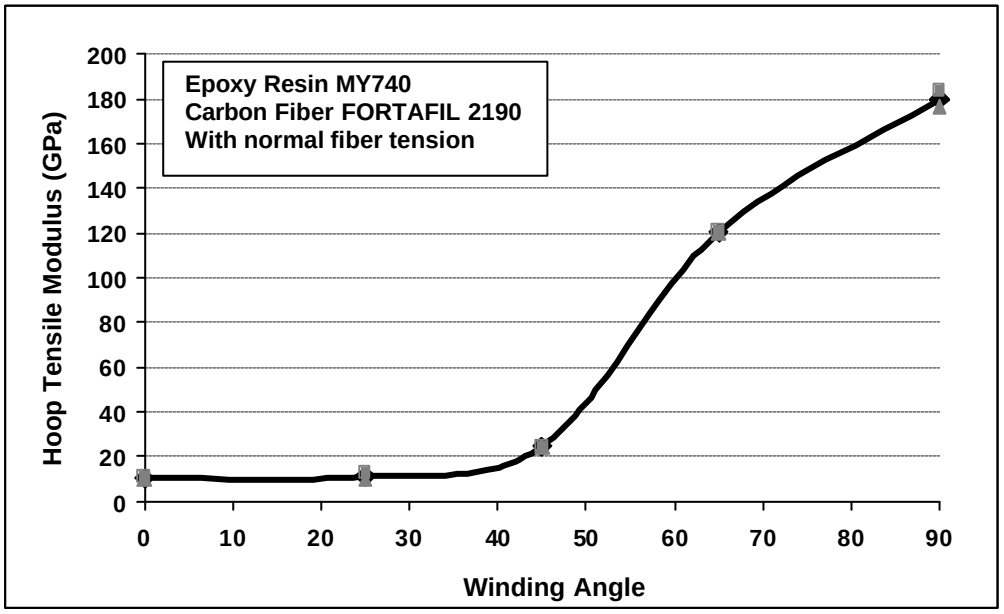

Figure 4.28 Hoop tensile modulus of elasticity vs. winding angle for specimens (fiber 5, resin 1, tension setting 1).

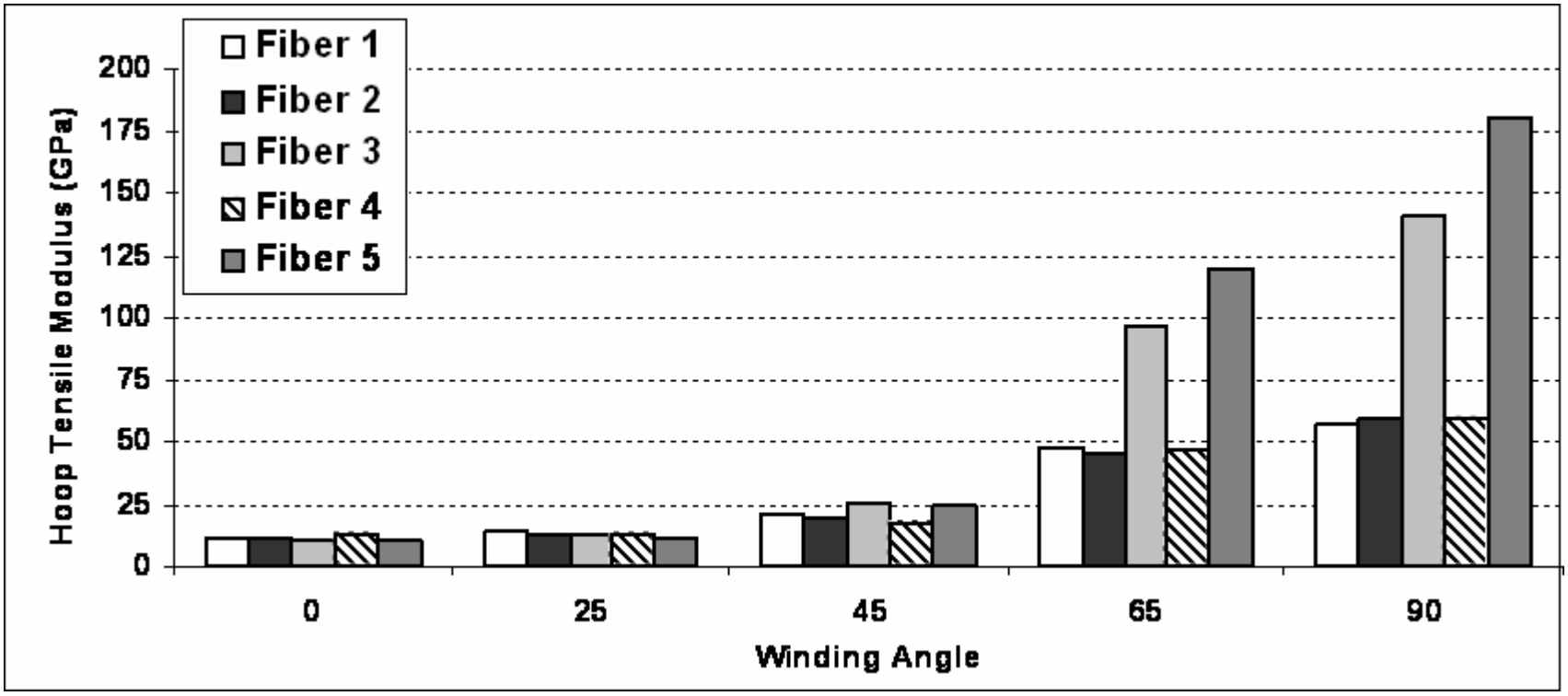

Figure 4.29 Comparison of hoop tensile modulus of elasticity of specimens having different fibers as a function of winding angle.

fibers, as long as the winding angles greater than 65^0 are concerned. This result can be better observed from Figure 4.29, which involves the comparison of hoop tensile modulus of elasticity of specimens having different fibers as a function of winding angle.

4.3.2 Tube Tensile Tests

The effect of winding angle, tension setting, and type of fiber and resin on the longitudinal tensile properties of tube tensile test specimens will be evaluated in this section of the thesis by using the tabulated results, given in the previous sections of the report.

In Figure 4.30, types of failure and their locations on tubular specimens, having $\pm 45^o$ (5231, 2231), $\pm 65^o$ (5241, 4141), and 90^o (3251, 1251) winding angles are compared. Photographs of both a carbon fiber and a glass fiber reinforced specimen are presented for each winding angles. As seen from the photographs, failure occurred usually at the middle section of the specimens. Less macroscopic damage was observed for these specimens compared to split-disk test specimens.

For specimens, having 90^o winding angle, cracking of matrix phase was observed dominantly, parallel to the winding direction of fibers (Figure 4.30(a - b)). Since rupture of fibers did not occur, less macroscopic damage and low failure strengths was obtained for these specimens.

For glass fiber reinforced specimens, having $\pm 65^o$ winding angle (Figure 4.30 d), the same mechanism was observed. In addition, delamination of $\pm 65^o$ layers was detected. The latter mechanism was observed more dominantly in $\pm 65^o$ carbon fiber reinforced specimens (Figure 4.30 (c)).

(a) Carbon fiber reinforced

$\theta = 90^o$

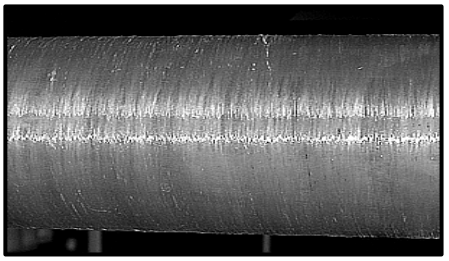

(b) Glass fiber reinforced

$\theta = 90^o$

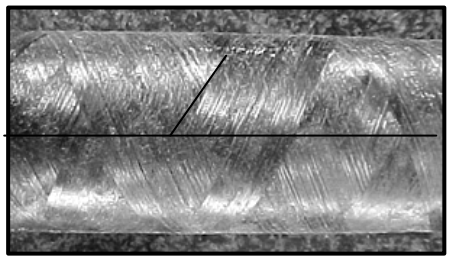

(c) Carbon fiber reinforced

$\theta = 65^o$

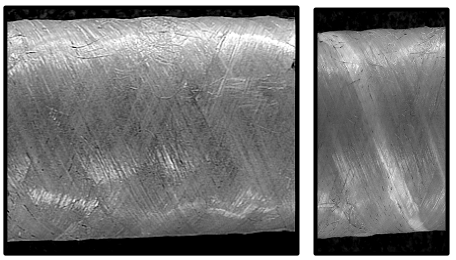

(d) Glass fiber reinforced

$\theta = 65^o$

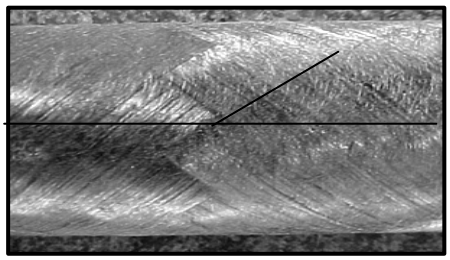

(e) Carbon fiber reinforced

$\theta = 45^o$

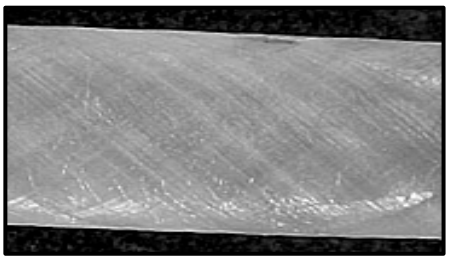

(f) Glass fiber reinforced

$\theta = 45^o$

Figure 4.30 Types of failure and their locations on carbon/glass fiber reinforced tube tensile test specimens.

For carbon fiber reinforced specimens, having ±45° winding angle (Figure 4.30 (e)), delamination of layers was also observed in a similar manner. For glass fiber reinforced specimens, having ±45° winding angle (Figure 4.30 (f)), delamination was observed less dominantly, which makes its macroscopic observation more difficult. Since the amount of fractured fibers is low for ±65° and ±45° winding angle specimens, comparable strength performance was obtained with 90° winding angle specimens.

According to Tables 4.18 and 4.19, it can be stated that tube tensile test specimens, having ±65°, and 90° winding angles showed similar performances. The tests, performed with ±45° filament-wound specimens resulted with relatively higher strength values, as expected. This result was plotted graphically in Figure 4.31, for specimens produced with resin system 1, and tension setting 1.

The effect of tension setting on longitudinal tensile properties of tube tensile test specimens can be understood by inspecting Figure 4.32. In that figure, longitudinal tensile strengths of tube tensile test specimens is plotted for the two cases, with tension and without tension. (The plot was obtained by using the results of the tests performed with specimens produced with resin system 1 and winding angle of ±45°).

From Figure 4.32, it was observed that the tube tensile test specimens, produced with extra tensioning of fibers show higher mechanical performance. Moreover, by comparing Figure 4.32 and 4.19-4.23, it can be stated that the effect of tension setting is more dominant for tube tensile test specimens compared to split-disk test specimens. This is actually an expected result since fiber tension is a processing parameter, effecting the defect-free production of specimens. Therefore, as the dimensions of the specimens increase, the effect of this parameter is expected to increase. (As the dimensions of specimens increase, defect-free production of specimens become more important).

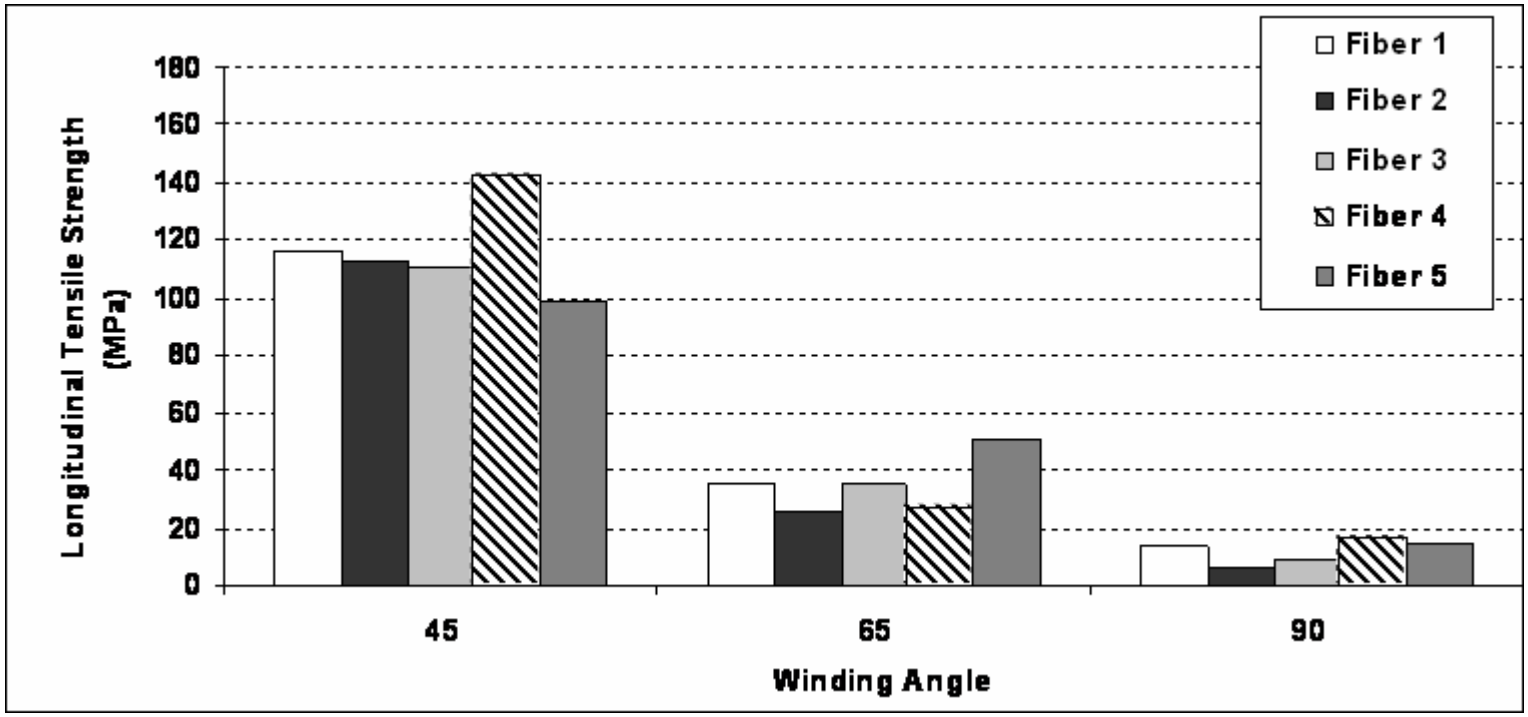

Figure 4.31 Comparison of longitudinal tensile strengths of tube tensile test specimens having different fibers as a function of winding angle.

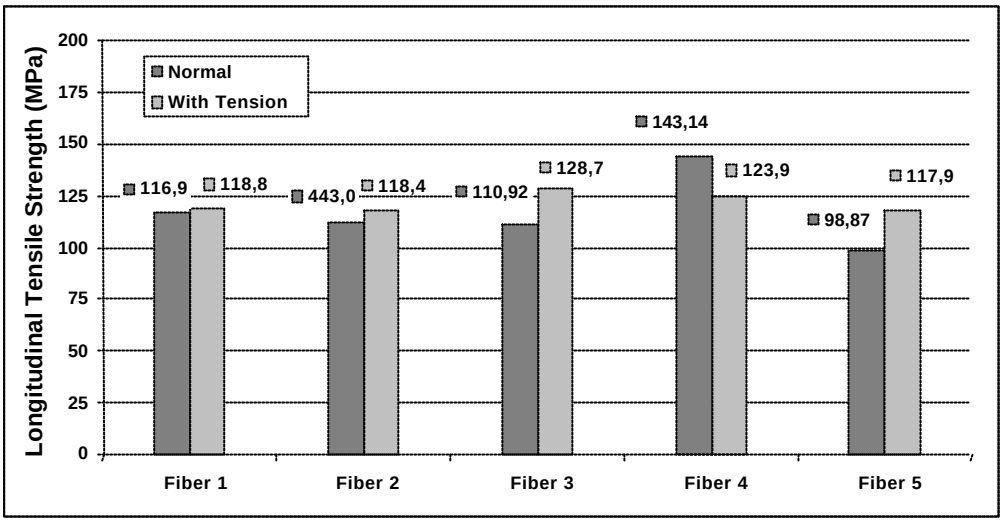

Figure 4.32 Comparison of longitudinal tensile strengths of tube tensile test specimens having ±45^{o} winding angle.

Differently from split-disk test results, carbon fiber reinforced specimens showed similar performance with glass fiber reinforced specimens. This difference was obtained since tube tensile test specimens tested under the scope of the thesis have winding directions, much different than the direction of loading (≥ 45^{o}). Due to the strong anisotropic character of graphitic structures of carbon fibers, even lower strength results was obtained compared to glass fibers. The graphitic structure consist of hexagonal layers, in which the bonding is covalent and strong, and the inter-layer bonds being weak Van der Walls bonds. This anisotropy arises due to this reason and can be clearly observed from Figure 4.31.

The effects of winding angle and fiber type on longitudinal tensile modulus of elasticity of specimens are presented in Figure 4.33. The plot was obtained by using the results of tube tensile tests, having resin system 1 and tension setting 2. According to figure, it is clear that tube tensile test specimens, having ±45, ±65°, and 90° winding angles showed similar performances. It is also obvious that stiffness results of carbon fiber reinforced specimens are more sensitive to structural anisotropy than strength results.

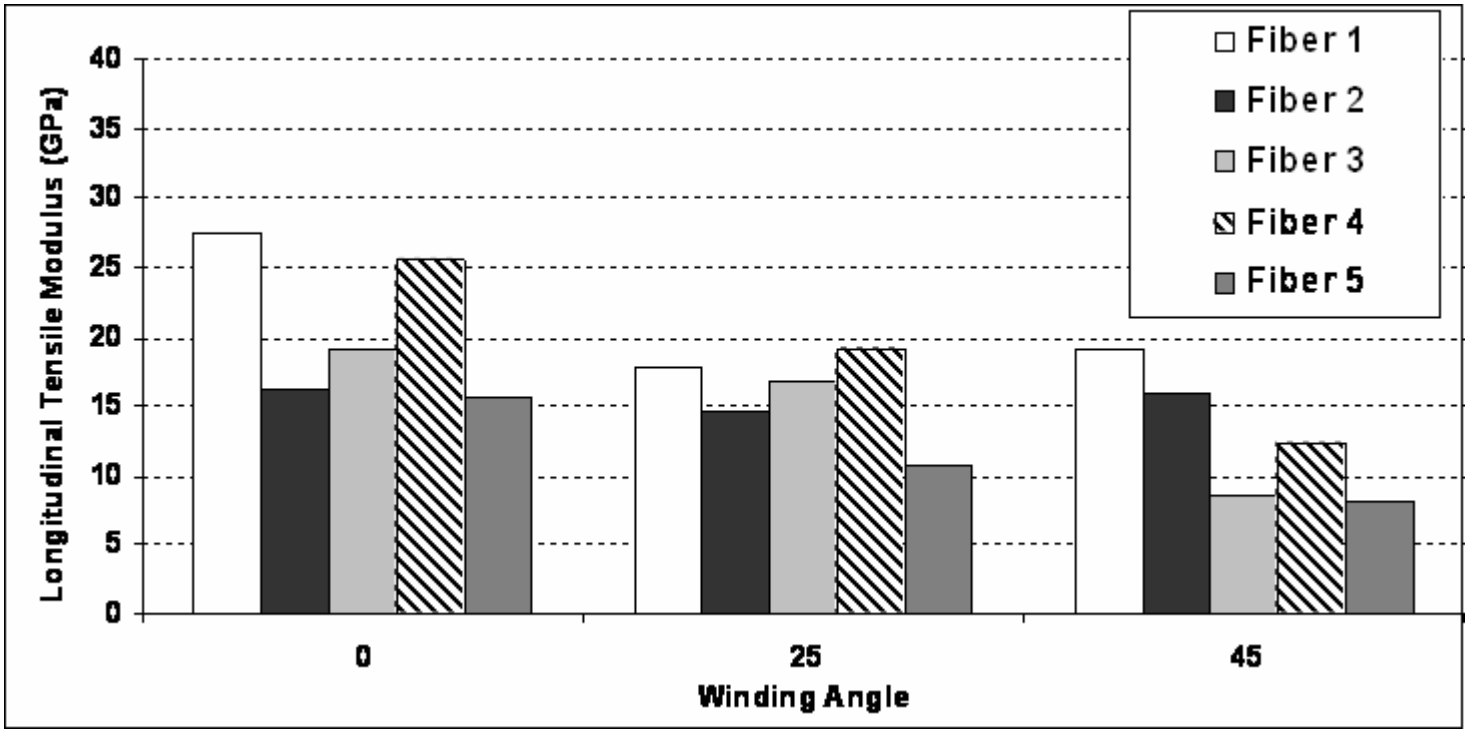

Figure 4.33 Comparison of longitudinal tensile modulus of elasticity of tube tensile test specimens having different fibers as a function of winding angle.

4.4 Results and Discussions of Simulation of Split-disk Tests

Modeling of split-disk testing of composite specimens, whose results were tabulated in the preceeding sections of this chapter, were performed mainly to verify the accuracy of the test results and to provide a comprehensive base to the study. This objective was fulfilled with the following procedure:

- During the split-disk testing of the specimens, the axial displacements of the two half split-disk sections, at the instant of maximum loading, were recorded.

- Loading of specimens was performed with small increments until the maximum loads, observed in the experiments was reached. These loads were applied as a distributed force on the inner surfaces (A_1) of the split disk test fixture (Figure 4.34). Therefore, the maximum pressure applied on these surfaces is:

$$\sigma_1 = \frac{P_{exp}}{A_1} \tag{4.1}$$

  where, P_{exp} is the maximum load observed in experiments, and σ_1 is the pressure applied on the inner surfaces(A_1) of the split-disk test fixture.

- The displacements of the split-disk test fixture (analysis output) were discussed comprehensively with the experimentally obtained data.

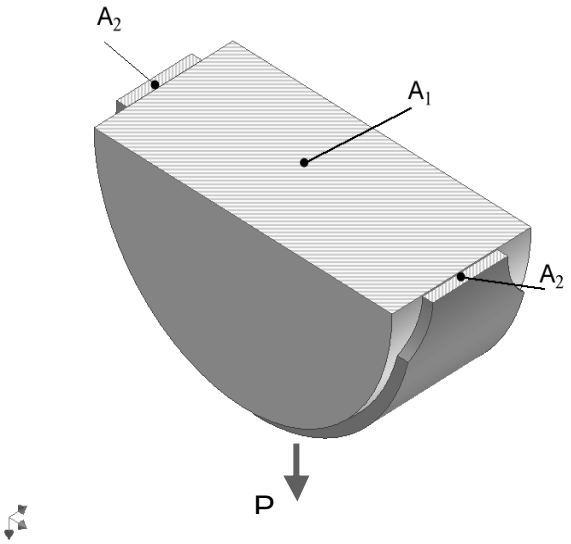

Figure 4.34 Schematic view of split-disk test fixture upon loading.

- The strain data, obtained in the analysis (from the gage section) were used in order to plot stress-strain graphs for the selected specimens. Load data were converted into strength data in correlation with Section 2.2.2.5, as follows:

$$\sigma_2 = \frac{P_{exp}}{2.A_2} = \sigma_h \qquad (4.2)$$

where, A_2 is the area of the gage section of specimens(Figure 4.43).

- These graphs were used so as to predict the hoop tensile modulus of elasticity of these specimens. (The slopes of the linear portion of these curves were determined, by least – square method, as stated in Section 4.2.1).

- This data were then compared with the experimental results.

The failure loads obtained in split-disk tests (the inputs for the analysis) and displacements of the two half split-disk sections, corresponding to these data (the experimental data, with which the results of the analysis was compared) are tabulated in Table 4.22, for the specimens, selected for the analysis. In Table 4.23, the displacements of the inner split-disk sections, computed in the analysis and the related percent errors are tabulated.

Table 4.22 Failure loads and maximum elongations of specimens, obtained experimentally.

Specimen Designation	Failure Load (P_{max}) (N)	Max. Elongation (mm)
1221	**2040.4**	**0.38**
1231	**6892.4**	**1.71**
1241	**25660.0**	**2.14**
3221	**1678.8**	**0.43**
3231	**6303.2**	**3.26**
3241	**31550.0**	**3.46**

Table 4.23 The displacement data of the inner split-disk sections, computed in the analysis and the related percent errors.

Specimen Name	Elongation at the	Error (%)
1221	**0.48**	**20,42**
1231	**0.92**	**85,25**
1241	**2.00**	**6,83**
3221	**0.39**	**10,63**
3231	**2.86**	**13,86**
3241	**2.49**	**39,07**

In Figures 4.35, 4.37, 4.39, 4.41, 4.43, and 4.45, the stress/strain plots, obtained from the analysis were presented. These graphs involve an initial linear region, followed by another linear region having relatively higher slope. This result is actually in good agreement with the experimentally obtained stress-strain curves (Figures 4.1 and 4.3). Due to the effect of the bending moment, imposed during the test at the split, between the split-disk test fixture, this unusual behaviour was observed.

In Figures 4.36, 4.38, 4.40, 4.42, 4.44, and 4.46 least square fitted stress-strain curves are presented. The initial linear region with a relatively smaller slope were not taken into account upon fitting the curve, due to the reason stated above. Therefore, these graphs were not ploted, starting from zero stress/strain. Hoop tensile modulus of elasticity results, obtained from these curves are tabulated in Table 4.24 and presented graphically in Figure 4.47. According to this figure, it can be stated that a good agreement between the results of the simulation and the experimental data was obtained as long as the glass fiber reinforced specimens were considered. The results of the simulation for carbon fiber reinforced specimens have larger errors.

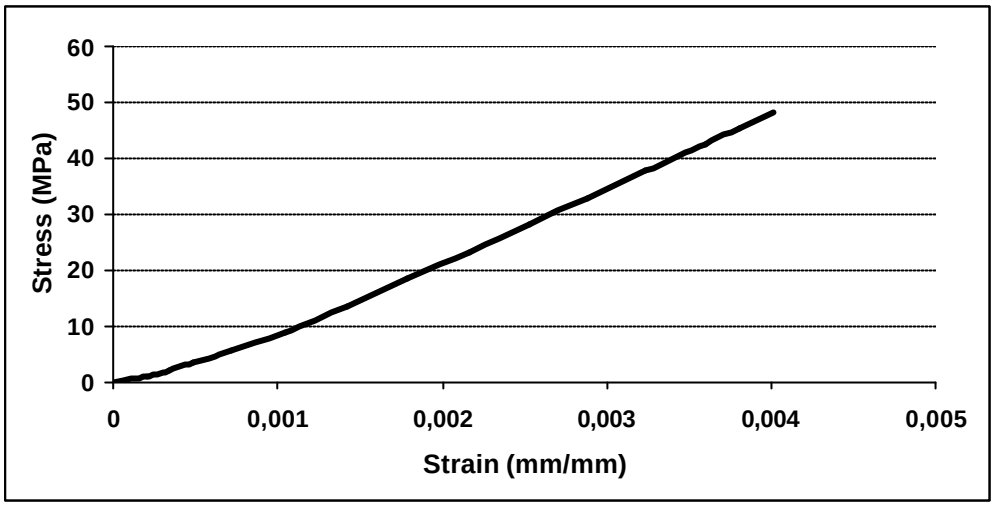

Figure 4.35 Hoop tensile stress–strain graph of split-disk test specimen 1221, obtained by FEM.

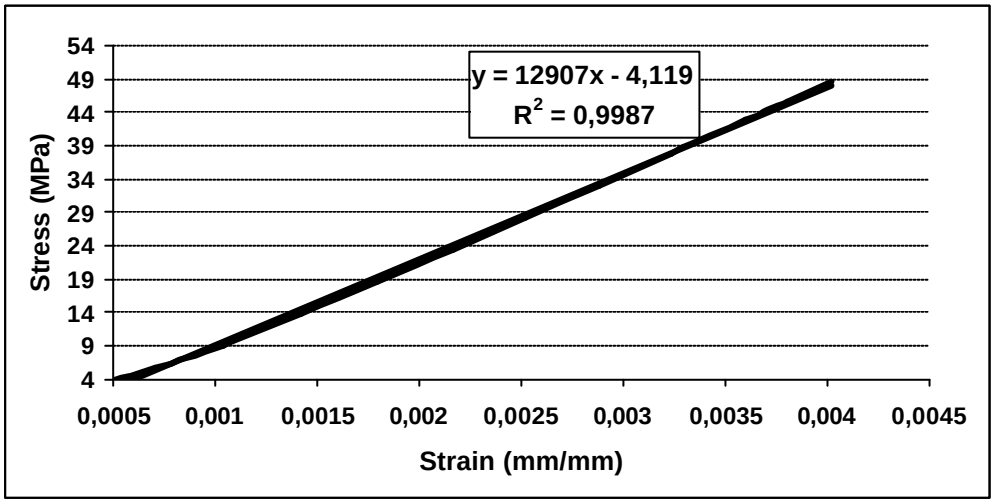

Figure 4.36 Least-square fitted stress-strain graph of 1221 split-disk test specimen, obtained by FEM.

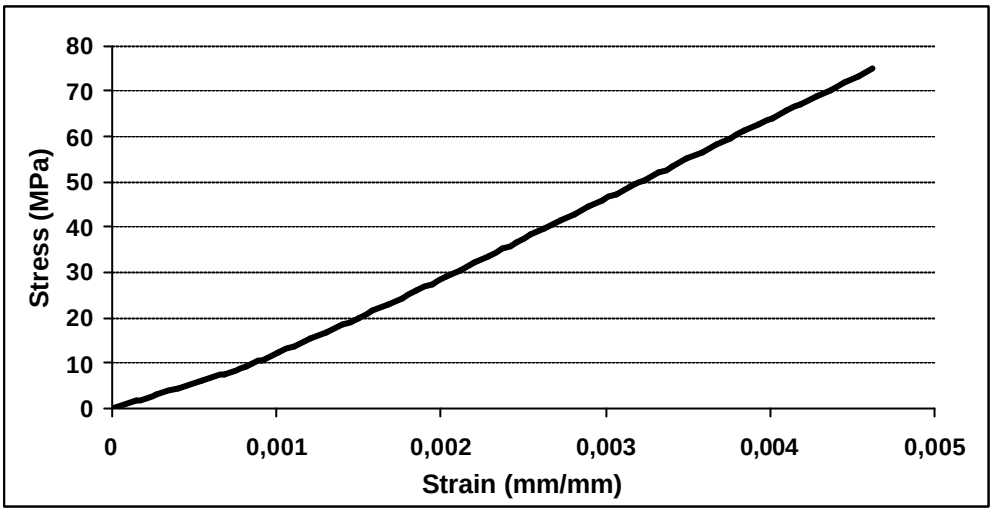

Figure 4.37 Hoop tensile stress–strain graph of split-disk test specimen 1231, obtained by FEM.

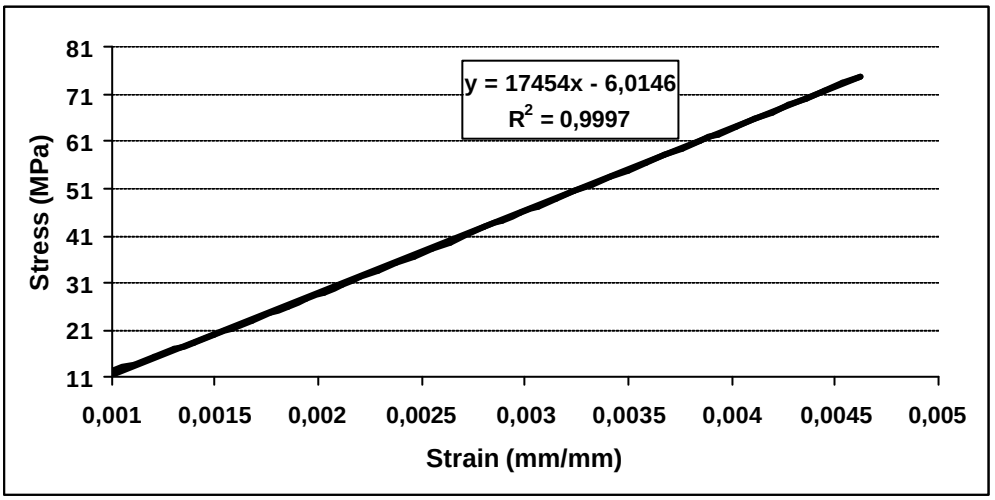

Figure 4.38 Least-square fitted stress-strain graph of 1231 split-disk test specimen, obtained by FEM.

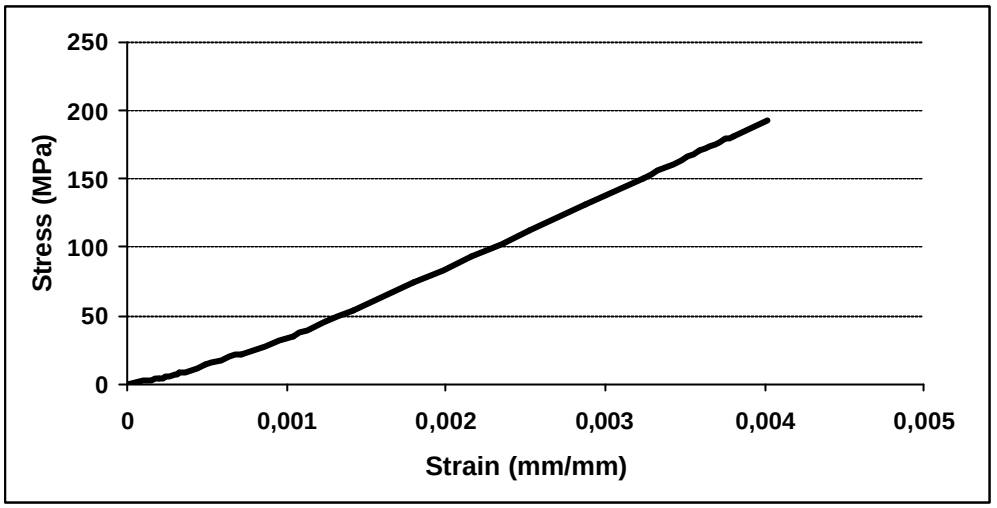

Figure 4.39 Hoop tensile stress–strain graph of split-disk test specimen 1241, obtained by FEM.

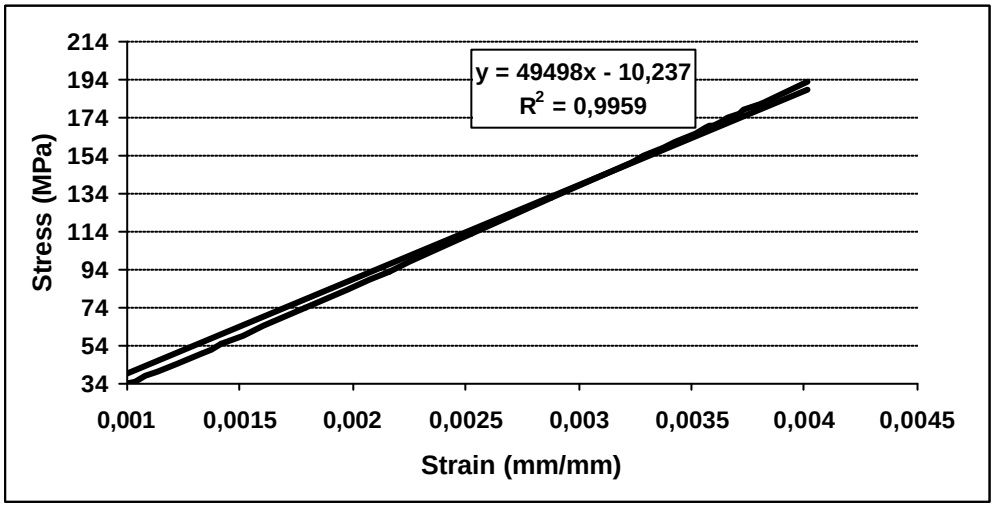

Figure 4.40 Least-square fitted stress-strain graph of 1241 split-disk test specimen, obtained by FEM.

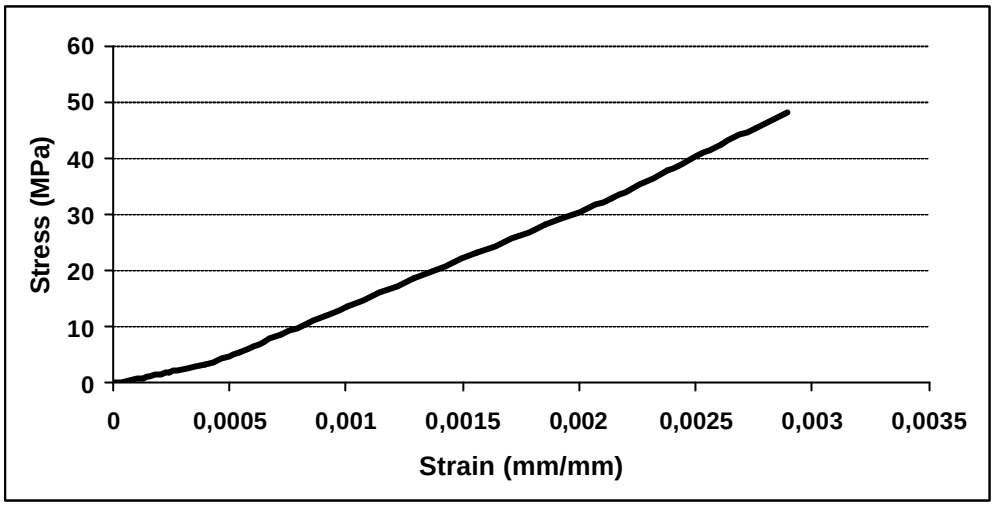

Figure 4.41 Hoop tensile stress–strain graph of split-disk test specimen 3221, obtained by FEM.

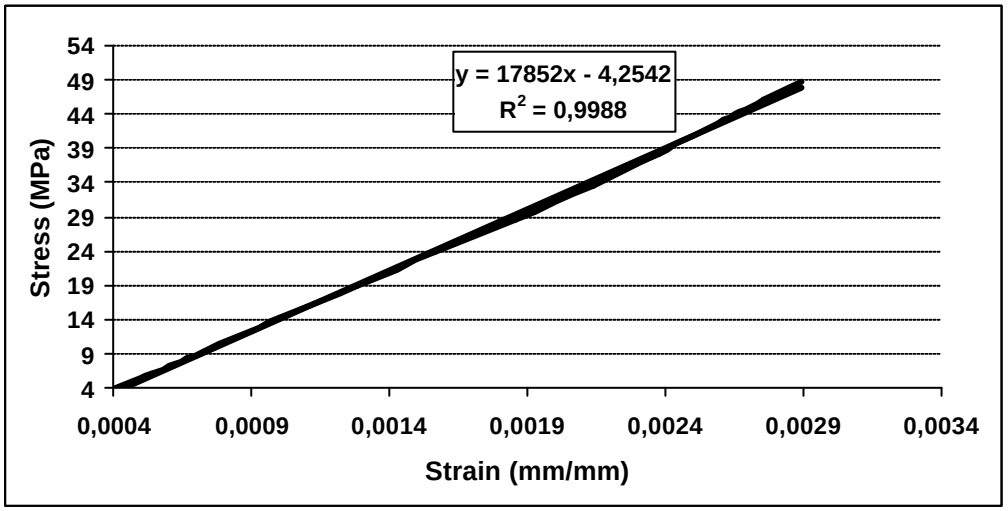

Figure 4.42 Least-square fitted stress-strain graph of 3221 split-disk test specimen, obtained by FEM.

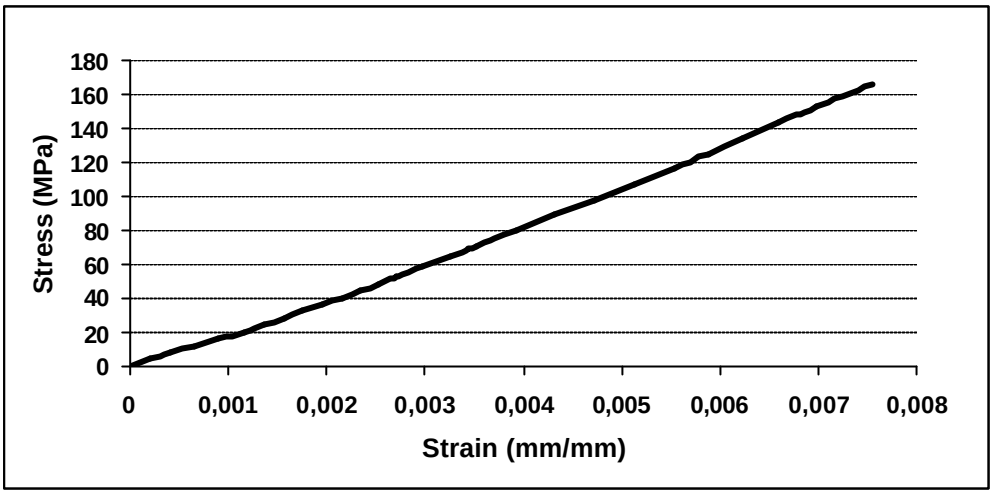

Figure 4.43 Hoop tensile stress–strain graph of split-disk test specimen 3231, obtained by FEM.

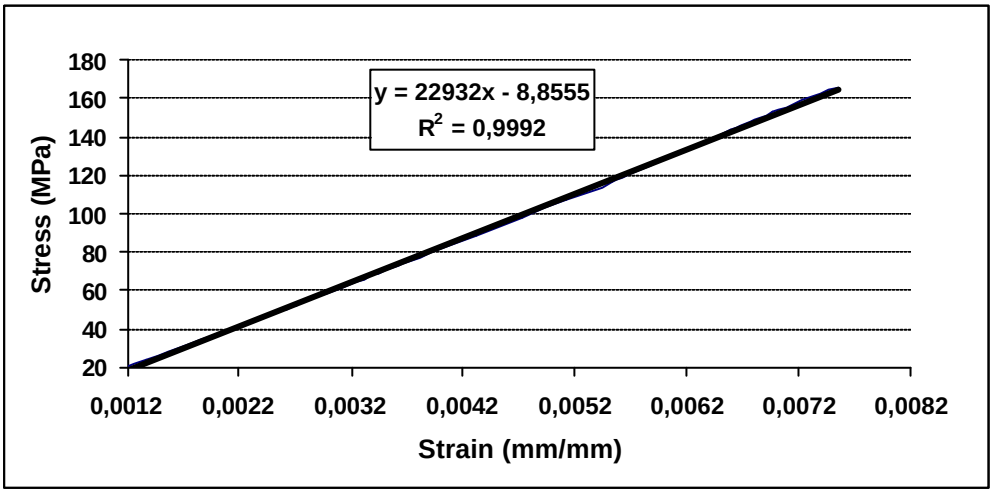

Figure 4.44 Least-square fitted stress-strain graph of 3231 split-disk test specimen, obtained by FEM.

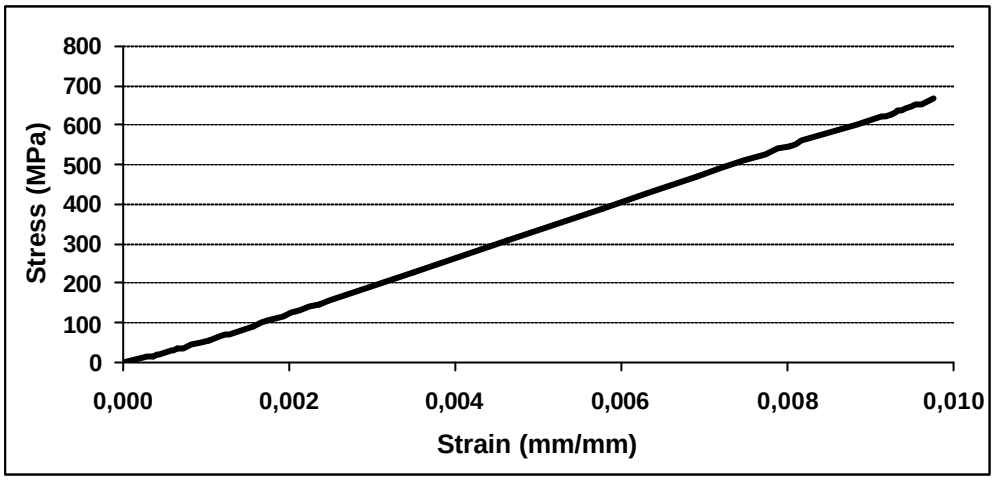

Figure 4.45 Hoop tensile stress–strain graph of split-disk test specimen 3241, obtained by FEM.

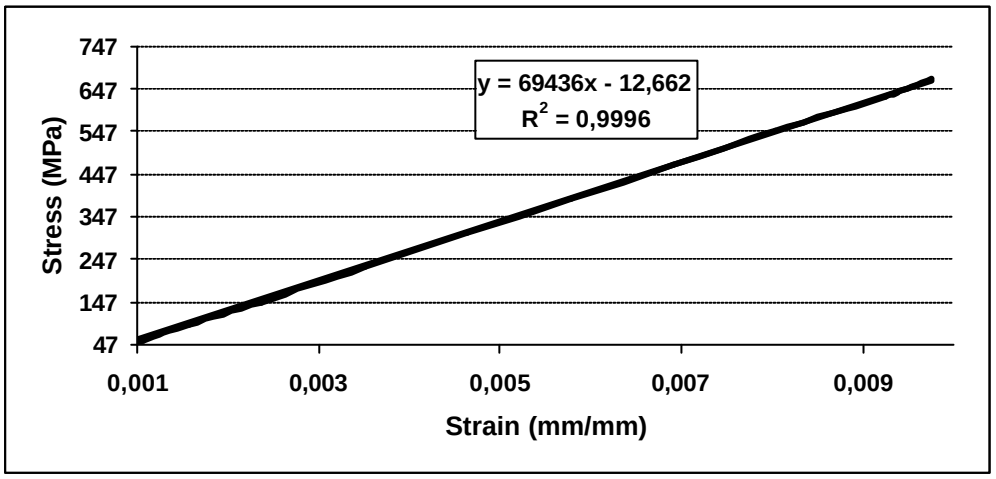

Figure 4.46 Least-square fitted stress-strain graph of 3241 split-disk test specimen, obtained by FEM.

Table 4.24 Tabulated hoop tensile modulus of elasticity results computed by FEM and obtained from experiments.

	Hoop Tensile Modulus (FEM) (GPa)	Hoop Tensile Modulus (Exp.) (GPa)	Error (%)
1221	**12.9**	**12.1**	**6.0**
1231	**17.5**	**18.1**	**3.6**
1241	**49.5**	**49.9**	**0.8**
3221	**17.9**	**8.8**	**51.0**
3231	**22.9**	**16.8**	**26.6**
3241	**69.4**	**94.0**	**35.3**

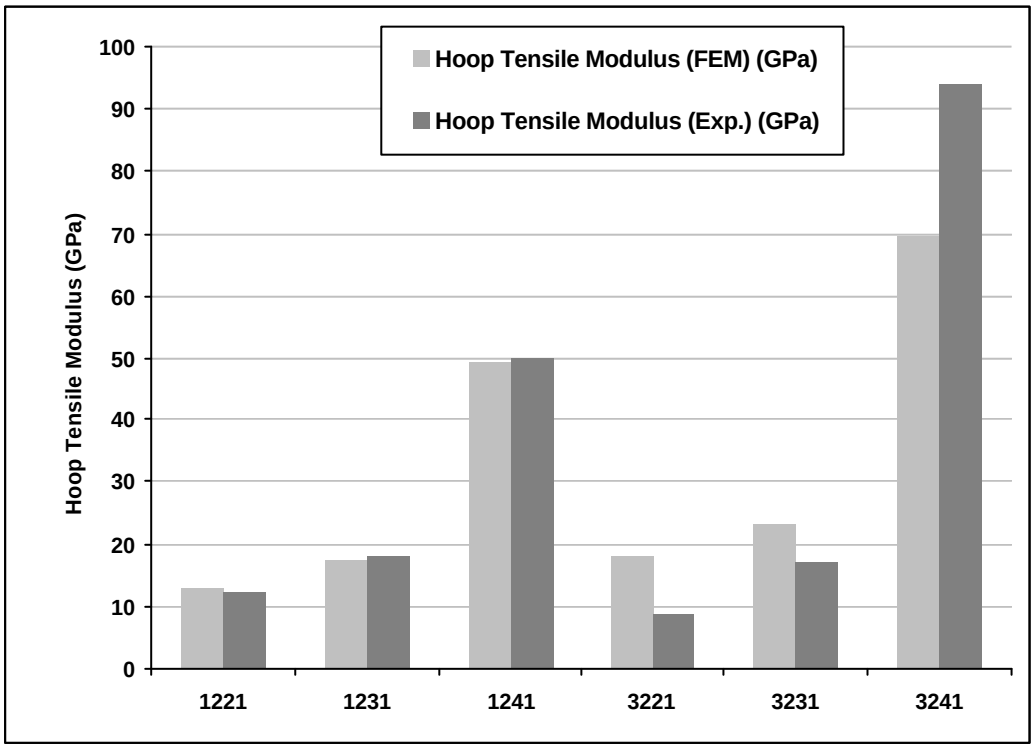

Figure 4.47 Comparison of hoop tensile modulus of elasticity results obtained by FEM and experiments.

CHAPTER 5

CONCLUSION

This study was aimed to fulfill the requirement of experimental data for the characterization of filament-wound composite tubes. For this purpose, hundred different testing groups were defined by considering five winding angles, two reinforcements, two resin systems and two tension settings. Tensile and split-disk tests were performed with specimens from each group. The results of these experiments were summarized in Table 5.1 – 5.2.

Table 5.1 Experimental results of glass fiber reinforced specimens

Tube Tensile Tests					
		45°	65°	90°	
Longitudinal Tensile Strength (MPa)		143-106	40-24	17-6	
Longitudinal Modulus (GPa)		28-20	22-15	20-14	
Split-disk Tests					
	0°	25°	45°	65°	90°
Hoop Tensile Strength (MPa)	11-6	50-28	198-141	584-482	895-701
Hoop Modulus (GPa)	14-9	14-11	30-17	55-45	65-55

Table 5.2 Experimental results of carbon fiber reinforced specimens.

Tube Tensile Tests					
		45°	65°	90°	
Longitudinal Tensile Strength (MPa)		129-97	51-36	18-8	
Longitudinal Modulus (GPa)		22-16	17-9	13-8	
Split-disk Tests					
	0°	25°	45°	65°	90°
Hoop Tensile Strength (MPa)	5-2	51-34	172-142	691-616	1201-1009
Hoop Modulus (GPa)	11-8	14-9	26-16	120-93	191-141

It was observed that the longitudinal and hoop tensile stress-strain curves are linear up to the point of failure. For split-disk test specimens having 0^o winding angle, deviation from linearity was detected as the failure occurs dominantly by matrix cracking. The experimental data were used to investigate the general distribution of hoop tensile properties of the selected composites as a function of winding angle. Winding angle dependence of hoop tensile properties of filament-wound composite tubes was visualized efficiently by least-square fitting through data points by using a higher order polynomial. It was observed that both hoop tensile stength and tensile modulus of elasticity depend strongly on the winding angle (fiber direction) of specimens.

It was observed that split-disk test is an effective method for determination of hoop tensile properties of filament-wound tubular structures. Reliable results were obtained with low standard deviations. Tests with carbon fiber reinforced specimens resulted with relatively larger deviations.

Fiber fracture and fiber-matrix debonding is observed to be the dominant failure mechanisms for split-disk test specimens, having 90^o winding angle. For specimens having 65^o winding angle, in addition to these mechanisms, delamination of layers was detected. For 45^o filament-wound specimens, fiber-matrix debonding occurred more dominantly. For specimens, having 25^o winding angle fiber breakage was very limited, and the specimens failed with the rupture of the matrix phase, which causes the formation of less macroscopic damage on the specimens and low failure strength.

In almost all of the split-disk tests, failure occurred in the gage section of the specimens. Less macroscopic damage was observed in tube tensile testing of specimens compared to split-disk tests. Failure of tube tensile test specimens occurred usually from the middle section.

Tests were performed with two different epoxy+hardener systems. The properties of these systems are quite similar, with a slight difference in glass transiton temperature and resin viscocity. The effect of resin system on mechanical performance was inspected and it was found that the effect of resin system is negligible as long as the resin systems stated above are considered.

It was observed that the specimens produced by carbon fibers showed much better mechanical properties compared to the ones produced with glass fibers for loading directions close to the direction of loading.

The effect of tension setting on longitudinal and hoop tensile properties of composite tubes were determined. An increase was observed in longitudinal/hoop tensile properties of tube tensile/split-disk test specimens, for winding angles close to the direction of loading. It can be further stated that tube tensile test specimens are more sensitive to the tension setting of fibers.

The split-disk test of selected composite specimens was simulated by finite element method. Hoop tensile modulus of elasticity and the elongation at the instant of maximum loading were computed for the selected specimens. The experimental results were used as material data to perform the simulation. The results of the analysis were then compared with the experimental results. A good agreement between the simulation results and the experimental work was obtained for glass fiber reinforced specimens.

For carbon fiber reinforced specimens, the deviation of the numerical results from the experimental data is significant. This is caused by the usage of inaccurate material data during the analysis for carbon fiber reinforced specimens. Some part of the deviation between the numerical results and the experimental data can be due to the friction model used in the analysis. Rough contac surface with infinite friction resistance was defined in the analysis between the target and contac surfaces whereas in reality sliding along the contac/target surface can occur.

In the computational study, structures were assumed to be defect-free. However, this assumption can not be strictly fullfilled for real test specimens. Test specimens can not be perfectly defect-free, which can result in early failure of specimens compared to numerical results.

As a future study, longitudinal tensile properties of tubular specimens having winding angles close to the direction of loading can be tested with tube tensile test method. This objective could not be achieved in this study due to the requirement of better test fixture design. Therefore, by the improvements in tube tensile test fixture, variation of longitudinal tensile properties as a function of winding angle can be obtained, which can then be compared with the split-disk test results.

Numerical solution for carbon fiber reinforced specimens can be improved by the usage of more accurate material data. Also, numerical solution can be further developed by using an iterative procedure to define failure loads, by the application of a suitable failure criteria.

There are some studies in literature, aiming to optimize the ring testing system [22]. In the proposed design, the lateral (or radial) displacement is blocked in order to reduce the bending moment to a minimum. Therefore, as a further study, this new design can be taken into consideration upon making split-disk tests.

REFERENCES

[1] I. M. Daniel, O. Ishai, Engineering Mechanics of Composite Materials, Oxford University Press, 1994.

[2] S. T. Peters, W. D. Humphrey, R. F. Foral, Filament Winding Composite Structure Fabrication, Second Edition.

[3] S. W. Tsai, Composite Design, Thick Composites, Ohio, USA, 1987.

[4] C. S. Chouchaoui, O. O. Ochoa, "Similitude Study for a Laminated Cylindrical Tube Under Tensile, Torsion, Bending, Internal and External Pressure" Composite Structures, 44 (1999) 221 – 229.

[5] C. Cazeneuve, P. Joguet, J. C. Maile and C. Oytana, "Predicting the Mechanical Behavior of Kevlar/epoxy and Carbon/epoxy Filament-wound Tubes" Composites, 1992, 23, 6, 415 - 424.

[6] C. Wüthrich, "Thick-Walled Composite Tubes under Mechanical and Hydrothermal Loading" Composites, 1992, 23, 6, 407-413.

[7] L. P. Kollar, M. J. Paterson and G. S. Springer, "Composite Cylinders Subjected to Hydrothermal and Mechanical Loads" International Journal of Solid Structures, 1992, 29, 12, 1519-1534.

[8] J. C. Prucz, J. D' Acquisto and J. E. Smith, "Dynamic-Response of Composite Pressure-Vessels to Inertia Loads", Journal of Pressure Vessel Technology, 1991, 113, 86-91.

[9] S. G. Lekhnitskii, Theory of Elasticity of an Anisotropic Body, Mir Publishers, Moscow, Soviet Union, 1981.

[10] P. M. Wild, G. W. Vickers, "Analysis of Filament-wound Cylindrical Shells Under Combined Centrifugal, Pressure, and Axial Loading", Composites Part A, 28A, 1997, 47 – 55.

[11] C. S. Chouchaoui, O. O. Ochoa, Composite Structures, 44, 1999, 221 – 229.

[12] C. T. Sun, S. Li, "Three-Dimensional Effective Elastic Constants for Thick Laminates", Journal of Composite Materials, 1988, Vol. 22, 629-639.

[13] S. Aleçakir,"Structural Design and Experimental Analysis of a Filament-Wound Composite Tube Under Combined Loading", M. S. Thesis, Middle East Technical University, 1998.

[14] K. Chandrashekhara, and P. Gopalakrishnan, "Elasticity Solution for a Multilayered Transversely Isotropic Circular Cylindrical Shell", Journal of Applied Mechanics, 1982, Vol. 49, 108 – 114.

[15] M. F. S. Al-Khalil, P. D. Soden, "Theoretical Through-thickness Elastic Constants for Filament-wound Tubes", Int. J. Mech Sci. Vol. 36, No. 1, pp 49-62, 1994.

[16] Qi Zhao, S. V. Hoa, "Triaxial Woven Fabric (TWF) Composites with Open Holes (Part 1): Finite Element Models for Analysis", Journal Of Composite Materials, Vol. 37. No 9, 2003, 763 – 789.

[17] Ala Tabiei, Ivelin Ivanov, "Fiber Reorientation in Laminated and Woven Composites for Finite Element Simulations", J. of Thermoplastic Composite Materials, Vol.16, September 2003, 457 – 473.

[18] Doh YD, Hong CS, J. Reinforced Plastic Composites, "Progressive failure analysis for filament wound pressure vessel", 1995, 14 (12), 1278-1306.

[19] Jeusette JP, Laschet G, Chapentier P, Deloo Ph, "Finite element analysis of composite revolution structures wound by wide plies", Composite Structures, 1987, 8, 221-237.

[20] K. A. Ilhan, "Computational Design of Composite Tubes and Pressure Vessels", M. S. Thesis, Middle East Technical University, 2001.

[21] M. G. Garrell, Albert J. Shih, Edgar Lara-Curzio, and Ronald O. Scattergood, "Finite-Element Analysis of Stress Concentration in ASTM-D 638 Tension Specimens", Journal of Testing and Evaluation, Vol. 31, No 1, 52-57, Paper ID JTE 11402_311.

[22] S. Arsene, J. Bai, "A New Approach to Measuring Transverse Properties of Structural Tubing by a Ring Test", Journal of Testing and Evaluation, Vol. 24, No. 6, November 1996, 386-391.

[23] D. Cohen, "Influence of Filament-winding Parameters on Composite Vessel Quality and Strength", Composites Part A 28A (1997) 1035-1047.

[24] D. Cohen, Y. T. Toombes, A. K. Johnson, M F. Hansen, "Pressurized Ring Test for Composite Pressure-Vessel Hoop Strength and Stiffness Evaluation", Journal of Composites Technology and Research, 1995, 17(4), 331-340.

[25] H. Wang, R. Bouchard, R. Eagleson, P. Martin, and W. R. Tyson, "Ring Hoop Tension Test (RHTT): A Test for Transverse Tensile Properties of Tubular Materials", Journal of Testing and Evaluation, Vol. 30, No. 5, September 2002, 382-391.

[26] C. S. Lee, W. Hwang, H.C Park, and K. S. Han, "Failure of Carbon/epoxy Composite Tubes under Combined Axial and Torsional Loading I. Experimental Results and Prediction of Biaxial Strength by the use of Neutral Networks", Composites Science and Technology, 59 (1999), 1779-1788.

[27] Jinbo Bai, Philippe Seeleuthner, and P. Bompard, "Mechanical Behaviour of $\pm 55^{o}$ Filament-wound Glass fiber/Epoxy Resin Tubes: I. Microstructural Analyses, Mechanical Behaviour and Damage Mechanism of Composite Tubes Under Pure Tensile Loading, Pure Internal Pressure, and Combined Loading", Composite Science ad Technology, 57 (1997), 141-153.

[28] M. Caroll, F. Ellyin, D. Kujawski, and A. S. Chiu, "The Rate Dependent Behaviour of $\pm 55^{o}$ Filament-wound Glass fiber/Epoxy Tubes Under Biaxial Loading", Composite Science and Technology 55 (1995) 391-403.

[29] A. E. Ayral, " Tensile, Flexural, Inplane Shear, and Impact Properties of Polyether-Ether-Ketone (PEEK) Matrix Reinforced by Carbon Fiber Composites", M. S. Thesis, Middle East Technical University, 2001.

[30] Baris Elektrik Endüstrisi A. S., MISAG 39 REPORT, Design of High Pressure Resistant Filament-Wound Composite Tubes, 1996.

[31] American Society for Metals, Metals Handbook. Ed. by Taylor Lyman, 8th edition.

[32] Annual Book of ASTM Standards D 3039/D 3039M-00, 'Standard Test Method for Tensile Properties of Polymer Matrix Composites'.

[33] Annual Book of ASTM Standards D 2290-00, 'Standard Test Method for Apparent Hoop Tensile Strength of Plastic or Reinforced Plastic Pipe by Split Disk Method'.

[34] Annual Book of ASTM Standards D 2105, 'Standard Test Method for Longitudinal Tensile Properties of "Fiberglass" (Glass-Fiber-Reinforced Thermosetting-Resin) Pipe and Tube'.

[35] John W. Bull, Finite Element Applications to Thin-Walled Structures, Elsevier Applied Science.

[36] ANSYS Workbench 7.1, User's Manual.

APPENDIX A

Table A.1 Winding configuration and tension setting for specimens 1111 through 3152 .

Specimen Designation	Winding Configuration	Tension Setting	Specimen Designation	Winding Configuration	Tension Setting
1111	$(0)_2$	Without weight	2112	$(0)_2$	With 1.5 kg weight
1121	$(\pm25)_2$	Without weight	2122	$(\pm25)_2$	With 1.5 kg weight
1131	$(\pm45)_2$	Without weight	2132	$(\pm45)_2$	With 1.5 kg weight
1141	$(\pm65)_2$	Without weight	2142	$(\pm65)_2$	With 1.5 kg weight
1151	$(90)_4$	Without weight	2152	$(90)_4$	With 1.5 kg weight
1112	$(0)_2$	With 1.5 kg weight	2211	$(0)_2$	Without weight
1122	$(\pm25)_2$	With 1.5 kg weight	2221	$(\pm25)_2$	Without weight
1132	$(\pm45)_2$	With 1.5 kg weight	2231	$(\pm45)_2$	Without weight
1142	$(\pm65)_2$	With 1.5 kg weight	2241	$(\pm65)_2$	Without weight
1152	$(90)_4$	With 1.5 kg weight	2251	$(90)_4$	Without weight
1211	$(0)_2$	Without weight	2212	$(0)_2$	With 1.5 kg weight
1221	$(\pm25)_2$	Without weight	2222	$(\pm25)_2$	With 1.5 kg weight
1231	$(\pm45)_2$	Without weight	2232	$(\pm45)_2$	With 1.5 kg weight
1241	$(\pm65)_2$	Without weight	2242	$(\pm65)_2$	With 1.5 kg weight
1251	$(90)_4$	Without weight	2252	$(90)_4$	With 1.5 kg weight
1212	$(\pm25)_2$	With 1.5 kg weight	3111	$(0)_2$	Without weight
1222	$(\pm25)_2$	With 1.5 kg weight	3121	$(\pm25)_3$	Without weight
1232	$(\pm45)_2$	With 1.5 kg weight	3131	$(\pm45)_3$	Without weight
1242	$(\pm65)_2$	With 1.5 kg weight	3141	$(\pm65)_4$	Without weight
1252	$(90)_4$	With 1.5 kg weight	3151	$(90)_6$	Without weight
2111	$(0)_2$	Without weight	3112	$(0)_2$	With 1.5 kg weight
2121	$(\pm25)_2$	Without weight	3122	$(\pm25)_3$	With 1.5 kg weight
2131	$(\pm45)_2$	Without weight	3132	$(\pm45)_3$	With 1.5 kg weight
2141	$(\pm65)_2$	Without weight	3142	$(\pm65)_4$	With 1.5 kg weight
2151	$(90)_4$	Without weight	3152	$(90)_6$	With 1.5 kg weight

Table A.2 Winding configuration and tension setting for specimens 3211 through 5252.

Specimen Designation	Winding Configuration	Tension Setting	Specimen Designation	Winding Configuration	Tension Setting
3211	$(0)_2$	Without weight	4212	$(0)_2$	With 1.5 kg weight
3221	$(\pm25)_3$	Without weight	4222	$(\pm25)_3$	With 1.5 kg weight
3231	$(\pm45)_2$	Without weight	4232	$(\pm45)_3$	With 1.5 kg weight
3241	$(\pm65)_4$	Without weight	4242	$(\pm65)_3$	With 1.5 kg weight
3251	$(90)_6$	Without weight	4252	$(90)_6$	With 1.5 kg weight
3212	$(0)_2$	With 1.5 kg weight	5111	$(0)_2$	Without weight
3222	$(\pm25)_3$	With 1.5 kg weight	5121	$(\pm25)_2$	Without weight
3232	$(\pm45)_3$	With 1.5 kg weight	5131	$(\pm45)_2$	Without weight
3242	$(\pm65)_4$	With 1.5 kg weight	5141	$(\pm65)_3$	Without weight
3252	$(90)_6$	With 1.5 kg weight	5151	$(90)_5$	Without weight
4111	$(0)_2$	Without weight	5112	$(0)_2$	With 1.5 kg weight
4121	$(\pm25)_3$	Without weight	5122	$(\pm25)_2$	With 1.5 kg weight
4131	$(\pm45)_3$	Without weight	5132	$(\pm45)_2$	With 1.5 kg weight
4141	$(\pm65)_3$	Without weight	5142	$(\pm65)_3$	With 1.5 kg weight
4151	$(90)_7$	Without weight	5152	$(90)_5$	With 1.5 kg weight
4112	$(0)_2$	With 1.5 kg weight	5211	$(0)_2$	Without weight
4122	$(\pm25)_3$	With 1.5 kg weight	5221	$(\pm25)_2$	Without weight
4132	$(\pm45)_3$	With 1.5 kg weight	5231	$(\pm45)_2$	Without weight
4142	$(\pm65)_3$	With 1.5 kg weight	5241	$(\pm65)_3$	Without weight
4152	$(90)_6$	With 1.5 kg weight	5251	$(90)_5$	Without weight
4211	$(0)_2$	Without weight	5212	$(0)_2$	With 1.5 kg weight
4221	$(\pm25)_3$	Without weight	5222	$(\pm25)_2$	With 1.5 kg weight
4231	$(\pm45)_3$	Without weight	5232	$(\pm45)_2$	With 1.5 kg weight
4241	$(\pm65)_3$	Without weight	5242	$(\pm65)_3$	With 1.5 kg weight
4251	$(90)_7$	Without weight	5252	$(90)_5$	With 1.5 kg weight

APPENDIX B

Table B.1 Split-disk test specimen dimensions for 1111-1 through 1212-5.

Specimen Designation	Minimum Thickness (mm)	Minimum Width (mm)	Reduced Sec. Area (mm^2)	Specimen Designation	Minimum Thickness (mm)	Minimum Width (mm)	Reduced Sec. Area (mm^2)
1111-1	0.99	14.76	14.61	1142-1	1.54	14.70	22.64
1111-2	0.99	14.76	14.61	1142-2	1.41	14.73	20.77
1111-3	0.94	14.80	13.91	1142-3	1.47	14.70	21.61
1111-4	0.93	14.78	13.75	1142-4	1.49	14.76	21.99
1111-5	0.99	14.76	14.61	1142-5	1.40	14.69	20.57
1121-1	1.73	14.86	25.71	1152-1	1.47	14.64	21.52
1121-2	1.78	14.77	26.29	1152-2	1.48	14.65	21.68
1121-3	1.68	14.83	24.91	1152-3	1.49	14.69	21.89
1121-4	1.64	14.77	24.22	1152-4	1.47	14.76	21.70
1121-5	1.67	14.81	24.73	1152-5	1.54	14.72	22.67
1131-1	1.54	14.72	22.67	1211-1	1.45	14.91	21.62
1131-2	1.68	14.71	24.71	1211-2	1.64	14.77	24.22
1131-3	1.53	14.77	22.60	1211-3	1.62	14.73	23.86
1131-4	1.47	14.75	21.68	1211-4	1.52	14.81	22.51
1131-5	1.68	14.74	24.76	1211-5	1.47	14.87	21.86
1141-1	1.43	14.60	20.88	1221-1	1.79	14.89	26.65
1141-2	1.52	14.67	22.30	1221-2	1.81	14.81	26.80
1141-3	1.51	14.27	21.55	1221-3	1.96	14.76	28.93
1141-4	1.44	14.67	21.12	1221-4	1.98	14.87	29.44
1141-5	1.49	14.66	21.84	1221-5	1.88	14.87	27.96
1151-1	1.49	14.58	21.72	1231-1	1.49	14.69	21.89
1151-2	1.56	14.66	22.87	1231-2	1.59	14.68	23.34
1151-3	1.54	14.64	22.55	1231-3	1.60	14.80	23.68
1151-4	1.54	14.64	22.55	1231-4	1.48	14.74	21.82
1151-5	1.56	14.66	22.87	1231-5	1.59	14.73	23.42
1112-1	1.45	14.91	21.62	1241-1	1.53	14.74	22.55
1112-2	1.64	14.77	24.22	1241-2	1.53	14.69	22.48
1112-3	1.62	14.73	23.86	1241-3	1.44	14.69	21.15
1112-4	1.52	14.81	22.51	1241-4	1.52	14.69	22.33
1112-5	1.47	14.87	21.86	1241-5	1.48	14.62	21.64
1122-1	1.79	14.72	26.35	1251-1	1.49	14.74	21.96
1122-2	1.76	14.87	26.17	1251-2	1.52	14.69	22.32
1122-3	1.84	14.73	27.10	1251-3	1.50	14.72	22.08
1122-4	1.88	14.77	27.77	1251-4	1.46	14.79	21.59
1122-5	1.82	14.86	27.05	1251-5	1.45	14.72	21.34
1132-1	1.55	14.85	23.02	1212-1	0.95	14.89	14.15
1132-2	1.46	14.77	21.56	1212-2	1.01	14.78	14.93
1132-3	1.46	14.75	21.53	1212-3	0.94	14.75	13.86
1132-4	1.56	14.81	23.10	1212-4	0.99	14.76	14.61
1132-5	1.56	14.78	23.06	1212-5	0.99	14.76	14.61

Table B.2 Split-disk test specimen dimensions for 1222-1 through 2241-5.

Specimen Designation	Minimum Thickness (mm)	Minimum Width (mm)	Reduced Sec. Area (mm^2)	Specimen Designation	Minimum Thickness (mm)	Minimum Width (mm)	Reduced Sec. Area (mm^2)
1222-1	1.61	14.85	23.91	2112-1	0.86	14.83	12.75
1222-2	1.55	14.83	22.99	2112-2	0.64	14.82	9.48
1222-3	1.58	14.85	23.46	2112-3	0.71	14.81	10.51
1222-4	1.55	14.83	22.99	2112-4	0.82	14.76	12.10
1222-5	1.60	14.89	23.82	2112-5	0.71	14.81	10.51
1232-1	1.61	14.88	23.96	2122-1	2.08	14.92	31.03
1232-2	1.56	14.80	23.09	2122-2	2.17	14.90	32.33
1232-3	1.55	14.77	22.89	2122-3	2.12	14.85	31.48
1232-4	1.59	14.84	23.60	2122-4	2.10	14.87	31.23
1232-5	1.59	14.81	23.55	2122-5	2.10	14.81	31.10
1242-1	1.52	14.70	22.34	2132-1	1.71	14.80	25.31
1242-2	1.48	14.72	21.79	2132-2	1.75	14.78	25.86
1242-3	1.50	14.61	21.91	2132-3	1.72	14.85	25.54
1242-4	1.50	14.71	22.06	2132-4	1.77	14.81	26.21
1242-5	1.47	14.75	21.68	2132-5	1.70	14.80	25.16
1252-1	1.54	14.71	22.65	2142-1	1.63	14.70	23.96
1252-2	1.32	14.64	19.32	2142-2	1.65	14.73	24.30
1252-3	1.47	14.62	21.49	2142-3	1.55	14.69	22.77
1252-4	1.47	14.61	21.48	2142-4	1.52	14.71	22.36
1252-5	1.50	14.64	21.96	2142-5	1.68	14.73	24.75
2111-1	0.86	14.83	12.75	2152-1	1.65	14.63	24.14
2111-2	0.64	14.82	9.48	2152-2	1.62	14.81	23.99
2111-3	0.71	14.81	10.51	2152-3	1.62	14.82	24.01
2111-4	0.82	14.76	12.10	2152-4	1.70	14.79	25.14
2111-5	0.71	14.81	10.51	2152-5	1.65	14.73	24.30
2121-1	1.92	14.91	28.63	2211-1	1.84	14.87	27.36
2121-2	1.90	14.81	28.14	2211-2	0.64	14.82	9.48
2121-3	1.87	14.85	27.77	2211-3	0.71	14.81	10.51
2121-4	1.95	14.87	29.00	2211-4	0.82	14.76	12.10
2121-5	1.92	14.87	28.55	2211-5	0.71	14.81	10.51
2131-1	1.78	14.83	26.40	2221-1	1.94	14.94	28.98
2131-2	1.65	14.82	24.45	2221-2	2.06	14.96	30.82
2131-3	1.81	14.80	26.79	2221-3	1.94	14.97	29.04
2131-4	1.74	14.71	25.60	2221-4	1.87	14.93	27.92
2131-5	1.67	14.85	24.80	2221-5	1.93	14.93	28.81
2141-1	1.61	14.68	23.63	2231-1	1.69	14.92	25.21
2141-2	1.59	14.61	23.23	2231-2	1.86	14.91	27.73
2141-3	1.63	14.68	23.93	2231-3	1.79	14.87	26.62
2141-4	1.63	14.67	23.91	2231-4	1.79	14.86	26.60
2141-5	1.62	14.69	23.80	2231-5	1.78	14.91	26.54
2151-1	1.53	14.76	22.58	2241-1	1.19	14.67	17.46
2151-2	1.62	14.72	23.85	2241-2	1.12	14.70	16.46
2151-3	1.56	14.67	22.89	2241-3	1.23	14.66	18.03
2151-4	1.60	14.70	23.52	2241-4	1.20	14.64	17.57
2151-5	1.58	14.72	23.26	2241-5	1.29	14.63	18.87

Table B.3 Split-disk test specimen dimensions for 2251-1 through 3221-5.

Specimen Designation	Minimum Thickness (mm)	Minimum Width (mm)	Reduced Sec. Area (mm^2)	Specimen Designation	Minimum Thickness (mm)	Minimum Width (mm)	Reduced Sec. Area (mm^2)
2251-1	1.59	14.73	23.42	3141-1	1.54	14.80	22.79
2251-2	1.70	14.71	25.01	3141-2	1.49	14.66	21.84
2251-3	1.67	14.81	24.73	3141-3	1.64	14.72	24.14
2251-4	1.71	14.63	25.02	3141-4	1.60	14.75	23.60
2251-5	1.67	14.71	24.57	3141-5	1.51	14.76	22.29
2212-1	0.86	14.83	12.75	3151-1	1.18	14.65	17.29
2212-2	0.64	14.82	9.48	3151-2	1.24	14.64	18.15
2212-3	0.71	14.81	10.51	3151-3	1.20	14.69	17.63
2212-4	0.82	14.76	12.10	3151-4	1.18	14.62	17.25
2212-5	0.71	14.81	10.51	3151-5	1.17	14.60	17.08
2222-1	2.03	14.97	30.39	3112-1	1.09	14.81	17.48
2222-2	2.00	14.90	29.80	3112-2	1.04	14.84	16.47
2222-3	2.01	14.97	30.09	3112-3	1.06	14.73	15.61
2222-4	2.04	14.97	30.54	3112-4	1.18	14.81	17.48
2222-5	2.04	14.83	30.25	3112-5	1.11	14.84	16.47
2232-1	1.65	14.82	24.45	3122-1	1.53	14.80	22.64
2232-2	1.75	14.79	25.88	3122-2	1.66	14.78	24.53
2232-3	1.86	14.83	27.58	3122-3	1.58	14.80	23.38
2232-4	1.79	14.89	26.65	3122-4	1.52	14.82	22.53
2232-5	1.76	14.89	26.21	3122-5	1.58	14.76	23.32
2242-1	1.63	14.75	24.04	3132-1	1.45	14.85	21.53
2242-2	1.53	14.75	22.57	3132-2	1.39	14.81	20.59
2242-3	1.63	14.77	24.08	3132-3	1.31	14.89	19.51
2242-4	1.47	14.72	21.64	3132-4	1.38	14.55	20.08
2242-5	1.66	14.47	24.02	3132-5	1.27	14.76	18.74
2252-1	1.58	14.81	23.40	3142-1	1.41	14.78	20.84
2252-2	1.70	14.80	25.16	3142-2	1.47	14.71	21.62
2252-3	1.63	14.74	24.03	3142-3	1.59	14.70	23.37
2252-4	1.70	14.52	24.68	3142-4	1.48	14.76	21.84
2252-5	1.67	14.73	24.60	3142-5	1.58	14.66	23.16
3111-1	1.05	14.80	15.54	3152-1	1.20	14.62	17.54
3111-2	1.06	14.86	15.75	3152-2	1.19	14.67	17.46
3111-3	1.02	14.84	15.14	3152-3	1.22	14.57	17.78
3111-4	1.05	14.80	15.54	3152-4	1.19	14.72	17.52
3111-5	1.06	14.86	15.75	3152-5	1.18	14.71	17.36
3121-1	1.70	14.85	25.24	3211-1	1.06	14.79	15.68
3121-2	1.68	14.90	25.03	3211-2	1.18	14.83	17.50
3121-3	1.64	14.88	24.40	3211-3	1.06	14.73	15.61
3121-4	1.74	14.86	25.86	3211-4	1.18	14.81	17.48
3121-5	1.73	14.88	25.74	3211-5	1.11	14.84	16.47
3131-1	1.29	14.61	18.85	3221-1	1.64	14.60	23.94
3131-2	1.33	14.75	19.62	3221-2	1.72	14.88	25.59
3131-3	1.37	14.85	20.34	3221-3	1.61	14.36	23.12
3131-4	1.32	14.81	19.55	3221-4	1.65	14.42	23.79
3131-5	1.30	14.72	19.14	3221-5	1.67	14.46	24.15

Table B.4 Split-disk test specimen dimensions for 3231-1 through 4152-5.

.

Specimen Designation	Minimum Thickness (mm)	Minimum Width (mm)	Reduced Sec. Area (mm^2)	Specimen Designation	Minimum Thickness (mm)	Minimum Width (mm)	Reduced Sec. Area (mm^2)
3231-1	1.40	14.82	20.75	4121-1	1.47	14.73	21.65
3231-2	1.43	14.66	20.96	4121-2	1.44	14.76	21.25
3231-3	1.42	14.73	20.92	4121-3	1.41	14.77	20.83
3231-4	1.40	14.55	20.37	4121-4	1.46	14.77	21.56
3231-5	1.35	14.75	19.91	4121-5	1.40	14.83	20.76
3241-1	1.72	14.86	25.56	4131-1	1.37	14.80	20.28
3241-2	1.62	14.85	24.06	4131-2	1.33	14.83	19.72
3241-3	1.75	14.80	25.90	4131-3	1.38	14.80	20.42
3241-4	1.71	14.86	25.41	4131-4	1.35	14.82	20.01
3241-5	1.68	14.79	24.85	4131-5	1.39	14.75	20.50
3251-1	1.22	14.78	18.03	4141-1	1.53	14.72	22.52
3251-2	1.23	14.79	18.19	4141-2	1.50	14.77	22.15
3251-3	1.20	14.69	17.63	4141-3	1.61	14.74	23.73
3251-4	1.21	14.67	17.75	4141-4	1.47	14.67	21.56
3251-5	1.23	14.73	18.12	4141-5	1.57	14.67	23.03
3212-1	1.06	14.79	15.68	4151-1	1.38	14.70	20.29
3212-2	1.18	14.83	17.50	4151-2	1.31	14.70	19.26
3212-3	1.06	14.73	15.61	4151-3	1.35	14.66	19.79
3212-4	1.18	14.81	17.48	4151-4	1.36	14.66	19.94
3212-5	1.11	14.84	16.47	4151-5	1.33	14.62	19.44
3222-1	1.72	14.86	25.56	4112-1	1.01	14.83	14.98
3222-2	1.57	14.83	23.28	4112-2	0.98	14.79	14.49
3222-3	1.55	14.73	22.83	4112-3	0.94	14.82	13.93
3222-4	1.64	14.89	24.42	4112-4	0.94	14.83	13.94
3222-5	1.50	14.86	22.29	4112-5	0.96	14.84	14.25
3232-1	1.49	14.67	21.86	4122-1	1.46	14.81	21.62
3232-2	1.42	14.73	20.97	4122-2	1.44	14.70	21.17
3232-3	1.38	14.58	20.12	4122-3	1.51	14.79	22.33
3232-4	1.40	14.73	20.62	4122-4	1.45	14.81	21.47
3232-5	1.54	14.77	22.75	4122-5	1.51	14.83	22.39
3242-1	1.67	14.85	24.80	4132-1	1.33	14.75	19.62
3242-2	1.53	14.62	22.37	4132-2	1.39	14.66	20.38
3242-3	1.61	14.67	23.62	4132-3	1.37	14.67	20.10
3242-4	1.68	14.81	24.88	4132-4	1.37	14.72	20.17
3242-5	1.59	14.76	23.47	4132-5	1.35	14.68	19.82
3252-1	1.18	14.76	17.42	4142-1	1.24	14.75	18.29
3252-2	1.24	14.85	18.41	4142-2	1.16	14.74	17.10
3252-3	1.15	14.62	16.81	4142-3	1.10	14.73	16.20
3252-4	1.18	14.61	17.24	4142-4	1.11	14.64	16.25
3252-5	1.21	14.65	17.73	4142-5	1.18	14.63	17.26
4111-1	1.01	14.83	14.98	4152-1	1.24	14.61	18.12
4111-2	0.98	14.79	14.49	4152-2	1.29	14.66	18.91
4111-3	0.94	14.82	13.93	4152-3	1.21	14.76	17.86
4111-4	0.94	14.83	13.94	4152-4	1.25	14.63	18.29
4111-5	0.96	14.84	14.25	4152-5	1.26	14.66	18.47

Table B.5 Split-disk test specimen dimensions for 4211-1 through 5132-5.

Specimen Designation	Minimum Thickness (mm)	Minimum Width (mm)	Reduced Sec. Area (mm^2)	Specimen Designation	Minimum Thickness (mm)	Minimum Width (mm)	Reduced Sec. Area (mm^2)
4211-1	1.01	14.83	14.98	4252-1	1.20	14.64	17.57
4211-2	0.98	14.79	14.49	4252-2	1.25	14.68	18.35
4211-3	0.94	14.82	13.93	4252-3	1.23	14.71	18.09
4211-4	0.94	14.83	13.94	4252-4	1.25	14.66	18.32
4211-5	0.96	14.84	14.25	4252-5	1.29	14.63	18.87
4221-1	1.48	14.73	21.80	5111-1	1.43	14.79	21.15
4221-2	1.40	14.74	20.64	5111-2	1.54	14.83	22.84
4221-3	1.45	14.76	21.40	5111-3	1.45	14.74	21.37
4221-4	1.46	14.74	21.52	5111-4	1.51	14.75	22.27
4221-5	1.43	14.81	21.18	5111-5	1.52	14.89	22.63
4231-1	1.29	14.76	19.04	5121-1	1.62	14.88	24.11
4231-2	1.36	14.84	20.18	5121-2	1.62	14.71	23.83
4231-3	1.32	14.85	19.60	5121-3	1.55	14.83	22.99
4231-4	1.30	14.84	19.29	5121-4	1.53	14.82	22.67
4231-5	1.33	14.81	19.70	5121-5	1.52	14.86	22.59
4241-1	1.14	14.75	16.81	5131-1	1.36	14.56	19.80
4241-2	1.19	14.90	17.73	5131-2	1.23	14.59	17.95
4241-3	1.12	14.68	16.44	5131-3	1.31	14.62	19.15
4241-4	1.13	14.74	16.66	5131-4	1.36	14.70	19.99
4241-5	1.17	14.72	17.22	5131-5	1.44	14.69	21.15
4251-1	1.29	14.67	18.92	5141-1	1.88	14.80	27.82
4251-2	1.26	14.50	18.27	5141-2	1.89	14.59	27.58
4251-3	1.36	14.63	19.90	5141-3	1.95	14.79	28.84
4251-4	1.28	14.57	18.65	5141-4	1.95	14.76	28.78
4251-5	1.29	14.62	18.86	5141-5	1.92	14.71	28.24
4212-1	1.01	14.83	14.98	5151-1	1.63	14.55	23.72
4212-2	0.98	14.79	14.49	5151-2	1.64	14.75	24.19
4212-3	0.94	14.82	13.93	5151-3	1.61	14.74	23.73
4212-4	0.94	14.83	13.94	5151-4	1.58	14.73	23.27
4212-5	0.96	14.84	14.25	5151-5	1.56	14.68	22.90
4222-1	1.45	14.79	21.45	5112-1	1.19	14.85	17.67
4222-2	1.44	14.75	21.24	5112-2	1.33	14.77	19.64
4222-3	1.48	14.77	21.86	5112-3	1.41	14.87	20.97
4222-4	1.53	14.80	22.64	5112-4	1.31	14.88	19.49
4222-5	1.46	14.77	21.56	5112-5	1.32	14.74	19.46
4232-1	1.26	14.65	18.46	5122-1	1.71	14.79	25.29
4232-2	1.18	14.68	17.32	5122-2	1.49	14.81	22.07
4232-3	1.26	14.60	18.40	5122-3	1.46	14.85	21.68
4232-4	1.18	14.64	17.28	5122-4	1.54	14.87	22.90
4232-5	1.17	14.61	17.09	5122-5	1.47	14.82	21.79
4242-1	1.34	14.84	19.89	5132-1	1.29	14.73	19.00
4242-2	1.39	14.83	20.61	5132-2	1.22	14.69	17.92
4242-3	1.28	14.61	18.70	5132-3	1.27	14.80	18.80
4242-4	1.35	14.83	20.02	5132-4	1.17	14.81	17.33
4242-5	1.35	14.83	20.02	5132-5	1.26	14.61	18.41

Table B.6 Split-disk test specimen dimensions for 5142-1 through 5252-5.

Specimen Designation	Minimum Thickness (mm)	Minimum Width (mm)	Reduced Sec. Area (mm^2)	Specimen Designation	Minimum Thickness (mm)	Minimum Width (mm)	Reduced Sec. Area (mm^2)
5142-1	2.01	14.81	29.77	5251-1	1.58	14.76	23.32
5142-2	2.01	14.80	29.75	5251-2	1.63	14.78	24.09
5142-3	2.00	14.75	29.50	5251-3	1.60	14.78	23.65
5142-4	1.95	14.78	28.82	5251-4	1.57	14.79	23.22
5142-5	1.99	14.74	29.33	5251-5	1.69	14.79	25.00
5152-1	1.62	14.78	23.94	5212-1	1.39	14.88	20.68
5152-2	1.64	14.78	24.24	5212-2	1.47	14.89	21.89
5152-3	1.62	14.66	23.75	5212-3	1.47	14.69	21.59
5152-4	1.64	14.77	24.22	5212-4	1.51	14.83	22.39
5152-5	1.63	14.81	24.14	5212-5	1.51	14.79	22.33
5211-1	1.52	14.86	22.59	5222-1	1.58	14.88	23.51
5211-2	1.55	14.88	23.06	5222-2	1.49	14.85	22.13
5211-3	1.49	14.73	21.95	5222-3	1.55	14.85	23.02
5211-4	1.52	14.86	22.59	5222-4	1.51	14.72	22.22
5211-5	1.55	14.88	23.06	5222-5	1.59	14.78	23.50
5221-1	1.02	14.78	15.08	5232-1	1.37	14.74	20.19
5221-2	0.94	14.79	13.90	5232-2	1.30	14.72	19.14
5221-3	0.92	14.79	13.61	5232-3	1.35	14.70	19.84
5221-4	0.94	14.78	13.89	5232-4	1.41	14.83	20.91
5221-5	0.97	14.78	14.34	5232-5	1.36	14.74	20.05
5231-1	1.38	14.77	20.38	5242-1	2.00	14.87	29.74
5231-2	1.33	14.71	19.56	5242-2	1.97	14.75	29.06
5231-3	1.39	14.75	20.50	5242-3	1.97	14.86	29.27
5231-4	1.39	14.74	20.49	5242-4	1.86	14.81	27.55
5231-5	1.35	14.71	19.86	5242-5	1.95	14.77	28.80
5241-1	1.90	14.73	27.99	5252-1	1.65	14.76	24.35
5241-2	1.96	14.78	28.97	5252-2	1.63	14.86	24.22
5241-3	1.88	14.70	27.64	5252-3	1.70	14.76	25.09
5241-4	1.91	14.86	28.38	5252-4	1.70	14.71	25.00
5241-5	1.83	14.81	27.10	5252-5	1.71	14.89	25.46

Table B.7 Tube tensile test specimen dimensions.

Specimen Designation	Outer Diameter (mm)	Thickness (mm)	Area (mm^2)	Specimen Designation	Outer Diameter (mm)	Thickness (mm)	Area (mm^2)
1131	63.05	1.52	294.76	3231	62.72	1.36	262.16
1141	62.83	1.41	272.72	3241	62.85	1.42	274.98
1151	62.96	1.48	285.85	3251	62.28	1.14	218.96
1132	63.00	1.50	289.8	3232	62.62	1.31	252.31
1142	62.75	1.37	265.11	3242	63.16	1.58	305.66
1152	62.96	1.48	285.85	3252	62.36	1.18	226.79
1231	63.18	1.59	307.64	4131	62.66	1.33	256.25
1241	62.80	1.40	270.04	4141	63.06	1.53	295.75
1251	62.90	1.45	279.92	4151	62.54	1.27	244.45
1232	63.05	1.52	294.76	4132	62.88	1.44	277.94
1242	62.80	1.40	270.04	4142	62.25	1.12	216.03
1252	62.93	1.47	283.27	4152	62.50	1.25	240.52
2131	63.25	1.62	314.59	4231	62.70	1.35	260.19
2141	63.20	1.60	309.63	4241	62.30	1.15	220.92
2151	63.24	1.62	313.6	4251	62.46	1.23	236.6
2132	63.20	1.60	309.25	4232	62.30	1.15	220.92
2142	63.12	1.56	301.69	4242	62.36	1.18	226.79
2152	63.19	1.59	308.64	4252	62.34	1.17	224.83
2231	63.30	1.65	319.56	5131	63.10	1.55	299.71
2241	62.30	1.15	220.92	5141	63.64	1.82	353.46
2251	63.21	1.60	310.62	5151	63.20	1.60	309.63
2232	63.40	1.70	329.51	5132	62.38	1.19	228.75
2242	63.06	1.53	295.75	5142	63.75	1.87	364.47
2252	63.22	1.61	311.61	5152	63.18	1.59	307.64
3131	62.70	1.35	260.19	5231	62.80	1.40	270.04
3141	63.04	1.52	293.76	5241	63.66	1.83	355.46
3151	62.34	1.17	224.83	5251	63.04	1.52	293.76
3132	62.50	1.25	240.52	5232	62.58	1.29	248.38
3142	63.08	1.54	297.73	5242	63.76	1.88	365.47
3152	62.46	1.23	236.6	5252	63.28	1.64	317.58